Numerical Modelling of Dynamics of FOWT

for Hardware-in-Loop Testing in Wind Tunnels

Shakthi Thinakaran

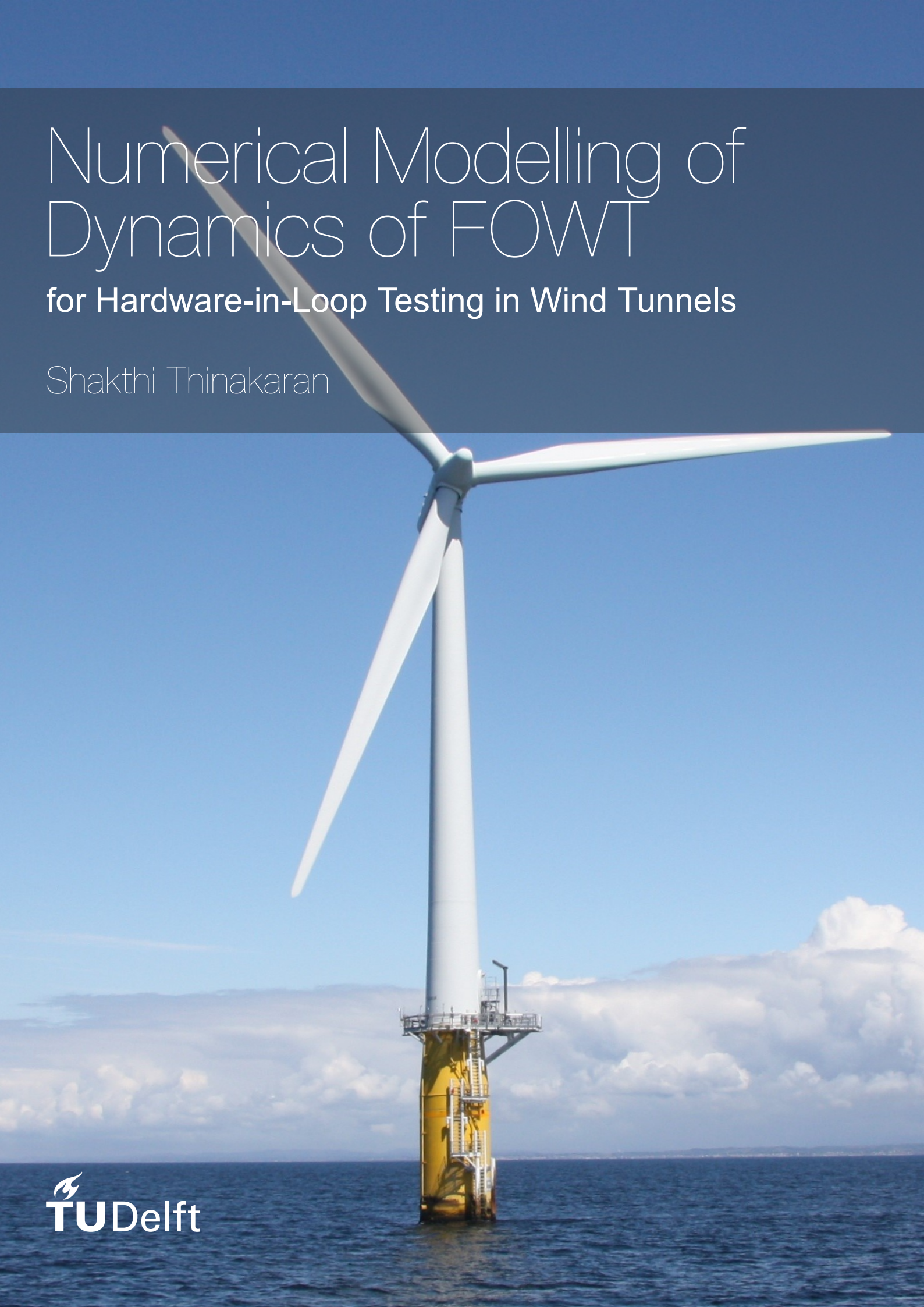

TU Delft

Numerical Modelling of Dynamics of FOWT

for Hardware-in-Loop Testing in Wind Tunnels

by

Shakthi Thinakaran

In partial fulfilment of the requirements to obtain the degree of
Master of Science in Sustainable Energy Technology (SET)
at the Delft University of Technology,
Faculty of Electrical Engineering, Mathematics and Computer Science

to be defended publicly on **August 26, 2024, at 9:00**.

Student number:	5817757	
Project duration:	November 15, 2023, – August 26, 2024	
Thesis committee:	Prof. dr. ir. A. Viré,	TU Delft, supervisor
	Dr. ir. F. Taruffi,	TU Delft, daily supervisor
	Dr. ing. S. Schreier,	TU Delft, committee member

An electronic version of this thesis is available at http://repository.tudelft.nl/.

TU Delft

Preface

This thesis is the culmination of the past nine months of discovering, understanding and developing. It was an incredible journey that was both challenging and rewarding and I could not have done it alone. I want to use this opportunity to express my gratitude to everyone who helped me reach the place I am today.

I want to start by thanking my supervisor Prof. Dr. Axelle Viré for introducing me to the world of floating offshore wind turbines and all its fascination. This topic perfectly suited my interests and was everything I hoped it would be. I also want to thank her for her support and trust in my capabilities. I also want to extend my thanks to Dr. Sebastian Schreier for showing interest in my work and agreeing to be a member of my thesis committee.

I am also deeply grateful to Dr. Federico Taruffi, my daily supervisor, whose guidance was indispensable. There were times when I felt lost and was not sure which direction to head in. His patience and insight helped me pick the right path and allowed me to learn and grow at my own pace. His experience on this topic was immensely beneficial to the project, as he could identify errors in places I wouldn't have thought to look. Moreover, his ability to empathise and offer advice tailored to my needs is truly commendable.

I also want to thank my family for being a constant source of encouragement, despite being spread across different corners of the world. Finally, I want to express my heartfelt appreciation to my boyfriend and all of my friends for sticking with me through all the ups and downs. Your presence made everything feel a little bit lighter and easier.

Shakthi Thinakaran
Delft, August 2024

Summary

Floating wind energy has the potential to revolutionize the offshore wind industry. It makes offshore wind energy more accessible to the majority of the countries around the world. To develop this technology further it is crucial to understand the effects of floating motion on aerodynamics, structural and control dynamics. Unsteady aerodynamic effects occur due to the pitching motion of the floating wind turbine, this phenomenon is still not understood and is an active research topic. Experimentally testing floating offshore wind turbines in a wind tunnel with a hybrid setup allows the simulation of floating dynamics. Furthermore, it enables a better understanding of the physics of unsteady aerodynamics.

A hardware-in-loop (HIL) methodology is used for experimentally testing floating offshore wind turbines (FOWT) in the wind tunnel. This is also referred to as hybrid experimental testing. Within this approach is a scaled physical wind turbine model designed with low-Reynolds number rotor blades to match aerodynamic performance. This wind turbine model is mounted on top of a hexapod, that can simulate the six degrees of freedom (6DOF) floating motion of the FOWT. A numerical model is used to solve the dynamics of the system based on the measured aerodynamic forces on the wind turbine model and the user-defined sea state conditions. Force and acceleration sensors are placed on the wind turbine model, and the hexapod records the actual position. These signals are used in the hardware-in-loop (HIL) numerical model.

The scope of this thesis is to create the numerical subsystem of the HIL model that can solve the dynamics of the system in real-time based on the inputs from the measurements and the user. The DTU10MW wind turbine model with the TripleSpar is used as the standard FOWT model for developing the numerical subsystem. This is because the wind turbine model used is a 1:148 scaled version of the DTU10MW model. The dynamics are solved by incorporating the structural and hydrodynamic properties of the wind turbine and the floater. The hydrostatics, hydrodynamics, aerodynamics, mass and inertia of the FOWT, mooring line effects and gravitational effects are incorporated into the equation of motion used to solve the floating dynamics.

The aerodynamic force measurements are also corrected before solving the dynamics. This is a crucial step because the force sensor on the wind turbine model also measures the inertial and gravitation forces of the wind turbine model's nacelle and rotor. Since the mass and inertia effects are also calculated within the numerical model, the measurements are corrected to provide only the force due to wind. On another note, the scaling methodology chosen does not follow the Froude similarity law, which means the accelerations have a scaling factor, due to this it is not possible to have a model whose inertial and gravitational forces are correctly scaled, making a correction methodology necessary.

The model was built in MATLAB's Simulink environment and run with the help of multiple '.mat' scripts. Once the model is built, the results of the simulation are verified with a well-established engineering tool, FAST/OpenFAST. The FAST model for the DTU10MW with the TripleSpar model was set up to operate with similar conditions as the Simulink model and the results were compared to validate the performance. In this project, the possibility of adapting the wind turbine model with the IEA15MW model is also tested since the IEA15MW's rotor is essentially an upscaled version of the DTU10MW's rotor. The scaling factors were determined and the numerical model in Simulink was also adapted to this wind turbine with the VolurnUS floater. This model was then validated with a similar OpenFAST setup.

After validation, the FOWT model is experimentally tested in the wind tunnel at the Open Jet Facility in TU Delft. The experimental tests proved the capability of the numerical model to solve the dynamics with applied aerodynamic loads and simulated hydrodynamic loads in a real-time setting. The results for the DTU10MW with the TripleSpar model were successfully tested. The IEA15MW with the VolturnUS model however was not successful in the preliminary HIL tests, the reasons for this are explored in the report.

Contents

1 Introduction **1**

1.1 Thesis Scope . . . 2
1.2 Research Questions . . . 2
1.3 Structure . . . 3

2 Background and Literature Study **4**

2.1 Background and Development of FOWT . . . 4
2.2 Numerical Modelling . . . 5
2.3 Modelling Techniques . . . 6
2.3.1 Aerodynamics . . . 7
2.3.2 Structural Dynamics . . . 7
2.3.3 Hydrodynamics . . . 8
2.3.4 Mooring Line Dynamics . . . 9
2.4 Experimental Testing . . . 9
2.4.1 Scaling . . . 9
2.4.2 Performance Matching of Turbine . . . 10
2.5 Physical Testing with Integrated Wind and Wave . . . 11
2.6 Real Time Hybrid Testing . . . 12
2.6.1 Hybrid Tests in Wave Basins . . . 12
2.6.2 Hybrid Tests in Wind Tunnels . . . 13

3 Setup **17**

3.1 Experimental Setup . . . 17
3.1.1 Wind Tunnel . . . 17
3.1.2 Hexapod . . . 18
3.1.3 Instrumentation . . . 18
3.1.4 Scaled Physical Wind Turbine Model . . . 19
3.2 Verification and Validation Setup . . . 21
3.2.1 Adapting to IEA15MW and VolturnUS . . . 23
3.2.2 OpenFAST Model: IEA15MW with VolturnUS . . . 23
3.2.3 OpenFAST Model: TU Delft Wind Turbine Model . . . 25
3.2.4 Scaling . . . 26

4 Numerical Modelling **28**
4.1 FOWT Motion Response . . . 28
4.2 Simulink HIL model . . . 30
4.3 Hydrodynamic Loads . . . 32
4.3.1 Radiation Loads . . . 33
4.3.2 Diffraction Loads . . . 34
4.4 Mooring Line Model . . . 34
4.5 Stiffness and Damping . . . 35
4.5.1 Hydrostatic and Gravitational Stiffness . . . 35
4.5.2 Viscous Damping . . . 36
4.6 Overall Dynamics . . . 36
4.7 Necessity for Force Correction . . . 37
4.8 Transformation Matrices . . . 37
4.9 Measured Force and Acceleration Estimation . . . 39
4.10 Determining Aerodynamic Forces . . . 41

5 Tuning, Validation and Testing **43**
5.1 Initial Testing in Open Loop . . . 43
5.1.1 Free Decay Tests . . . 44
5.1.2 Testing Irregular Waves . . . 49
5.2 Preliminary Closed Loop HIL Testing . . . 55
5.3 Feasibility of IEA15MW + VolturnUS model . . . 56
5.4 Final HIL test in the Wind Tunnel . . . 57
5.4.1 Preparation for the Test Campaign . . . 58

6 Results and Discussion **59**
6.1 Static Case . . . 59
6.2 Decay Test Cases . . . 61
6.2.1 Open-loop vs Closed-loop . . . 61
6.2.2 Large Displacement . . . 63
6.2.3 Medium displacement . . . 65
6.2.4 Small Displacement . . . 67
6.3 Irregular Wave Cases . . . 69

7 Conclusion **74**

References **77**

A Property Matrices **82**
A.1 DTU10MW + TripleSpar . . . 82
A.2 IEA15MW + VolturnUS . . . 83

A.3 Structural Matrices 85

B Force Correction MATLAB Script **86**

C Response Amplitude Operators **88**

List of Figures

2.1 Types for floaters: a semi-submersible, a tension leg platform and a spar buoy. In order from left to right. [10] . . . 5

2.2 Set up of a scaled wind turbine with 6DOF 'HexaFloat' robot for HIL testing in the wind tunnel at Politecnico di Milano [69] . . . 15

3.1 OJF schematic [77] . . . 17

3.2 Schematic of the Simulink program and the HMI . . . 19

3.3 Scaled Wind Turbine Model . . . 20

3.4 Diagram of the experimental setup with dimensions [76] . . . 21

3.5 Thrust curve comparison between the DTU 10MW reference turbine and the scaled wind turbine model. Modified from [76] . . . 22

3.6 Sketch of the IEA15MW reference wind turbine with the VolturnUS semi-submersible floater [13] . . . 23

3.7 Comparision between results from OpenFAST and values from the documentation. From left to right, power, thrust and torque values are compared. . . . 25

3.8 Decay test for VolturnUS simulated in OpenFAST . . . 25

4.1 Coordinate System of a FOWT with degrees of freedom [86] . . . 29

4.2 Simplified flowchart of the HIL simulink model in the closed loop condition. The blocks in blue are user-defined inputs and the blocks in red are the major calculations required. 31

4.3 Quasi-static mooring line model approximation compared with a dynamic model [89] . . 35

4.4 Representation of the frame transformation from rotating to fixed frame . . . 38

4.5 Image of the rotor nacelle assembly on the wind turbine model. The coordinate axes, the positions of the accelerometer and the loadcell are also mentioned. . . . 39

5.1 Free decay plot comparison between outputs from the HIL Simulink model and FAST tool for the DTU10MW wind turbine with TripleSpar floater. The decays from all six degrees of freedom are compared. . . . 46

5.2 Free decay plot comparison between HIL Simulink model and OpenFAST for the IEA15MW wind turbine with VolturnUS floater. . . . 48

5.3 Wave elevation spectrum for an irregular wave at rated wind speed for the DTU10MW wind turbine with H_s of 3.04m and T_p of 9.50s. The spectrum of the wave generated in FAST is compared with that generated by the HIL Simulink Model (SLX). . . . 50

5.4 Diffraction force spectra for an incoming irregular wave with H_s of 3.04m and T_p of 9.50s. The spectra are compared between the output from FAST and the HIL Simulink model for the DTU10MW wind turbine with TripleSpar floater. . . . 50

5.5 Motion time history of DTU10MW FOWT model with TripleSpar floater for the wave case at rated wind condition compared between HIL simulink model and FAST. The cases are compared assuming no wind. . . . 51

5.6 Motion spectra of DTU10MW FOWT model with TripleSpar floater for the wave case at rated wind condition compared between HIL simulink model and FAST. The cases are compared in all DOFs assuming no wind. 51

5.7 Comparision of RAO between the Simulink model and FAST for the simulated rated wave condition without wind. 52

5.8 Wave elevation spectrum for an irregular wave at rated wind speed for the IEA15MW wind turbine with H_s of 1.53m and T_p of 7.65s. The spectrum of the wave generated in OpenFAST is compared with that generated by the HIL Simulink Model (SLX). 53

5.9 Motion time history of IEA15MW FOWT model with VolturnUS floater for the wave case at rated wind condition compared between HIL Simulink model and OpenFAST. The cases are compared assuming no wind. 54

5.10 Motion spectra of IEA15MW FOWT model with VolturnUS floater for the wave case at rated wind condition compared between HIL simulink model and OpenFAST. The cases are compared in all DOFs assuming no wind. 54

5.11 Comparision of the platform displacement RAO obtained for the Simulink and the OpenFAST model for the IEA15MW wind turbine with VolturnUS using the wave case at rated conditions assuming no wind. 55

6.1 Comparison of torque and power (left and right resp.) values from the motor and the loadcell with the values from the DTU10MW definition. 60

6.2 Thrust curve 60

6.3 Power curve 60

6.4 Torque curve 60

6.5 Schema of the step-by-step process taken for HIL testing in wind tunnels 61

6.6 Decay motion history comparison between open-loop and closed-loop setting in 6DOF with maximum initial displacement. The DTU10MW model with the TripleSpar floater is used for the simulation. 62

6.7 Decay motion spectra comparison between open-loop and closed-loop setting in 6DOF with maximum initial displacement. The DTU10MW model with the TripleSpar floater is used for the simulation. 62

6.8 Decay motion history in 6DOF with maximum initial displacement. The decay tests were held with the HIL setup in the windtunnel with the DTU10MW with TripleSpar numerical model. The motion history from open-loop, closed-loop and closed-loop with wind are compared. 63

6.9 Spectrum of decay motion done with HIL testing in 6DOF with maximum initial displacement. The sprectrum from decays in open-loop, closed-loop and closed-loop with wind are compared. 64

6.10 Decay motion history with medium displacement from HIL testing with and without wind in a closed-loop setting. The decays are done in model scale for all the 6DOFs with the DTU10MW numerical model. 65

6.11 Spectrum of decay motion with medium initial displacement. The decay motion tests were conducted in a HIL setup with and without the presence of wind. 66

6.12 Decay motion history with small initial displacement from HIL testing with and without wind in a closed-loop setting. The decays are done in model scale for all the 6DOFs with the DTU10MW numerical model. 67

6.13 Spectrum of decay motion with small initial displacement. The decay motion tests were conducted in a HIL setup with and without the presence of wind. 68

6.14 Sprectrum obtained after FFT of motion history for irregular wave case 1 tested in the wind tunnel. 70
6.16 Sprectrum obtained after FFT of motion history for irregular wave case 3 tested in the wind tunnel. 70
6.15 Sprectrum obtained after FFT of motion history for irregular wave case 2 tested in the wind tunnel. 71
6.17 Sprectrum obtained after FFT of motion history for irregular wave case 4 tested in the wind tunnel. 71
6.18 Sprectrum obtained after FFT of motion history for irregular wave case 5 tested in the wind tunnel. 72
6.19 RAO obtained from the platform motion for wave case 4 73

C.1 RAO of Wave Case 1 tested in the wind tunnel. 89
C.2 RAO of Wave Case 2 tested in the wind tunnel. 90
C.3 RAO of Wave Case 3 tested in the wind tunnel. 90
C.4 RAO of Wave Case 4 tested in the wind tunnel. 91
C.5 RAO of Wave Case 5 tested in the wind tunnel. 91

List of Tables

2.1 Representative physical model experiment projects.[33] 11

2.2 Overview of FOWT model experiments with different actuators. 14

3.1 Scaling Factors of the model DTU10MW for HIL testing are provided in the format of model scale/full scale. Modified from [69] 19

3.2 Main characteristics comparison between full-scale DTU10MW reference turbine and the model-scale wind turbine [76] 22

3.3 Main Characteristics of IEA15MW wind turbine [84] 24

3.4 Natural frequency comparison for VolturnUS between OpenFAST setup and documentation 25

3.5 Wind Turbine Model Performance Values from OpenFAST model 26

3.6 Scaling Factors of the model IEA15MW for HIL testing. 27

5.1 Initial conditions for free decay tests for the DTU10MW with TripleSpar model. The offset is added to the final motion history before comparison. 45

5.2 Comparison of natural frequencies and damping ratios between FAST and Simulink numerical model for the DTU10MW+TripleSpar model 47

5.3 Initial conditions for free decay tests for the IEA15MW with VolturnUS model 47

5.4 Comparison of natural frequencies and damping ratios between OpenFAST and the Simulink HIL model for the IEA15MW with VolturnUS FOWT design. 49

6.1 Natural frequencies and damping ratios obtained from decay tests done using the HIL setup with large initial displacements, for different DOFs under different test settings. The values have been scaled from model-scale to full-scale. 65

6.2 Natural frequencies and damping ratios obtained from decay tests done using the HIL setup with medium initial displacements, for different DOFs under different test settings. The values have been scaled from model-scale to full-scale. 66

6.3 Natural frequencies and damping ratios for different degrees of freedom (DOFs) under closed-loop and closed-loop with wind conditions. 69

6.4 Irregular wave test cases with corresponding wind speeds, rotor speeds, wave heights (H_s), and wave peak periods (T_p). 69

List of Acronyms

BEM Boundary Element Method

BEMT Blade Element Momentum Theory

CDPM Cable-Driven Parallel Manipulators

CFD Computational Fluid Dynamics

DAQ Data Acquisition

DOF Degree of Freedom

DTU Denmark Technical University

FDI Frequency Domain Identification

FEM Finite Element Method

FFT Fast Fourier Transform

FOWT Floating Offshore Wind Energy

HIL Hardware-in-Loop

HMI Human Machine Interface

IEA International Energy Association

JONSWAP Joint North Sea Wave Project

LCOE Levelised Cost of Electricity

MAP Mooring Analysis Program

NREL National Renewable Energy Laboratory

OJF Open Jet Facility

PF Potential Flow

PIV Particle Image Velocimetry

RAO Response Amplitude Operator

SWL Still Water Level

TLP Tension Leg Platform

TSR Tip Speed Ratio

WAMIT Wave Analysis MIT

WTM Wind Turbine Model

1

Introduction

The global temperature rise has become apparent across the globe, marked by several countries reporting the hottest consecutive months in a row compared to data from pre-industrial levels [1]. The number of natural disasters and their severity are on the rise, posing a risk of biodiversity loss [2]. To combat this and avoid a more disastrous future, the world needs to shift towards using renewable sources of energy and making energy-efficient infrastructure and technologies.

The landmark Paris Agreement, ratified by 196 nations, calls for collective commitment to limit global warming to 1.5°. To meet this target, achieving net zero emissions by 2050 is paramount [3]. The energy sector is responsible for three-quarters of all emissions, thus this sector must make a transition to renewable energy sources. In the 2050 net zero emissions scenario, two-thirds of the energy demand is met by renewable energy. To make this happen, wind energy production almost needs to quadruple [4].

Offshore wind energy holds immense promise, it often has more energy potential than the total electricity consumption of entire countries [5]. In the past decade, the growth of offshore wind energy has been remarkable with a boom in installed capacity. Offshore wind energy capacity has increased tenfold from 2013 to 2023. The cost of installing wind turbines at sea has also reduced making it more economical [6]. However, a lot of developed countries are now facing a plateau in growth, since they are running out of shallow seas for installation and it's becoming economically unviable to go to deeper seas with the same concept.

Enter Floating Offshore Wind Turbines (FOWTs) with the potential to revolutionize the offshore wind energy industry. They have access to better-quality wind and can produce more energy than any other wind turbine technology. They are also not hindered by neighbouring infrastructures and there is more space to avoid negative wake effects. However, their viability is hindered by cost barriers related to installation and maintenance. Bottom-fixed offshore wind turbines are more economically feasible, but observing the trend these wind turbines took in the past decade the same is predicted to happen for the floating wind turbines. Nevertheless, to make this a reality substantial research efforts need to be taken into FOWT to understand the engineering challenges and adapt and improve the FOWT designs to make them better suitable for an offshore floating environment.

The engineering challenges faced by FOWT are diverse. Some are due to the combined loading of wind and waves and the effects of their interaction on the dynamics of the FOWT. Another cause is the floater's motion in six degrees of freedom. This causes additional gravitational loading in directions that bottom-fixed turbines did not experience. The interaction of the turbine with its wake could also cause unsteady aerodynamic effects. Developing numerical models and experimental testing methodologies are imperative for analysing these engineering challenges. Studying these scenarios is necessary for making suitable design adjustments in structure, control systems or other aspects.

With attaining a considerable technology readiness level for FOWTs, the other industries connected to it such as offshore cable laying, platform construction, and FOWT maintenance and installation are

poised with parallel growth to support the development of this field, resulting in a huge socio-economic benefit. With the realization of a robust FOWT industry, a clean and more reliable source of renewable energy will be available for nations worldwide. This will bring more diversity to the energy mix in the future. The energy generated by floating offshore wind turbines is more consistent compared to other wind turbine technologies because they are less affected by daily fluctuations in wind patterns. A consistent energy source is crucial for system integration with renewable energy sources.

1.1. Thesis Scope

The many engineering challenges inherent in FOWTs can be effectively understood and tackled with the help of experimental testing. Experimentally testing a FOWT in a smaller-scale laboratory environment enables research possibilities regarding various critical aspects such as assessing the stability of a FOWT structure, the loading and fatigue under wave and wind conditions, the changes in aerodynamics due to platform motion, and testing control systems for the FOWT. Experimental tests can be done with physically simulated wind and waves or employ hybrid tests where either wind or waves are physical and the other is numerically modelled. These tests are also crucial for validating or tuning numerical models that simulate FOWT behaviour.

At TU Delft a hybrid experimental setup is being developed in the Open Jet Facility (OJF) wind tunnel. This hybrid experimental setup involves a scaled wind turbine that is attached to a parallel kinematics robot with six degrees of freedom (DOF), also referred to as Hexapod. It also involves a numerical model that mimics the floater's motion depending on the wind and wave conditions. A model capable of simulating 3DOFs (surge, heave and pitch) dynamics has been developed for the DTU(Denmark Technical University)10MW reference wind turbine with the TripleSpar floater. The setup works as a closed loop system where the aerodynamic loads produced by the wind tunnel are measured and corrected, this is later used to determine the motion of the FOWT with the help of the numerical model. Due to this reason, this experimental setup is referred to as Hardware-in-Loop (HIL) testing. The main purpose of this setup is to analyse the complex aerodynamic effects created by the motions of a FOWT.

The primary aim of this thesis is to devise a numerical model to simulate the complete 6DOF dynamics exhibited by the DTU10MW reference wind turbine with the TripleSpar floater. This model is crucial for the HIL wind tunnel test setup since it is the tool that will be used to integrate the measured aerodynamic loads and modelled hydrodynamic loads. An important requirement for the model is the real-time constraint, this allows the successful coupling of the loads and the experimental tests would not be possible without this. It is also necessary to validate the developed dynamic numerical model, this will be done by comparing the results obtained with the outputs from an identical setup in the established engineering tool OpenFAST.

Another aim of the thesis is to make the experimental setup adaptable to different reference FOWT systems. For this, the IEA15MW reference wind turbine is chosen with the VolturnUS semi-submersible floater. To make this adaptation multiple feasibility tests will be done before creating the real-time dynamic numerical model. New scaling factors for the chosen reference FOWT system will be decided and validated. After this, the numerical model for the reference FOWT would be built and tested for tuning and validation.

Another important aspect of devising the numerical model for dynamics is correcting the measured forces to result in only aerodynamic forces. This requires a robust correction methodology. Developing this methodology for a complex 6DOF system with coupling and interactions is another challenge that will be tackled as part of this research. The developed methodology will be tested and validated numerically and with the HIL setup.

1.2. Research Questions

1. How are the dynamics of a fully coupled FOWT system with given aerodynamic loads and met-ocean conditions modelled in real-time for use in Hardware-in-loop testing in a wind tunnel?
2. What is the methodology for correcting the aerodynamic force for a non-Froude scaled FOWT in HIL wind tunnel testing?

3. How to make the numerical model adaptable with different floaters and wind turbines?
4. How accurate is the HIL model at modelling dynamics of FOWT compared to established engineering models like OpenFAST?

1.3. Structure

This report starts by explaining the background behind floating offshore wind turbines and the need for experimental testing. This is followed by a literature study on the types of experimental testing and the techniques used in numerical models. After this research, the subsequent chapter explains the methodology of the project, later this methodology is verified and used for experimental testing. The results of the tests are documented and discussed and finally, the conclusions for this project are made.

This work is organized into a total of 7 chapters including the introduction, the titles of the other chapters are listed below,

- Chapter 2: Background and Literature Study
- Chapter 3: Setup
- Chapter 4: Numerical Modelling
- Chapter 5: Tuning, Validation and Testing
- Chapter 6: Results and Discussion
- Chapter 7: Conclusion

2

Background and Literature Study

This chapter aims to provide an overview of the evolution of testing methods for floating offshore wind energy. The chapter starts with an introduction to floating offshore wind energy and contemporary developments in the field in section 2.1. The numerical models developed so far are described in section 2.2 followed by section 2.3 which explains the modelling techniques in detail. At last in section 2.4, various experimental testing methodologies are discussed extensively.

2.1. Background and Development of FOWT

Floating Offshore Wind Energy is becoming an increasingly attractive option as fixed-bottom offshore wind turbines run out of suitable spaces, especially in the North Sea. The depth in which offshore wind turbines have been installed has been increasing gradually from 10m depths in 2005 to 30m depths as of the present day. However, this trend is projected to decline as it becomes more difficult to install bigger turbines in deeper waters. For depths over 60m, having bottom-fixed turbines becomes unfeasible [7].

So, the development of FOWT is the next step in expanding the energy potential of offshore wind. In fact, 80% of offshore wind potential in Europe is in deeper waters where floating offshore wind turbines are necessary [8]. It also has great potential as a suitable energy source for countries that lack shallow seas such as Japan, France, Italy, Norway, and the western coast of the United States.

The wind available in deeper seas is also stronger and more consistent. Hence, floating wind turbines are predicted to have a higher capacity factor, thus producing more energy annually compared to their fixed-bottom counterparts. Having more space in deeper seas also means the turbines can be installed further apart from each other to avoid wake effects, wave effects of wind farms can also be similarly avoided.

However, this technology is still not commercial and data to validate models to predict performance have higher margins of error. The extra degrees of motion that the FOWT experiences create new situations of gravitational, inertial and hydrodynamic loads. These play an effect on the loading and the lifetime of the floating wind turbine. It also has different wakes and other aerodynamic effects due to the extra degrees of motion.

Another difficulty that floating offshore wind turbines face in their commercialisation is the difficulty of installing and maintaining these turbines and providing a connection to shore with electricity lines. This makes this technology fairly expensive compared to bottom-fixed turbines. Currently, there are also multiple designs for floaters and various ideas, standardization is necessary to grow this field of energy and reduce the costs. Since, this is still a developing field, understanding more about the dynamics of FOWT and the unsteady aerodynamics caused by the motions and its effect on performance, energy production and the structure's lifetime is crucial at this stage.

FOWT requires structures from different manufacturers due to confidentiality issues. For example, the wind turbine is commonly made by the turbine manufacturers, and the tower and the floater are

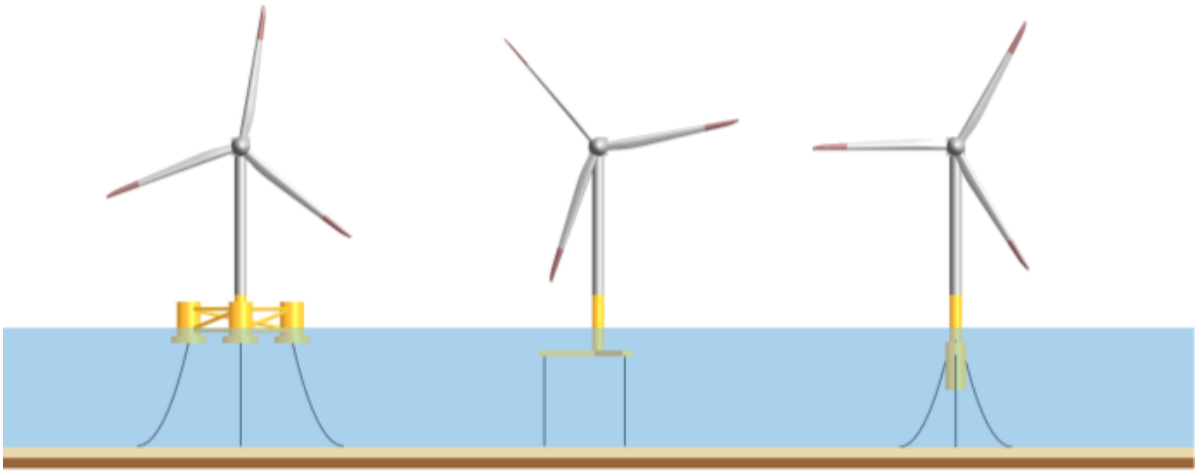

Figure 2.1: Types for floaters: a semi-submersible, a tension leg platform and a spar buoy. In order from left to right. [10]

designed and manufactured by other parties. Towers are commonly designed after the floater and the turbine specifications have been decided since it needs to be specific to both those structures and the location. The floaters are usually designed by manufacturers depending on the location.

Floaters are often designed with borrowed knowledge from the offshore oil and gas industry. The stability for these floaters is based on three concepts: buoyancy, using ballasts or mooring lines. The stability of barge-type floaters is based on buoyancy, spar-type floaters are based on ballast stabilisation, and Tension Leg Platforms (TLPs) are stabilized with taut mooring lines. Semi-submersible floaters use both buoyancy and ballasts for stability. All these designs behave differently and have their pros and cons. [9]

The earliest installation of a floating offshore wind turbine farm was in Scotland in 2008. This was the Hywind Scotland wind farm with a capacity of 30MW [11]. This has been running for 16 years and has provided enough data to validate and improve various models. FOWT design improvements have also been made. Several other floating wind farms were also installed in other parts of the world. Currently, the Hywind Tampen wind farm in Norway which was installed in 2022 has a capacity of 88MW making it the biggest farm so far [12].

The data from these floating wind farms are used to validate numerical models which are imperative for testing developed FOWT designs. They also open a window into understanding the issues with the current design and the areas of improvement. Experimental tests with scaled models are also crucial in understanding special cases and improving the model.

The developed numerical models were also used to create new floater and turbine designs. The NREL (National Renewable Energy Laboratory) 5MW wind turbine with the DeepCWind floater has been the most researched FOWT system till now. Currently, 15MW floaters are becoming more relevant, the common floater design combined with this turbine is the VolturnUS semi-submersible floater developed by the University of Maine in the United States [13].

On the other hand, novel floating offshore wind energy technologies are also being developed. Several concepts for vertical axis floating offshore wind turbines are being researched, some concepts have straight blades, but the number of blades and the distance from the centre differ and some other concepts have curved blades. Airborne wind energy is also a growing topic in the field of FOWT. There are also concepts with multiple rotors with a single floater or multiple pillars supporting a single rotor.

2.2. Numerical Modelling

Numerical models are an essential tool required in the design process of FOWTs. They are often validated with data from model-scale experimental testing or using full-scale prototypes. These numerical

models also prove to help in analysing energy production, making lifetime analyses or the wake effects of the platform motion. Different fidelity numerical models are used based on the requirement.

In the beginning, numerical models were created to only simulate the linear dynamics of the FOWT in the frequency or the time domain. Frequency domain models are easily used to model the linear dynamics. Time domain methods are better used to deal with non-linear dynamics. Low-fidelity models often assumed rigid body systems and only solved for particular DOFs. Some examples of this are earlier versions of the open-source software FAST developed by Jason Jonkman in NREL [14] and other private software such as QuLAF[15] and SLOW.

Recent versions of FAST (now OpenFAST) have improved to include non-linearities in the system and all the DOFs. They have become a standard model for the development of many other engineering models. It also serves as a tool to validate newly developed numerical models [16][17][18]. These models are still considered mid-fidelity models since they use multiple approximations and do not capture all the non-linearities perfectly. Using the Blade Element Momentum Theory (BEMT) is one such approximation. However, there are multiple additions and modifications to this theory in FAST [19]. There are more commercial numerical models such as Bladed designed by DNV GL [20], HAWC2 developed by DTU, and Simpack by Dassault Systems.

Higher fidelity models are developed using concepts of computational fluid dynamics. These models are better at modelling the unsteady aerodynamic effects. The potential flow-free wake-vortex method is a lower fidelity method compared to computational fluid dynamics (CFD) but provides better accuracy than the BEMT model [17]. These higher fidelity models are also more computationally expensive. The level of fidelity required in the model often depends on the applications.

The models discussed above were designed originally for onshore fixed turbines. For offshore and floating offshore wind turbines new modules have to be added to simulate the entire system. Fully coupled numerical models are much more difficult to design for floating offshore wind turbines since there is an addition of hydrodynamic and mooring loads to the system. For example, Orcaflex and SIMA are hydrodynamic solvers for floating platforms. SIMA was developed for the offshore oil and gas industry. WAMIT and Ansys AQWA are some programs that solve for the wave forces using a panel method. These models are later coupled with models such as FAST or Bladed. Higher fidelity models can be set up to solve the dynamics simultaneously for better accuracy, the way most CFD models do. But, again the trade-off for this is the cost.

2.3. Modelling Techniques

The modelling techniques of most numerical models involve considering the dynamic effects of various structural and environmental sources. For FOWTs it is crucial to couple the aerodynamic and hydrodynamic effects. To better understand the dynamics of a FOWT, it is important to identify all the forces acting on the system. The system experiences various sources of loading as listed below,

- Wind causes loading on the rotor and the tower.
- Incident waves and ocean currents cause loading on the floater.
- The wind and wave direction misalignment also causes loading on the floater.
- The weight of the system causes inertial and gravitational loads on the system.
- The mooring lines also contribute to some loads on the floater.
- Floater loads can also be from other environmental conditions like tides or icing.
- The turbine control system also influences the loading on the system. Sudden failures can cause extreme loads.

However, not all the loading sources mentioned above are equally influential. Numerical models commonly divide the system dynamics into hydrodynamics, aerodynamics, structural dynamics, mooring line dynamics and control dynamics. They each deal with their respective loading cases. After solving for all the dynamics separately they are combined into a single equation of motion to define the dynamics of the whole system (this is discussed in detail in chapter 4). More details about the techniques of

modelling used in the different fields are given in the following subsections. Control dynamics is not focused on in this section, since its influence is limited to specific operating conditions which are not relevant to the topic of this thesis.

2.3.1. Aerodynamics

Accurately modelling the aerodynamics is crucial since it allows for modelling the performance of the wind turbine. For a FOWT, this comes with extra challenges since the platform's motion results in a varying relative velocity of the wind. This is commonly referred to as dynamic inflow or unsteady aerodynamics. [21].

Motion that is the direction of the wind is damped with aerodynamic damping, however, side motions or yawing motions caused due to the irregularities in the wind are difficult to damp. This needs to be mitigated using control. Understanding the aerodynamics is necessary for this.

The conventional low and mid-fidelity model, the steady or quasi-steady BEMT fails to model unsteady aerodynamics effectively. But with an additional dynamic inflow model added to the BEMT model, the results are promising when compared to higher fidelity CFD models [22]. Oye's unsteady aerodynamic model and a modified Beddoes-Leichman model for dynamic stall are tested in OpenFAST and validated by Branlard et al.[23]

The next step in fidelity from the BEMT model is the Free Vortex Wake (FVW) model. This model has more computational efficiency than CFD models and is gaining popularity in many commercial and open-source models, due to its better accuracy. With increasing turbine sizes the need to accurately model the blade deflections becomes more important. Shaler et al. added the FVW method to OpenFAST [24].

Higher fidelity models use either the potential flow method or a computational fluid dynamics solver. These models give a greater accuracy but at a lower computational efficiency. In the industry, it is still common to use mid-fidelity numerical models.

2.3.2. Structural Dynamics

Structural dynamics involves modelling the motion of the individual parts of the floating wind turbine due to forcing. The dynamics of the rotor, the tower and the floating platform are some of the most crucial. In lower fidelity models, the whole set-up is considered a fixed rigid body. In mid-fidelity models, the different parts of the structure are modelled as approximate rigid structures with flexible connections [25].

Sometimes, particular structure's flexibility is taken into account, for example, the tower or the blades. A modal analysis is done on these structures and specific deformation shapes in the relevant DOFs for the different modes are identified. These shapes are then used in numerical codes for the structural modelling [26]

Another approach would be to calculate the responses using multibody dynamics, this does not restrict the number of DOFs considered. This approach is used in the numerical code ADAMS and SLOW [17]. Higher fidelity models use the finite element method to analyse the forces and derive the displacement of each element of the structure. They provide accurate results and might be crucial at the end stages of the design process.

The importance of structural dynamics lies in identifying the excitation frequencies of the structures to avoid resonance. It is also necessary for the Ultimate limit state, fatigue limit state and accidental limit state assessments which need to be satisfied according to the standards for the FOWT design [16]. The most common tools used are mid-fidelity numerical models in the time domain.

More often than not, various numerical models that emphasize understanding the aerodynamics or the performance, assume a low-fidelity solution for the structural dynamics. However, with the growing sizes of turbines, the influence of structural dynamics is increasing. Also with the introduction of waves and floater dynamics, the range of resonance frequencies to avoid becomes larger, making FOWT design more challenging.

2.3.3. Hydrodynamics

Modelling the hydrodynamics involves analysing the loading caused by the met-ocean conditions and the interactions with the floating platform. Understanding the loading from incident waves was previously considered for bottom fixed offshore wind turbines, the motion of the floating platform and its influence on the FOWT dynamics are recent additions to the numerical models for FOWT.

There are two basic approaches to modelling the hydrodynamics in mid-fidelity models. The most common approach is using the Potential Flow (PF) model. They involve solving the Laplace equation for continuity with irrotational and inviscid assumptions. They are also called panel methods or boundary element methods due to the method of solution [16]. Another method uses Morison equations, which solve for the hydrodynamic forces assuming the floating structure does not disturb the incoming waves.

The potential flow method is often chosen when D»L where,
D: characteristic length of floater
L: length of wave
This method solves based on the following sources of loading,

- Incident wave loads: Due to the unsteady pressure field created by incident waves on the floater. They are also called the Froude-Krylov forces.
- Radiation loads: Due to the wave generated by the oscillating floating body.
- Diffraction loads: Due to the disturbance of the incident wave after interaction with the floater.
- Hydrostatic loads: The restoring forces and moments caused by a displacement of the centre of buoyancy.

The viscous forces are often ignored in this method, although there are modifications that allow its addition.

Numerical methods based on the potential flow theory or the Boundary Element Method (BEM), divide the geometry into panels and derive the hydrodynamics loads in each panel. Most numerical codes achieve this by precalculating a set of hydrodynamic coefficients for the particular floater. WAMIT for example is a widely used frequency domain potential flow solver that provides the hydrodynamic coefficients which can be used in the numerical time domain model [21].

Often the potential flow is solved linearly and the non-linearities are added separately. Froude-Krylov loads are the most important non-linear forces and it is significant with bigger waves, as it depends on the pressure of the wetted surface area. Non-linear diffraction forces also influence the dynamics. A common way to calculate the non-linearities in conventional numerical models is using the Quadratic Transfer Function (QTF) or Newman approximations.

Viscous forces become important with bigger waves or rougher sea states. Since viscous forces are ignored in the potential flow theory, they need to be modelled with Morison's equation [16]. Solvers based on Morison take into account inertial and viscous drag loads. This model assumes the structure is too small to have any impact on the incident wave and ignores diffraction effects. This method is usually chosen when D«L [25].

The choice between Morisons and PF often depends on the sea state and the type of floating platform. Often, hybrid methods are used to solve the hydrodynamics, where slender parts of the floating structure are modelled with Morisons while the rest are modelled using the potential flow theory. This is done because the potential flow theory does not account for flow separation. Rougher seas are also sometimes modelled with Morision instead of potential flow theory. [21] It is also common to use Potential flow theory and include the viscous forces from Morison to capture all the effects. [27][28]

Popular numerical models such as OpenFAST and OrcaFlex for FOWT dynamics include both potential flow theory solvers and Morison solvers. They can be used in a hybrid way or separately. They also include QTF or Newman approximations for non-linearities. Hybrid methods are a cheaper alternative to using high-fidelity tools such as CFD. OpenFOAM and QBlade are some common CFD solvers used to model the hydrodynamics of a FOWT. The mid-fidelity tools are often validated with results from

CFD simulations. Smoothed Particle Hydrodynamics (SPH) is also a high-fidelity tool for modelling hydrodynamics [29].

2.3.4. Mooring Line Dynamics

Mooring lines are an essential part of FOWT system that keeps the floating platform at a fixed position. Most floater designs are equipped with catenary mooring lines. They have fairleads connected to the floater approximately at the still water level (SWL) and anchors fixed to the bottom of the ocean. The lines are normally synthetic ropes.

The mooring lines contribute to tension forces that depend on the motion of the floating platform. The mooring line dynamics are also influenced by currents, soil and hydrodynamics. Mooring line dynamics for catenary mooring lines can be modelled by a range of numerical models with increasing fidelity as listed below,

1. Static model: Assuming the static spring-mass system with a fixed stiffness coefficient.
2. Quasi-static model: Assuming a static spring mass system but the stiffness differs with the displacement. It is still a static method, so an equilibrium position is assumed at all times.
3. Quasi-dynamic model: Assuming all the catenary lines to have mass and inertia but still act as a spring mass system with stiffness and damping. Drag is also considered in this model.
4. Dynamic model: Assuming nodes over the catenary line connected by massless springs, where each node is a spring mass system. It is also referred to as a lumped mass system. A higher fidelity fully dynamic system uses Finite Element Methods (FEM) or Finite Difference (FD). They are similar to the lumped mass method but the number of nodes considered is significantly higher.

The quasi-dynamic model is often used in mid-fidelity models such as Orcaflex. The Orcaflex model includes springs and dampers to model the axial, torsional and bending behaviour of the mooring line. OpenFAST utilizes the lumped mass model as part of its MoorDyn module, it also includes lower-fidelity models for simulation.

2.4. Experimental Testing

Experimental testing of FOWT turbines in laboratory conditions is often an essential step of the design process. Experimental testing ensures structural stability and gives insight into the motion of the FOWT. Since the system deals with both wind and wave loads, their interaction can also be understood further. This can further help develop the operational strategies, design the control system, study the unsteady aerodynamics or analyse the fatigue.

Experimental testing is done in various ways to study the dynamic response and performance of the FOWT. Scaled wind turbines are tested in wave basins or in wind tunnels. Sometimes prototype turbines are installed at sea and monitored. Often a hybrid setup is used where some physical phenomena are numerically simulated and others are experimentally applied. They can be in a wind tunnel or a wave basin. These tests provide valuable data that can be used to validate numerical models.

Sometimes full-scale or lightly scaled testing is done at sea to validate the numerical models or the FOWT design [30, 31, 32]. However, this is an expensive step and the disturbances in the real world are difficult to model accurately in a numerical model, hence laboratory tests with scaled models are often preferred. The reliability of the results of these tests is important since they are used for validation. However, laboratory tests do have shortcomings in simulating the real-world environment, mostly due to the issues of scaling.

2.4.1. Scaling

The first step in any experimental testing is to create a scaled model of the FOWT. The physical substructures such as the blades, tower and floater are geometrically scaled down based on a scaling length factor. This is fairly straightforward, however, the physical aspects of wind and wave loading cannot be scaled with just geometric length scaling. A velocity scale factor is also necessary.

The aerodynamics of the system are influenced by viscous forces and are normally scaled using the Reynolds scaling laws. The hydrodynamics are mostly based on inertial loading and need to be scaled

with the Froude scaling law. This means either the Reynolds or Froude number needs to match before and after scaling. The Reynolds and Froude number expressions are given below,

$$Re = \frac{\rho v L}{\mu}, \tag{2.1}$$

$$Fr = \frac{v}{\sqrt{gL}}, \tag{2.2}$$

where ρ is the density of the fluid, v is the velocity, L is the characteristic length of the structure interacting with the fluid, μ is the dynamic viscosity and g is the gravitational acceleration. As seen from Equation 2.1 and Equation 2.2, the Reynolds number depends on the ratio of inertial and viscous forces. While the Froude number represents a ratio of inertial and gravitational forces. Since they signify different physical characteristics only one scaling law can be achieved at a time. This leads to the scaling law conflict.

Choosing the Reynolds scaling law produces correct aerodynamic loading but compromises hydrodynamic and gravitational loading and choosing Froude does the vice versa. Choosing the Reynolds scaling law is generally not done for experimental testing of FOWT due to the high velocities required for testing the scaled model. The velocity scaling factors for Reynold's and Froude's scaling are given below. From Equation 2.3, it can be seen that velocities for achieving the Reynolds scaling law for a 1:50 model scale would already be 50. This is a number that is not practical for HIL testing.

In Reynolds scaling,

$$\lambda_v = 1/\lambda_l \tag{2.3}$$

In Froude Scaling,

$$\lambda_v = \sqrt{\lambda_l} \tag{2.4}$$

Another approach that is commonly used is to decide a velocity factor that is a trade-off between both scaling laws. This scaling factor is chosen after taking into consideration the operating range of the model, the capabilities of the equipment and frequency analysis to mitigate resonance effects. This scaling method is commonly used for hybrid tests in wind tunnels where violating the Froude law has smaller consequences since the hydrodynamic and gravitational loads are simulated and not measured. Yet, since the gravitational loads are not correctly reproduced, additional correction is often needed.

Wave basin tests still commonly use the Froude scaling law to have high-fidelity hydrodynamics. This is also because the Froude scaling is easier to achieve compared to Reynolds scaling. The influence of hydrodynamic and gravitational loads on the dynamics is also considered significant for a FOWT. Thus the Froude scaling is the most popular scaling method used in laboratory tests. With the Froude scaling law the Reynolds number of the model is considerably lower thus the mismatch is high, and the performance of the turbine is not matched. With Froude scaling the velocity scale is also quite low, hence really low wind speeds need to be used. Assessing the aerodynamic effects with such low wind speeds is a hurdle faced in full physical testing.

Therefore, the choice of scaling is a significant and crucial decision in experimental testing. The choice depends on the objectives of the tests and the facilities available. Each scaling method has its advantages and limitations, and there are plenty of ideas to overcome the limitations. Some of the ideas will be discussed in later sections.

2.4.2. Performance Matching of Turbine

To match the aerodynamic performance of the rotor the C_t, C_p and the Tip Speed Ratio (TSR) need to be matched for different wind speeds. Of this, matching the C_t is the most relevant for any dynamic model, since it corresponds to the aerodynamic thrust force. This is the main aerodynamic input for the dynamics of the FOWT system.

To match the aerodynamic thrust, initial test campaigns used a pulley mechanism or thrust disks. However, these methods failed to model the aerodynamic damping caused due to the rotation of the turbine.

Gyroscopic loads and their influence on the dynamics of other DOFs such as yaw were also not modelled with this method.

Later geometry-scaled blades were used to include rotational loads. But these blades failed to match the performance of the full scale, to combat this higher wind velocities were used, and the blades were roughened at the leading edges to increase the effective wind velocity. But this resulted in a mismatch of the TSR. With a TSR mismatch the torque and the aerodynamic damping were also not accurate. Thus, the importance of performance-based scaling of the wind turbine blades was soon realized.

Performance-based scaling of the blades involves redesigning the model scale rotor blades with lower Reynolds number airfoils to match the aerodynamic performance after Froude Scaling. This showed a good matching of thrust values (C_t) and rotational speed (TSR). The blades were also able to simulate the gyroscopic effects accurately, hence the dynamics in all DOFs were satisfied. Aerodynamic damping was also achieved with these blades. However, the mass distribution of the blades and the control were still not able to match the full-scale prototype.

2.5. Physical Testing with Integrated Wind and Wave

These full physical tests were done mostly in wave basins with Froude scaling. Initial studies used thrust disks and geometry-matched blades based on Froude scaling, this shifted to performance scaling. A summary of the projects done is provided in Table 2.1 below. A summary of the relevant literature available in this field is given in this section.

Institution	Year	Project	Floater Type	Wind Turbine	Scale	Aerodynamic Equivalence
SINTEF Ocean	2006	Hywind	Spar	2 MW	1:47	Geometry-matched Blades
UC Berkeley	2009	Windfloat	Semi	5 MW	1:67	Thrust Disk
MARIN	2011/2013	DeepCwind	Spar, Semi, TLP	5 MW	1:50	Geometry-matched Blades/Performance-Matched Blades
MARIN	2014	GICON	TLP	5 MW	1:37	Performance-matched Blades
MARIN	2014	Tri-floater	Semi	5 MW	1:50	Performance-matched Blades
SJTU	2016	SJTU-S	Spar	5 MW	1:50	Geometry-matched Blades
IFREMER	2017	EOLINK	Semi	12 MW	1:50	Performance-matched Blades
DTU	2020	KIER	TLP	10 MW	1:60	Performance-matched Blades
DUT	2020	TWWC	TLP	5 MW	1:50	Performance-matched Blades
SJTU	2021	SPIC	Semi	10 MW	1:64	Performance-matched Blades
SJTU	2021	SJTU-S4	Spar	5 MW	1:50	Performance-matched Blades

Table 2.1: Representative physical model experiment projects.[33]

Cermelli and Aubault [34]describe the experimental campaign at the University of California Berkeley Ship Model Testing Facilities, where they used a 1/67 scaled model of a 5MW turbine. A thrust disk was used to model the aerodynamics. The test took place in a wave basin and the Froude scaling law was followed. The main aim of this test was to validate numerical models built in OrcaFlex. The emphasis in the test was given to studying the hydrodynamics and the mooring lines and electrical cables.

Bahramiasl, Abbaspour, and Karimirad [35]tested a 1/100 scaled model of a FOWT with TLP. The FOWT including the turbine was scaled using the Froude Scaling Law. The experiments were done in a wave basin with applied wind. The motor was controlled manually. The results were used to analyse the gyroscopic effect of the FOWT and analyse the response amplitude operator (RAO) frequencies. The gyroscopic effects of the turbine were found to have a damping effect on the floater motion, the RAOs of the floater were shifted.

Goupee et al. [36] reports the test campaign with the 1/50 scaled model of NREL 5MW FOWT as part of the DeepCWind consortium. Three different floater types were used for the tests: TLP, semi-submersible and spar buoy. The testing was done at MARIN in the Netherlands in a wind/wave basin. Froude scaling was done for the FOWT. Test cases were run for free decay and various operating conditions. The main objective was to compare the performance of the three different floater types. The tests also revealed the drawback of using geometrically scaled turbines as the aerodynamic forces were not reciprocated. [37].

Soon, the turbine was redesigned with performance-based scaling by the University of Maine. Goupee et al. [38] retested the newly scaled turbine with the floater in the wind/wave offshore basin at MARIN and concluded the benefits of having a performance-based scaling for the turbine. The data from these experiments were later used for the validation of the FAST model [39]. This turbine was also later used by Ridder et al. [40] to test the GustoMSC Tri-floater semi-submersible and a new active pitch control. The tests provided a good relation between the collected data and results from CFD simulations.

Bredmose et al. [41] used a 1:60 scaled 10MW DTU turbine with a Triple Spar floater, which is a combination of the semi-submersible and the spar type floaters. The turbine was performance-scaled and was fitted with an active blade pitch control system. The project was aimed at analysing aerodynamic damping, understanding the interaction between wind and wave forces and analysing different pitch control strategies.

Zhao et al. [42] conducted an experimental study at a deep water basin at Shanghai Jiao Tong University using the scaled WindSpar TLP system with the NREL 5MW wind turbine. A 1:50 scaling factor was taken. The performance scaling of the blades and the scaling for the overall system are explained in detail. The objective of this study was to analyse the dynamics of the system including natural periods, damping, and RAOs.

In 2018, the EOLINK concept turbine where the nacelle is connected to the floater with multiple pillars was experimentally tested in the Ifremer's ocean basin in France. For the test, a 1:50 model was developed with Froude scaling and performance-matched blades. The rotor was also equipped with pitch control[43]. Numerical models were developed by Connolly et al. [44] to validate and optimize the FOWT design.

Most of the experimental testing is now done with performance-based scaling for the turbine. This has proved to show better results than the geometry-scaled turbines, especially with matching the aerodynamic thrust. However, there are still multiple shortcomings with this approach [45].

1. Other aerodynamic forces are not represented correctly, such as torque and blade inertia.
2. Mass inconsistency is a problem since it influences the centre of gravity, the rotational loads and the control system.
3. Having wind generators in a wave basin obstructs the quality of the waves.

To overcome these problems, hybrid testing is growing as a potential method of testing with better reliability and accuracy.

2.6. Real Time Hybrid Testing

Real-time hybrid testing represents an approach where the forces/ dynamics are bifurcated into two parts. The main advantage of this method is its ability to eliminate the scaling law conflict. The first part is physically tested and the second part is numerically simulated. This is achieved with a network of sensors and actuators which detect, correct and respond in real-time. This is also called real-time HIL testing.

This type of testing originated in the civil engineering industry when they wanted to test the effect of seismic forces on structures [46]. It later grew into the offshore industry where it was used to simulate floating objects with mooring lines, where the mooring lines were numerically simulated to represent depth in wave basins[47].

Now, in the field of FOWT, there are two ways of hybrid testing. One is in a wave basin, with the physical model of the floater and mooring lines. The hydrodynamics are physically modelled using the wave basin. The second method is in a wind tunnel with a real turbine and a numerically simulated floater. The turbine and the tower are scaled-down physical models, while a numerical model is used to make a robot behave as a floater.

2.6.1. Hybrid Tests in Wave Basins

Wave basin tests require physical models of the floater and the mooring lines. The aerodynamic loads are numerically simulated and applied to the system with the help of actuators. Depending on the

wave elevation and loads, a numerical model defines the wind velocity at each particular time step and translates them into aerodynamic forces that the full-scale turbine would face. The calculated forces are then scaled down according to the Froude scaling law and applied to the system with the help of one or multiple actuators.

Several kinds of mechanical actuators have been used in past research projects, some of them are 1. Ducted Fans or Propellers, 2. Multifans or Multipropellers, 3. Cable-driven parallel manipulators (CDPM). These methods have been investigated in various research projects, and they were found to have particular strengths and weaknesses.

The ducted fan actuator was the first approach to hybrid experimental testing in wave basins. Azcona et al. [48] experimented first by using a ducted fan to apply aerodynamic forces to a 1:40 scaled model of a 6MW semi-submersible. This was done in real-time with a numerical code based on FAST. They called this the Software-in-Loop (SIL) testing. Variable thrust forces were applied to the system by adjusting the rotational speed of the fan, which was fixed in place of the turbine.

The method was also utilized in later research projects with different turbines to study the effects of non-linear hydrodynamics in low-frequency ranges[49]. Oguz et al. [50] also used this methodology to test a 1:36.67 scaled 5MW NREL reference turbine with a TLP. They found that the experimental results predicted complex behaviours better than the numerical model, but the experiment also had some discrepancies with the numerical model in other cases.

Wright et al.[51] also used the SIL methodology with a 1:30 and 1:50 scaled model of a 5MW turbine with a hexagonal TLP. The study aimed to do a comparative analysis of TLP concepts. Some other research works that used the SIL methodology are referred [52][53][54]. The research projects are summarized in Table 2.2 below. All the research concluded that having an SIL methodology is better at reproducing the aerodynamic thrust force at the model scale than otherwise.

However, since only a single fan was used, only aerodynamic thrust was reproduced correctly, and aerodynamic torque and the gyroscopic effects were ignored. Even though aerodynamic thrust is the most significant aerodynamic force, it does not allow for the full dynamic modelling of the system. To address this issue several research institutes developed SIL methodologies with multiple fans.

They often used actuators that were modelled similarly to drone technology. For example, the multi-propeller developed by Otter, Murphy, and Desmond[55]. had 6 aerial drone propellers in order to model aerodynamic forces in other DOFs. The device was proven to perform well with some DOFs but underperforms in others The multipropeller SIL methodology was also used for the validation of the FOWT concept TELWIND [56]. In 2020 the NREL 5MW wind turbine at MARIN with the DeepCWind Semi-submersible was upgraded from the ducted fan to a multi-propeller actuator with 4 fans for SIL testing [57].

Another popular approach was using cable-driven parallel manipulators (CDPM). Researchers at SINTEF, Norway developed this methodology and validated it. They named the testing methodology Real-Time Hybrid Model (ReaTHM) [58]. ReaTHM involved generally using a rectangular frame at the top of the tower which was connected to multiple winch cables, six were used in this case. The tension of the cables was adjusted to emulate the aerodynamic forces.

ReaTHM methodology was also used in projects to validate FOWT designs and study the dynamics [59, 60]. Hall and Goupee [61] used a similar methodology, but only used the winches for thrust force emulation and used a scaled rotor with wind for other forces .

A summary of all the real-time hybrid testing in wave basins is provided in the table below,

2.6.2. Hybrid Tests in Wind Tunnels

Hybrid testing in wind tunnels involves the integration of a physical model of the scaled wind turbine and an actuation system that behaves as the floater. The wind tunnel and the performance-scaled wind turbine provide good aerodynamic fidelity. A numerical model is used to model the hydrodynamics and determine the position of the floater. This kind of testing is gaining popularity since it provides good-quality aerodynamics and is a great method for testing the effects of FOWT motion on wake effects.

Table 2.2: Overview of FOWT model experiments with different actuators.

Authors/Reference	FOWT Model	Scale	Objectives
Ducted Fan Actuators			
Azcona et al.[48]	6MW- Semi-sub	1:40	Validity of SIL methodology
Oguz et al.[50]	5MW- TLP	1:36.67	TLP Design validation
Wright et al.[51]	5MW-TLP	1:30, 1:50	Effect of spring dampers
Desmond, Hinrichs, and Murphy[52]	2 rotor- Semi-sub	1:36	Uncertainty incorporating aerodynamics
Andersen[54]	5MW - fixed operation	1:60	Aerodynamic forces emulation without real-time operation
Matoug et al.[53]	10MW HAWT, VAWT - Semi-sub	1:42	Competitive study with and without SIL
Multipropeller Actuator			
Otter, Murphy, and Desmond[55]	5MW - fixed operation	1:37	Development of multi propeller
Meseguer and Guanche[62]	5MW - fixed operation	1:40	Design and validation of the multi-propeller SIL methodology
Pires et al.[57]	5MW - Semi-sub	1:50	Model improvement from ducted fan, testing control strategies
Cable-driven Actuators			
Bachynski, Chabaud, and Sauder[60]	5MW - Semi-sub	1:30	ReaTHM methodology assessment
Thys et al.[59]	10MW - Semi-sub	1:36	Dynamic analysis of FOWT
Hall and Goupee[61]	5MW - Semi-sub	1:50	Validating hybrid methodology with scaled turbine and floater

HIL tests at Politecnico di Milano

Hybrid testing in wind tunnels was introduced first by researchers in Politecnico di Milano (PoliMi), Italy. Initially, they used the DTU 10MW turbine scaled down by a factor of 1:75. The detailed methodology for scaling the rotor and matching the thrust, torque, natural frequencies of the blades and mass is reported by Bayati et al.[64]. A non-Froude scaling method was chosen, they decided the scaling factors for length and velocity based on the turbine model and the operational capabilities of the wind tunnel [63]. The turbine was designed as part of the LIFES50+ project [65].

First, a 2-DOF motion platform was created to simulate the surge and pitch motions of the floater. These motions are the most relevant since they are in the direction of the incoming wind and have the highest influence over downwind aerodynamics. A hot-wire anemometer was set up behind to measure the wind speeds in the wake. Imposed motion in surge and pitch with three different wind speeds were tested, below rated, rated and above rated. Steady wind speeds were applied with a 2% turbulence. The results showed the behaviours of wave deficit behind the turbine at different imposed motion frequencies and wind speeds [66]. An extensive analysis of the 2DOF HIL set-up and the results is done in [67].

To obtain more realistic results, a 6DOF parallel kinematics robot was designed and named the 'HexaFloat'. The robot was designed to reproduce the floater motions of a scaled FOWT in different sea states. The system was validated with results from a scaled NREL 5MW spar buoy FOWT [68]. The 'HexaFloat' is later used in HIL tests with the International Energy Association (IEA) 15MW, DTU 10MW as well as the NREL 5MW scaled rotors. The final HIL set-up can be seen in the Figure 2.2 below.

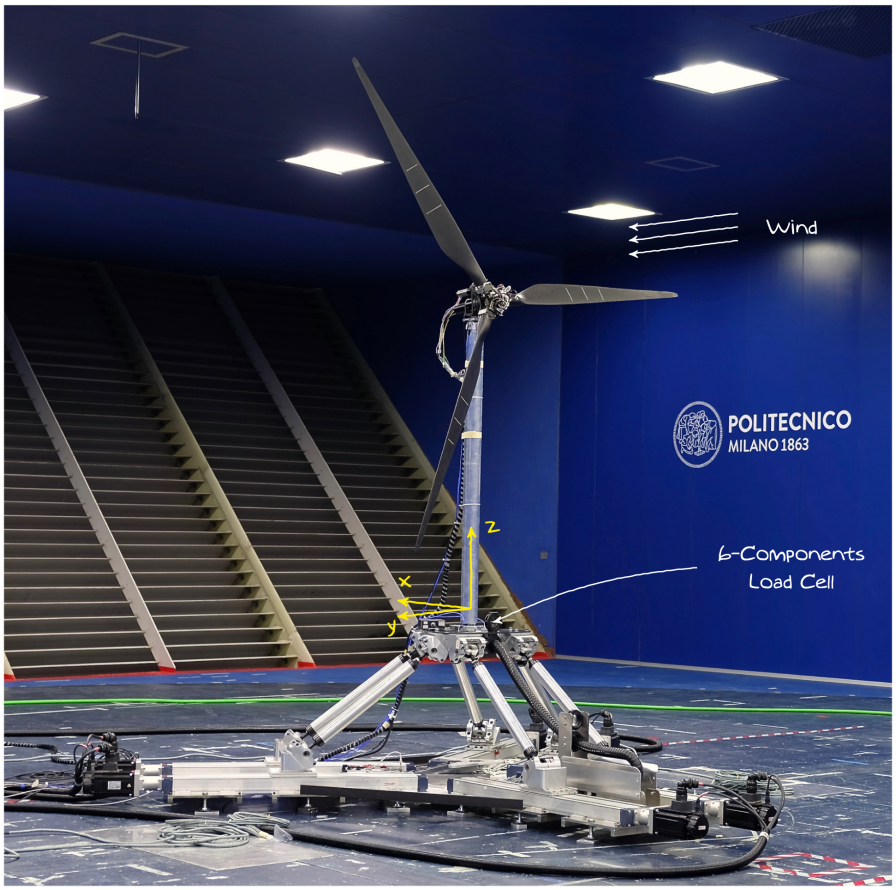

Figure 2.2: Set up of a scaled wind turbine with 6DOF 'HexaFloat' robot for HIL testing in the wind tunnel at Politecnico di Milano [69]

For a fully functioning HIL set-up, a numerical model for the hydrodynamics is also necessary. The 6DOF hydrodynamic numerical system was developed in the Simulink environment of MATLAB and deployed using a dSPACE real-time machine by Bayati et al. [70] The Cummins equation was used to model the dynamics of the floating platform as is standard in the industry. WAMIT was used to obtain the added mass, hydrostatic stiffness and damping coefficients for the equation. The external forces were divided into two parts, hydrodynamic forces and aerodynamic forces.

The hydrodynamic forces considered were, wave excitation, radiation, viscous and mooring line forces. The wave excitation forces were computed using the potential flow theory with the help of the WAMIT solver. The radiation forces were solved using a state-space implementation, also identified using WAMIT. The viscous forces were calculated using Morison's equation and a lumped mass model was used to calculate the mooring line forces.

The aerodynamic forces were measured with load cells at the top and bottom of the tower. These values were used to correct the force measurement to obtain aerodynamic effects and subtract the effects of inertia and mass of the rotor and nacelle. The detailed methodology of design and optimization of the real-time numerical model is provided in [70].

A critical overview of the HIL testing methodology with the scaled turbine and the HexaFloat is presented in [71]. The methodology is further used in testing the 10MW DTU wind turbine model with 1:75 length scaling and 1:3 velocity scale with a Triple Spar floater[70]. It is also further tested with the OO-Star Wind Floater, a semi-submersible floater and the Nautilus floater with the same turbine model [69, 72]. This is part of the project in partnership with SINTEF. The FOWT models were tested in the wave basin in SINTEF, Norway and the results were compared [72].

Recently, an upgrade from a 10MW wind turbine to a 15MW turbine was made, including improvements

to the HIL methodology by Fontanella, Facchinetti, and Belloli. The IEA 15MW turbine model was used along with the Activefloat semi-submersible floater design. The scaling factors chosen for length are 1:100 and the velocity scale factor was set at 1:4, as this was the most optimal value for reproducing the aerodynamic effects in the Politecnico di Milano wind tunnel [73].

Other Recent Research

In 2014, Rockel et al. [74] used an innovative method of testing FOWTs, by installing a 1:400 performance-scaled wind turbine on a rotating gimbal to emulate the floating motion. The setup was tested in wind tunnels. The effects of pitch motion on the wakes were studied in this experiment . Another researcher used a 1:500 scaled model of a 2MW wind turbine with a FLOATGEN FOWT and tested it in a wind tunnel. Only surge motion was applied to the FOWT and the rotor was replaced with a porous disk. Studying the wake characteristics under surge motion was the main aim of this project as well [75]

In 2023, HIL wind tunnel tests were held in the OJF at TU Delft by Taruffi et al. [76]. The HIL set-up consisted of a 6DOF parallel kinematics robot and a 1:148 performance-scaled DTU 10MW wind turbine. First imposed motion cases in surge, sway and pitch were done to study the thrust load variation in different scenarios and for system identification. Unsteady aerodynamic effects were observed and the thrust variation at higher frequencies did not match with the quasi-static numerical model.

A numerical model to simulate the hydrodynamics was also developed in Simulink and run with the dSPACE real-time machine which sends signals to control the 6DOF robot. Force and motion sensors were used as feedback to the dynamic system. The TripleSpar floater design was numerically modelled and coupled with the scaled DTU 10MW turbine. The numerical model was developed only for a 3DOF system with surge, pitch and heave, which are the dominant motions observed in aligned wind and wave scenarios [76]. More detailed explanations about the experimental HIL tests at TU Delft will be provided in the subsequent chapters.

3

Setup

This chapter covers the setup for Hardware-in-Loop wind tunnel testing and describes each entity in detail. It starts with the experimental setup which involves the wind tunnel, the scaled rotor, the 6DOF robot, the test instrumentation system and most importantly the numerical model for simulating the hydrodynamics. Another setup is used for verifying and validating the numerical model, and the HIL model's floating motion response. The engineering tool FAST/OpenFAST is used for this purpose since it is a well-researched and validated open-source numerical code.

The experimental setup is described in section 3.1. In this section, all the necessary hardware is listed and explained. As the work of this thesis is a continuation of previously done experiments, the details are kept short. For further information, the referenced document can be consulted [76]. The numerical model that simulates the floating dynamics is a crucial part, this is discussed in detail in the next chapter. Lastly, section 3.2 introduced the FAST/OpenFAST setup for tuning and validation purposes.

3.1. Experimental Setup

The experimental setup for Hardware-in-Loop testing typically involves a scaled wind turbine model with aerodynamic performance matching, a wind tunnel facility, a motion platform or a robot that can impose motions on the turbine, and an instrumentation system. As discussed in the previous section, the physical set-up for the hybrid experimental testing has already been established in previous works by Taruffi et al.[76] who held an experimental campaign to access and validate the setup and collect data. Another test campaign took place in November 2023 with the same set-up but with the addition of the 3DOF numerical model for simulating the hydrodynamics. Particle Image Velocimetry (PIV) was also done for studying the wake effects. At the time of writing this report, the results of this test campaign have not been published yet.

3.1.1. Wind Tunnel

For the experiment, the OJF is used to reproduce aerodynamic loads on the scaled wind turbine. The OJF is a low-speed wind tunnel at TU Delft, it has a huge fan that is powered by a 500kW motor. The created wind flow is conditioned with two diffusers. After this, the flow is passed through a settling chamber which reduces the turbulence and sharp velocity gradients. There is also a radiator-based cooling system that maintains the temperature [77]. An assessment of the quality of wind in the tunnel is done by Lignarolo et al.[78], who confirms quality wind with low turbulence levels around 0.5% near the nozzle and less than 2% 6m away from the nozzle. The nozzle is octagonal with dimensions 2.85m×2.85m. The uniform speeds in the wind tunnel are measured by a pitot tube.

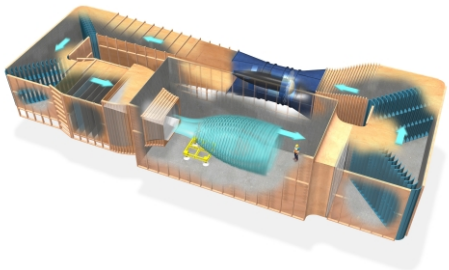

Figure 3.1: OJF schematic [77]

3.1.2. Hexapod

To reproduce the floating motions a 6DOF parallel kinematics robot is used, also commonly referred to as the 'Hexapod' due to its ability to impose motion in six degrees of freedom. The Hexapod used for this setup is a commercial parallel manipulator called the Quanser Hexapod [79]. It has the ability to manage payloads up to 100kg. The maximum bandwidth of the hexapod is 15Hz with no payloads and small displacements. Its workspace is limited to around ± 10cm for surge and sway motions and ± 5cm for heave. The rotational limits are around 15°to 25°. Row and Pitch motions have lower ranger compared to Yaw. Limitations also exist in velocity and acceleration [80].

However, with a rotating turbine as the payload, the workspace and the maximum frequency are reduced. An assessment was made in April 2023 before the HIL test campaign at the OJF. The revised frequency limitation with the rotating turbine at rated wind speeds is 5Hz. The imposed motion limits were also tested and the maximum amplitude for translation at low frequency was found to be 75mm and 10mm for the maximum frequency. The rotational constraints are from 10°amplitudes for low frequency and 1°for maximum frequency [76].

3.1.3. Instrumentation

The instrumentation involves all the sensors used for measurement, the data acquisition (DAQ) system, and control and monitoring systems. For measurement, load cells and accelerometers are installed on the turbine itself. One load cell is placed on top of the tower, directly beneath the nacelle. This load cell measures the forces and torques on the rotor such as loading due to turbine rotation, incoming wind, and inertial and gravitational loads. The load cell used is a 6-component load cell, so the output signal from the sensors includes the forces and moments corresponding to the six degrees of freedom. A calibration device is used to condition the signals.

There are two accelerometers on the turbine, one is placed on top of the nacelle and the other one at the bottom of the tower. These are MEMS (Microelectromechanical Systems) triaxial accelerometers, so they output only translational acceleration. These accelerometers are used for motion tracking as well as for correction in the numerical model. There is an encoder in the motor of the wind turbine which measures the rotational speed and current produced. The current values can be used to calculate the torque, but they would not be the most accurate because the current constantly fluctuates. The Hexapod also measures the actual position.

Apart from this the electric motor used to operate the turbine, the gearbox and the breaking resistor are also part of the instrumentation setup. The motor used is powered by a DC power input. The turbine operates at a fixed rotational speed and has no torque control. This could be developed in future works. The motor is equipped with a gearbox with a transmission ratio of 5.8:1. At higher wind speeds, the turbine produces current, and an extra unit to dissipate this produced electricity is necessary for the operation. A breaking resistor is used for this purpose, it dissipates the excess electricity as heat. The power source for the rotor and the sensors is DC at a fixed voltage of 24V.

A crucial component of the system is the dSPACE, which is a real-time machine that manages all the signals from the measurement devices, the control system, the motor in the wind turbine, and the actuation system (Hexapod). This is the device that runs the numerical simulation for the floater dynamics and sends the output signals to the hexapod. The dSPACE acquires all the measurement signals with the same sampling frequency of 1000Hz. The sampling frequency is fixed for the unit and is what determines the time step for the numerical model's simulation. The dSPACE is equipped with a Human Machine Interface (HMI) which can be used to send commands to the turbine and the Hexapod. The dSPACE is also the main data acquisition system for the experimental tests. The data/signals can also be visualized in real-time by the HMI setup, which makes the operation easier.

All the functions of the dSPACE are achieved with the help of a Simulink program that manages the input and output signals, the HIL numerical model, and data acquisition. This program also controls the commands to the hexapod and the turbine. The schematic of the simulink program can be visualized in Figure 3.2. The HMI setup is a user-friendly interface that is connected to the Simulink program for easier control.

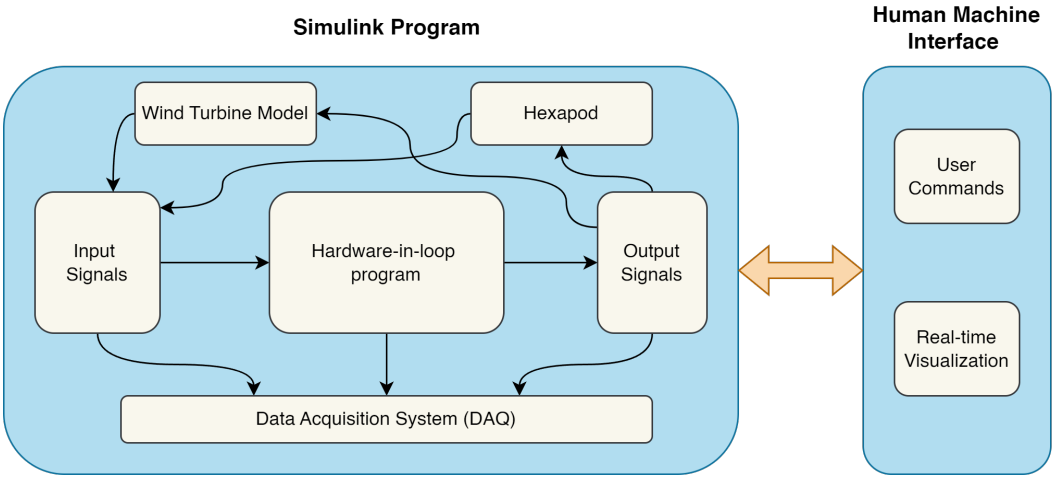

Figure 3.2: Schematic of the Simulink program and the HMI

3.1.4. Scaled Physical Wind Turbine Model

The wind turbine model used for the setup is a scaled-down version of the DTU10MW reference wind turbine [81]. This wind turbine design can be coupled with the TripleSpar floater which was developed as part of the LIFES50+ project [82]. But for the scaled model only the wind turbine is of relevance since the floater is numerically simulated. The main emphasis of the hybrid tests in wind tunnels is to test the aerodynamics of a FOWT. To achieve the best reproduction of aerodynamic loads, Reynold's scaling law needs to be followed. But, this results in very high wind speeds that are outside the capability of most wind tunnels. Hence, a new scaling approach was taken where the length and velocity factors were determined empirically, based on the capabilities of the wind tunnel at Politecnico di Milano and the selected wind turbine model. More details of the scaling methodology taken are described in [63].

The scaling factors decided for the wind turbine model were 1:148 for the length and 1:3 for the velocity factor. These factors are in the ratio model scale/full scale. The other necessary scaling factors for the HIL tests are determined by dimensional analysis. The results of this are summarized in the Table 3.1. As seen from the table, neither the Froude nor the Reynold's number is matched with the full scale. The selection of the factors is a tradeoff between Froude and Reynold's scaling law. More details about this are described in subsection 2.4.1 With the decided scaling factors, Reynolds number at the model scale is lower than 100k while the full-scale wind turbine model experiences Reynolds numbers around 1.5×10^7. Hence, to match the aerodynamic performance, low Reynolds number airfoils need to be chosen for the scaled wind turbine.

Quantity	Expression	Value
Length	λ_l	$1/148$
Velocity	λ_v	$1/3$
Mass	$\lambda_m = \lambda_l^3$	$1/148^3$
Time	$\lambda_t = \lambda_l/\lambda_v$	$3/148$
Frequency	$\lambda_\omega = \lambda_v/\lambda_l$	$148/3$
Acceleration	$\lambda_a = \lambda_v/\lambda_t$	$148/3^2$
Force	$\lambda_F = \lambda_m\lambda_a$	$1/444^2$
Reynolds number	$\lambda_v\lambda_l$	$1/444$
Froude number	$\lambda_v/\sqrt{\lambda_l}$	$\sqrt{148}/3$

Table 3.1: Scaling Factors of the model DTU10MW for HIL testing are provided in the format of model scale/full scale. Modified from [69]

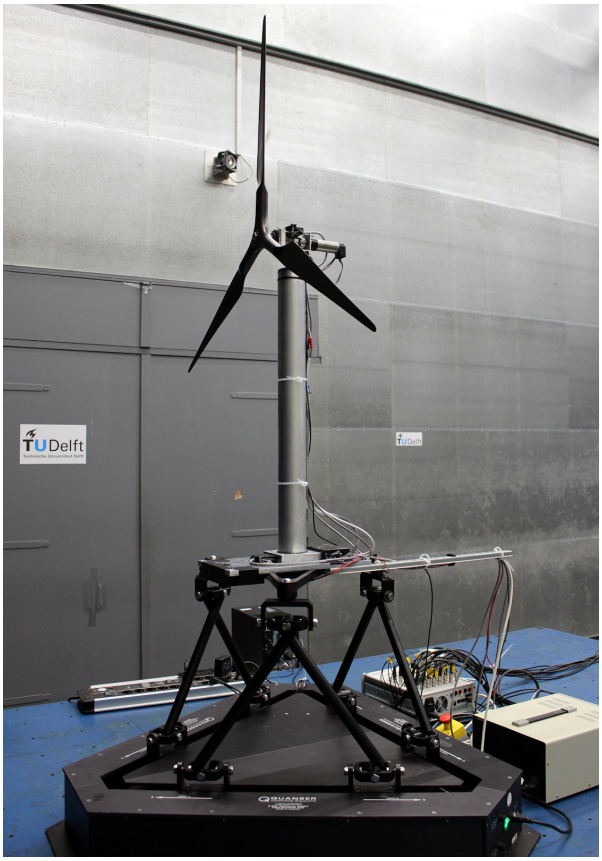

Figure 3.3: Scaled Wind Turbine Model

A detailed analysis of the design of the aerodynamic performance-matched blades for the scaled wind turbine is done by A. Fontanella et al. [83]. The chosen low-Reynolds number airfoil for the model wind turbine is SD7032, its lift (C_l) and drag (C_d) coefficients at the low Reynolds number experienced by the model match those of the full-scale model at a higher Reynolds number. They also designed a FAST model with the polars of the blade to numerically test and validate the aerodynamic performance of the scaled wind turbine. After this, the aerodynamic thrust, power and torque at different operating points of the wind turbine were tested and validated. Matching the aerodynamic performance with the designed wind turbine was possible with the chosen length and velocity factors. Although, the velocity factor has the freedom to be adjusted between 1:2 and 1:3 and still reproduce the aerodynamic performance with good results.

With the scaling factors decided, the resulting built wind turbine model had a diameter of 1.2m and a tower height of 0.8m. A general comparison of the important characteristics of the model scaled and the full-scale turbine is provided in Table 3.2. The rotor of the wind turbine is moulded with carbon fibre layers glued with epoxy resin. Hence, the blades are fixed and there is no pitch control, they are at a static pitch of 0°. This rotor is attached to a nacelle with a motor and a gearbox through the means of an Oldham joint. The nacelle weighs about 1.03kg and the rotor weighs about 0.58kg. They are connected to the tower which is made of a stiff cylindrical aluminium block. The setup can be visualized better with Figure 3.4. The tower has been made stiff to avoid the 1P and 3P frequencies of the rotor and the natural frequencies of the floater motion. The fore-aft natural frequency of the designed tower is 12.5Hz, which is well out of range [76].

In the previous test campaigns, the setup for the HIL testing with the scaled wind turbine model was tested and validated [76]. Static tests were done with just wind and rotor operation to assess the aerodynamic performance of the wind turbine. This was done multiple times for better accuracy and reliability. The performance of the wind turbine was validated by matching the performance curves of the scaled wind turbine model with the steady-state simulation results from FAST. This is also compared

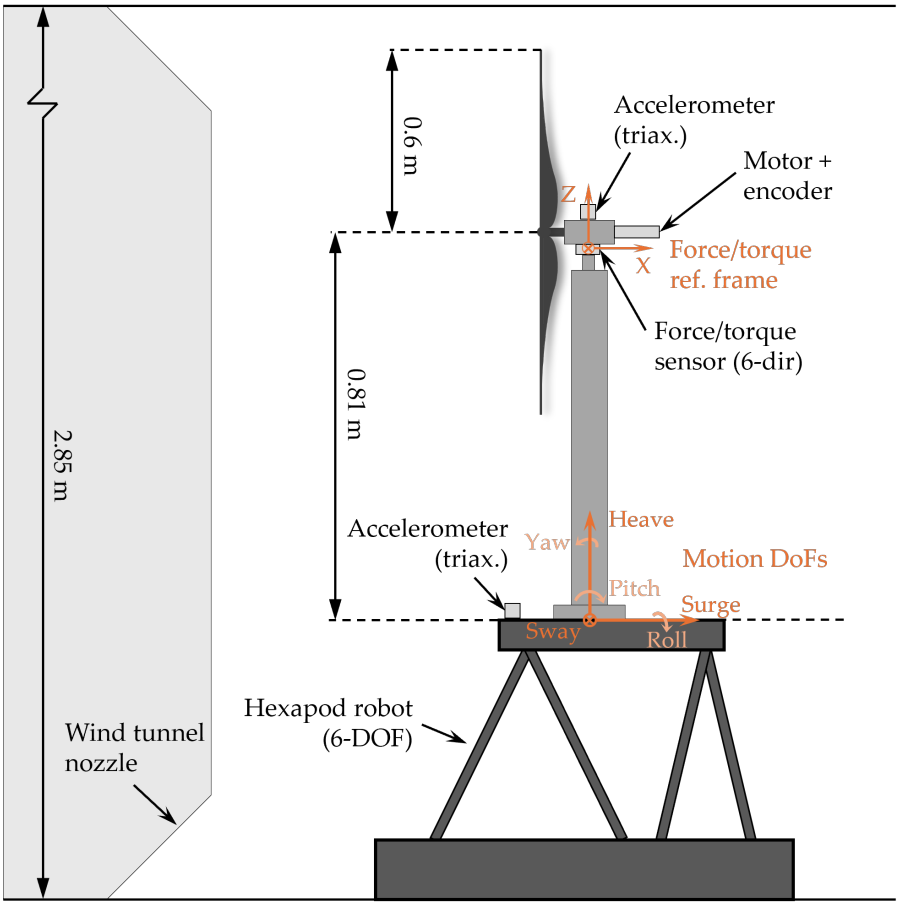

Figure 3.4: Diagram of the experimental setup with dimensions [76]

with the values from the documentation of the reference turbine. However, tests with this model can only be reproduced for below-rated and rated conditions due to the lack of pitch control. There is also no torque control and the rotational speed of the rotor is controlled by the motor at user-determined speeds. Rotor torque, power and TSR comparisons were also done. However, complete performance matching was not achieved for the other parameters, and a margin or error exists. The results of the test can be visualized with the comparison plot in Figure 3.5.

3.2. Verification and Validation Setup

Validation of the developed model is necessary to assess its accuracy. The open-source, fully coupled, multi-fidelity dynamic solver OpenFAST/ FAST [14] is used to validate the results from the experiment and the numerical dynamics model. This engineering tool was developed by researchers at NREL (National Renewable Energy Laboratory) and extensively tested and validated with measured data from experimental tests. It is also the most widely used validation tool for newly developed numerical models among researchers.

OpenFAST functions through the use of multiple modules that separately calculate the different dynamics involved with the floating wind turbine. This is done in a coupled manner with information exchange between the modules. This engineering tool simulates the dynamics in the time domain and has options to choose the fidelity. For example, the mooring dynamics can be simulated dynamically with a lumped mass system or quasi-statically using the Mooring Analysis Program (MAP). There are also options within OpenFAST to turn off certain degrees of freedom and the use of modules, these options are useful to assess specific dynamics such as floater decays or rotor performance. The different modules within OpenFAST and their primary objectives are listed below,

Parameter	Full Scale	Model Scale	Units
Rotor Diameter	178.3	1.2	m
Cut-in Speed	4	1.33	m/s
Rated Speed	11.4	3.8	m/s
Cut-Out Speed	25	8.33	m/s
Minimum Rotor Speed	6	296	rpm
Maximum Rotor Speed	9.6	473.6	rpm
Rated Thrust	1619	0.012	kN
Rated Torque	10738	0.529	kNm

Table 3.2: Main characteristics comparison between full-scale DTU10MW reference turbine and the model-scale wind turbine [76]

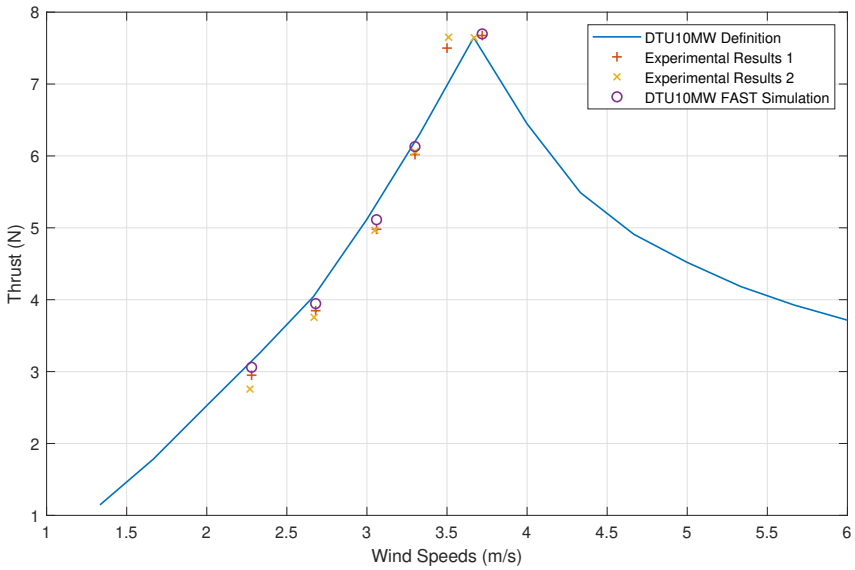

Figure 3.5: Thrust curve comparison between the DTU 10MW reference turbine and the scaled wind turbine model. Modified from [76]

- InflowWind - simulates incoming wind
- Aerodyn - simulating the aerodynamics of the turbine.
- Moordyn - simulates the mooring dynamics of the floater as a lumped mass system. MAP is a lower fidelity quasi-static method of simulating the mooring line dynamics.
- Servodyn - simulates the control dynamics of the FOWT
- Hydrodyn - simulates the hydrodynamic forces and platform motion depending on the given met-ocean conditions.
- Elastodyn - simulates the structural dynamics of the whole system depending on the initial conditions and constraints. Separate subdivisions exist to simulate the dynamics of the tower and the blades.

Recent work in the research community of FOWT is getting oriented towards bigger turbines since this is the best way to reduce the levelised cost of electricity (LCOE). This trend is also followed in the industry, for example, the 14MW GE-Halide-X offshore wind turbines are being installed in 2021,

whereas 6.2MW turbines were the standard in 2018. The IEA15MW wind turbine [84] is the ideal open-source reference offshore wind turbine for understanding, specific design elements and the physics of bigger FOWTs. This wind turbine was designed in 2020 by a collaboration of researchers from NREL, DTU and the University of Maine, this was part of the IEA wind task 37.

3.2.1. Adapting to IEA15MW and VolturnUS

The IEA 15MW wind turbine is a 3-bladed IEC Class 1B direct drive turbine with a 240m rotor diameter and 150m hub height. It was originally designed as a bottom fixed monopile offshore wind turbine, however it is adaptable for floating applications. The VolturnUS floater was developed for this purpose by the University of Maine and NREL as an addendum to the IEA task 37. The tower of the reference wind turbine was modified for floating purposes to be stiffer and slightly shorter. The floater itself is a steel semi-submersible floater with 4 buoyant columns with one column placed in the centre, on top of which the tower is installed. The structure is kept in place with three catenary mooring lines. A diagram of the design with the coordinate system can be visualized in Figure 3.6.

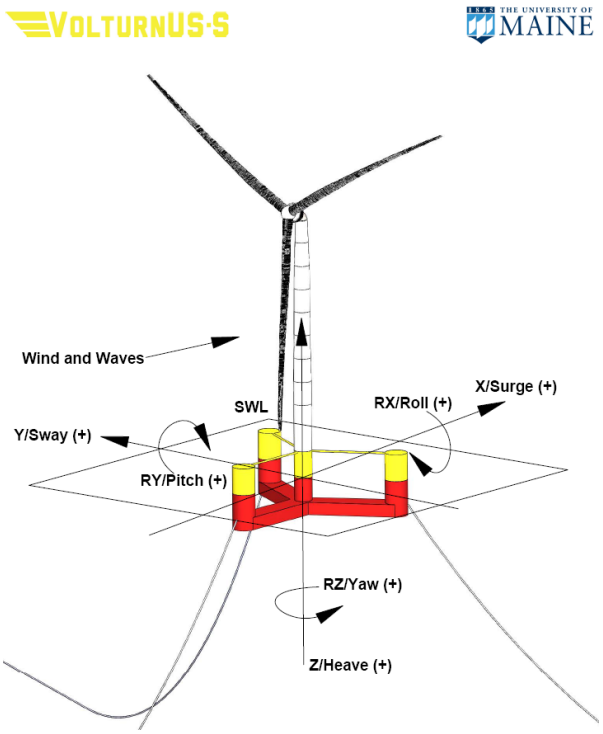

Figure 3.6: Sketch of the IEA15MW reference wind turbine with the VolturnUS semi-submersible floater [13]

Technically, it is possible to represent the IEA15MW wind turbine with the model wind turbine described in subsection 3.1.4 if the performance of the model turbine matches the full-scale reference turbine. The series of airfoils used in the IEA15MW wind turbine is the DTU FFA-W3 airfoil series, and this is the same series of airfoils used for the design of the DTU10MW wind turbine. The airfoil data for both wind turbines were also tested at 10^7 Reynolds number using 2D CFD simulations and adjusted. A table with the main characteristics of the IEA15MW is provided in Table 3.3. Despite the similarities, there are differences in the geometry involving, the length, chord and twist distribution of the blades. Thus simulations are necessary to check for performance matching.

3.2.2. OpenFAST Model: IEA15MW with VolturnUS

An aerodynamic code is needed to check the aerodynamic performance of the wind turbine and compare it with that of the model wind turbine. As part of the IEA task 37, an OpenFAST model of the reference wind turbine and the floater was also created [13]. The OpenFAST model of the reference wind turbine with the semi-submersible floater was installed successfully with OpenFAST version 3.5.1. It includes all the relevant modules to simulate a fully coupled floating wind turbine.

Parameter	Value	Units
Power Rating	15	MW
Cut-in Wind Speed	3	m/s
Rated wind speed	10.59	m/s
Cut-out wind speed	25	m/s
Rotor Diameter	240	m
Hub Height	150	m
Design TSR	9.0	-
Minimum Rotor Speed	5	rpm
Maximum Rotor Speed	7.56	rpm
RNA mass	1017	kg
Tower mass	860	kg

Table 3.3: Main Characteristics of IEA15MW wind turbine [84]

The OpenFAST model is run first and the results are compared by matching the results from the simulation with the documentation. First, the aerodynamic performance of the turbine is compared. The necessary modules for this are the InflowWind, Aerodyn and the Elastodyn module. The degrees of freedom of the platform the tower and the generator are restricted for this simulation. Steady-state simulations are run in OpenFAST with different operating conditions, the performance values and coefficient obtained are then matched with values from the documentation. The relevant performance metrics are the aerodynamic thrust, torque and power values and C_p and C_t values at rated conditions.

For the simulation, a MATLAB script is used to run OpenFAST. The operating points were chosen in the below rated region with the final operating point being the rated condition. The rated condition is the most important for validating the OpenFAST model. For comparing these values with the wind turbine model, only below-rated conditions are relevant due to the lack of pitch control. Since the pitch is set at 0, in the wind turbine model, conditions above rated wind speed cannot be accurately simulated in the experiment. A uniform wind speed is applied in the simulation and the rotational speed for that wind speed is set based on the values from documentation, which identifies the rotational speed through the design TSR (= 9).

$$TSR = \omega R/v \tag{3.1}$$

, where ω is the rotational speed (rad/s), R is the rotor radius (m) and v is the incoming velocity (m/s). The results from the simulation are compared with the results from the documentation. These can be visualized in the Figure 3.7. The design C_p and C_t values from the simulations were 0.49 and 0.80, which matched the values from the documentation.

Simulating the floater and the hydrodynamics in OpenFAST is done mainly in the Hydrodyn and the Elastodyn module, where all the hydrodynamics is handled by Hydrodyn and the hydrostatics and structural dynamics of the floater are handled by the Elastodyn module. The mooring line dynamics are handled by the MoorDyn module. The hydrodynamic model of the OpenFAST model is validated by doing rigid body-free decay simulations to match the natural frequency and the damping ratio with the definition. The results of the natural frequency comparison are provided in Figure 3.8

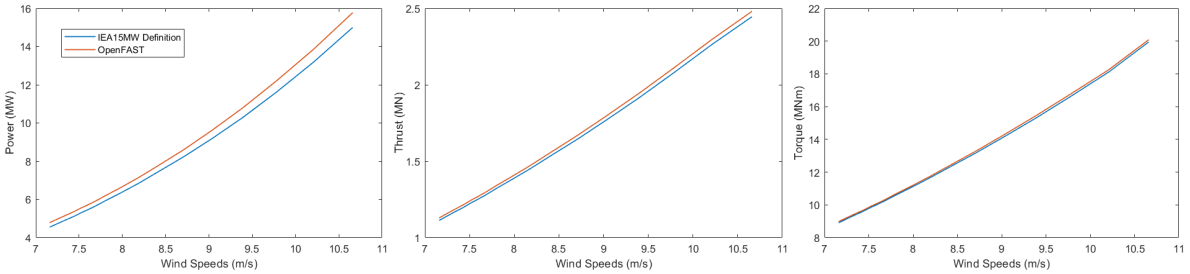

Figure 3.7: Comparision between results from OpenFAST and values from the documentation. From left to right, power, thrust and torque values are compared.

DOF	OpenFAST	Definition
Surge	0.007	0.007
Sway	0.007	0.007
Heave	0.048	0.049
Roll	0.035	0.036
Pitch	0.035	0.036
Yaw	0.011	0.011

Table 3.4: Natural frequency comparison for VolturnUS between OpenFAST setup and documentation

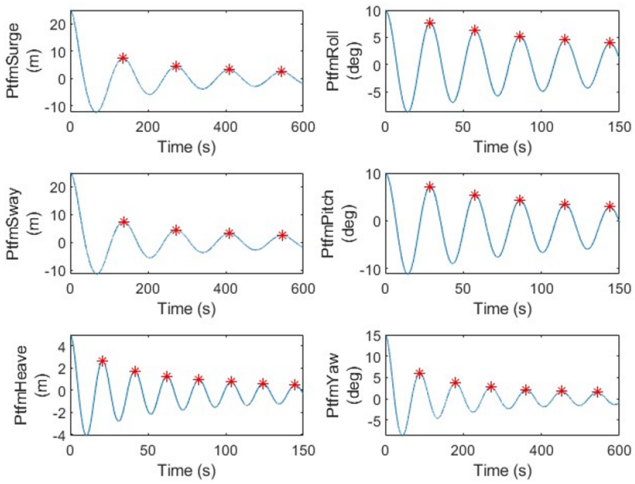

Figure 3.8: Decay test for VolturnUS simulated in OpenFAST

3.2.3. OpenFAST Model: TU Delft Wind Turbine Model

The aerodynamic design of the wind turbine model was done by Fontanella et al. [83] as described in the previous section. They also created a numerical model for the turbine design in FAST using the Aerodyn module. This included the polars of the blades designed so that the aerodynamics of the rotor could be numerically modelled. This model was built in Aerodyn14 with FAST v8. This was updated to a newer version of OpenFAST for this project, mainly for consistency reasons.

The OpenFAST model of the TU Delft Wind Turbine Model, which we will call TUD-WTM hereafter, was

validated with previously recorded performance values and from the experiment values from previous test campaigns [76]. The two main operating points of the wind turbine model were below-rated and at-rated conditions. The velocities were determined using the scaling factors for the DTU 10MW reference model, the two speeds were chosen as 2.5m/s and 4m/s, and the rotational speed was determined using the TSR (Equation 3.1). The design TSR for the DTU 10MW reference wind turbine is 7.5.

The values for the thrust and power obtained with the OpenFAST model are listed in Table **??**. These values are the same as the results from the FAST model used for previous tests. The experiment results also provide values that match the thrust values from OpenFAST. The power values from the experiment are lower than the power estimated by OpenFAST, this is expected since the scaling of the WTM is done mainly to match the thrust and not the power.

Wind Speed (m/s)	Rotational speed (rpm)	Thrust (N)	Power (W)
2.5	300	3.4517	0.8565
3.8	480	8.5056	9.017
4	480	9.0895	11.9858
4.3	480	9.9267	16.3568

Table 3.5: Wind Turbine Model Performance Values from OpenFAST model

3.2.4. Scaling

Before checking for aerodynamic performance matching between the wind turbine model and the IEA15MW reference wind turbine, the reference turbine needs to be scaled down to match the dimensions of the wind turbine model. The length scaling factor can be easily determined by comparing the rotor diameters. However, additional steps are necessary for determining the velocity factor. Having a lower velocity factor results in a lower Reynolds mismatch and a better thrust force reproduction. However, it also increases the rotational speed of the wind turbine which pushes the safe operating range of the rotor.

The length scaling factor (λ_l) is fixed at 1:199 (rounded up from 1:199.17) since that is the ratio of the rotor diameters. The velocity scaling factor (λ_v) was chosen to have a smaller denominator than the λ_v used for the DTU10MW scaling because the λ_l for the IEA15MW is larger. This follows the reasoning of having a low Reynold's mismatch value. As seen in Table 3.1 the scaling factor of the Reynolds number is a multiplication of the length and velocity scales. For the DTU10MW, this value was 1:444. The scaling factor of the Reynolds number is also referred to as the Reynolds mismatch. If the same λ_v is used then the Reynolds mismatch increases to almost 1:600. Hence a range of values for λ_v between 1:2.5 and 1:3 is tested.

The parameters to check for verifying the scaling are the scaling factors used in Table 3.1 and the cut in wind speed, rated wind speed, maximum rotational speed of the rotor, rated thrust and power. The scaled natural frequencies of the floater and the maximum displacement, velocity and acceleration in all DOFs for the wave cases were also tested to make sure they were within the capability of the Hexapod. Priority was given to having a high enough rated thrust since the loadcell has a higher difficulty sensing the aerodynamic thrust force. The rotational speeds of the rotor are also taken into consideration since there is a limit to the maximum speed on the rotor and also to avoid resonance with the stiff aluminium tower. The tower has a natural frequency of 12.5Hz [76], this results in a resonance at 750RPM for the rotor. The maximum rotor speed limit is fixed at 650 RPM to avoid this.

The numerically scaled factors and the operating parameters were first identified. The promising velocity factors were used in the OpenFAST wind turbine model and the resulting thrust values were compared with the scaling values from the full-scale IEA15MW OpenFAST results. The thrust force experienced in the bottom of the tower is compared since the thrust on the rotor is perpendicular to the plane of the rotor and not on the x-axis due to the rotor tilt angle. The WTM has no tilt, hence to avoid confusion the tower base values are selected since they represent the thrust force experienced at the

inertial x-axis. Error percentages were found to be around 15% between the OpenFAST models. To further access the scaling, the floater was scaled next.

The natural frequencies of the floater were scaled using dimensional analysis with the different velocity scale factors and the length scale. The natural frequencies for all the DOFs of the floater were within range. Heave has the highest natural frequency, between 3.2Hz and 3.5Hz for the range of velocity factors tested. Following this, different sea states were simulated in OpenFAST based on values from the documentation. The maximum displacement, velocity and acceleration in all the degrees of motion are identified for all DOFs.

Quantity	**Expression**	**Value**
Length	λ_l	$1/199$
Velocity	λ_v	$1/2.5$
Mass	$\lambda_m = \lambda_l^3$	$1/199^3$
Time	$\lambda_t = \lambda_l/\lambda_v$	$2.5/199$
Frequency	$\lambda_\omega = \lambda_v/\lambda_l$	$199/2.5$
Acceleration	$\lambda_a = \lambda_v/\lambda_t$	$199/2.5^2$
Force	$\lambda_F = \lambda_m\lambda_a$	$1/497.5^2$
Reynolds number	$\lambda_v\lambda_l$	$1/497.5$
Froude number	$\lambda_v/\sqrt{\lambda_l}$	$\sqrt{199}/2.5$

Table 3.6: Scaling Factors of the model IEA15MW for HIL testing.

These extremums were scaled down for all velocity scale factors. The maximum velocity and acceleration limits of the Hexapod are $0.67m/s$ and $9.8m/s^2$ respectively [80]. The displacements and frequency were well within the limits of the Hexapod. The velocity in all DOFs was also within the limits. The acceleration in rougher sea states was out of limits for smaller velocity scale factors. However, the sea-states with wind speeds up to rated were operable with the whole range of scaling factors chosen. Hence, the choice of scaling was left to the factor which produced the best aerodynamic thrust and the least Reynolds mismatch. This was the velocity factor of 1:2.5. The table with all the scaling factors and the significant parameters is given in the Table 3.6.

4

Numerical Modelling

This chapter describes the methodology for modelling the dynamics of the FOWT for HIL testing in wind tunnels. It begins with the description of the numerical model and later the force correction methodology is explained. It starts with section 4.1 that describes the equation of motion and the general coordinate system. This is followed by section 4.2 that details the methodology followed in the HIL numerical model. Later the different dynamic effects are discussed starting with hydrodynamics in section 4.3 which explains the modelling of the radiation and diffraction forces. Then mooring line loads are discussed in section 4.4 followed by the stiffness and damping terms in section 4.5 and section 4.6 describes the overall dynamics which couples all the various dynamic effects together in the same system. The specifics of modelling the various dynamics involved are discussed for both the chosen FOWT designs.

The aerodynamic forces and the correction methodology followed are discussed in the subsequent sections. The section 4.7 discusses the necessity for having a force correction module. The section 4.8 details the rotational transformation matrix that allows the switching between fixed and rotating reference frames. section 4.9 explains thoroughly the theoretical force and acceleration measurements that lay the foundation for determining the correction term. Finally section 4.10 lists the correction terms and discusses the transformation to derive the final aerodynamic forces.

4.1. FOWT Motion Response

The motion response of the FOWT is determined by solving the equations of motion. For FOWT, this is commonly done with a derived version of the Cummins equation [85], which models the complete dynamics of the floater as a damped spring-mass system approximately with external forces which are generally determined by aerodynamics and hydrodynamics. The Cummins equation is generally taken as the equation of motion for floating objects in the field of offshore engineering, this is represented as,

$$(M + A)\ddot{x} + R\dot{x} + R_2\dot{x}^2 + Kx = F_{\text{external}} \tag{4.1}$$

$$F_{\text{external}} = F_{\text{hydro}} + F_{\text{aero}} \tag{4.2}$$

where, M is the mass matrix , A is the added mass, R is the linear damping, R_2 is the quadratic damping, K is the stiffness and x is the position vector, $\dot{x}$ is the velocity vector, and $\ddot{x}$ is the acceleration vector. F_{external} includes all the external forces acting on the system. F_{hydro} is the external force due to hydrodynamics and F_{aero} is the loading experiences from the aerodynamics. All the terms in the equation of motion are represented as 6×6 matrices since they are modelled as a 6DOF system.

Other sources of loading such as gravitational loads, viscous forces, hydrostatics, or mooring line dynamics are added as part of the stiffness, damping or mass terms in the system. For the scope of HIL modelling, the aerodynamics is physically simulated with the wind tunnel. The aerodynamic forces on the rotor can be measured with the help of a load cell on top of the tower. The external force then

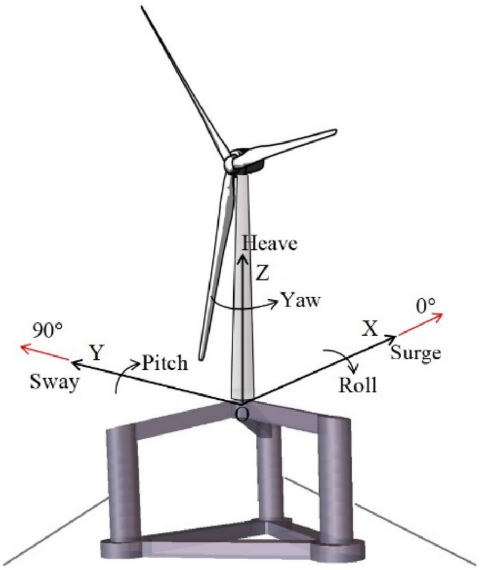

Figure 4.1: Coordinate System of a FOWT with degrees of freedom [86]

consists of the measured aerodynamic force and the simulated hydrodynamic forces. The measured forces need to be corrected before addition.

The definition of the coordinate system is crucial for solving the dynamics. The origin of the floating wind turbine is often fixed at the point exactly at the SWL height and at the mean of the floating platform. This point is commonly in the tower. The six degrees of motion of a FOWT are surge, sway, and heave in the translational directions and roll, pitch and yaw in the rotational directions. This can be better visualized by the Figure 4.1. This can be defined as the fixed reference frame or the inertial reference. The reference frame that moves along with the FOWT motions is defined as the rotating frame or the body-fixed frame.

With these extra degrees of motion, it becomes imperative to take into account the resultant position (x), velocity ($\dot{x}$) and acceleration ($\ddot{x}$) vectors, since they drastically differ from bottom fixed turbines. The positions in surge, sway and heave are taken as X, Y and Z. The rotational positions are referred to as ϕ, θ, and ψ as the roll, pitch and yaw angles respectively. This can be used to define the position vector as follows,

$$x = \begin{bmatrix} X \\ Y \\ Z \\ \phi \\ \theta \\ \psi \end{bmatrix} \tag{4.3}$$

To handle the dynamics in 6DOF, converting from a fixed reference frame to a rotating reference frame and vice-versa is necessary. This can be done by assuming the rotational angles as Euler angles or taking small angle approximations. The latter is done in the FAST (now OpenFAST) model. However, the FAST model also takes extra steps to ensure the orthogonality of the rotational matrices. This was later validated with the numerical model ADAMS which uses Euler angles [87].

In this project, the coefficients for all the hydrodynamic and hydrostatic effects used in the HIL model are obtained from the BEM solver WAMIT, which provides the coefficients in the fixed reference frame

hence no transformations are necessary and the dynamics can be solved directly. However, the force measurements are used to solve for the aerodynamics which requires transformation. The Euler angles are used for this transformation.

4.2. Simulink HIL model

The numerical model for simulating the dynamics is run with the help of MATLAB's Simulink environment. The timestep for the model is defined by the real-time machine dSPACE, described in the previous chapter. The role of the Simulink model is to obtain data on the positions, force and acceleration measurements from the experimental setup and use this information to find the position of the FOWT in the next time step. This involves correcting the force measurements and numerically simulating the hydrodynamics based on the user-set met-ocean conditions. The other physical effects such as hydrostatics, mooring lines, and structural dynamics are also simulated within the model, with the help of MATLAB scripts.

The Simulink HIL model is common for both the selected FOWT design and the inputs that go into the model, which are stored as separate MATLAB scripts. The Simulink model is also initiated and run with the help of a MATLAB script. This script initializes the simulation setting, the wind turbine and floater chosen for the simulation, the chosen FOWT's properties, and the respective scaling factors. The MATLAB script does the scaling necessary for all the involved physical properties before the start of the HIL simulation. From the Figure 4.2 the wind turbine model properties and the sea state condition is defined within the main MATLAB script for running the simulation. Since there are two different FOWT models used, the design is specified with its scaling factor within the main script, which then calls another MATLAB script containing all the detailed properties of the selected FOWT design.

The basic principle of the Simulink model can be understood with the help of the flowchart in Figure 4.2. It starts with the initialisation of the position vector which is defined as zero position initially and then becomes the position vector that is the solution of the previous time step. The flowchart only describes the condition with the HIL setup in a closed loop. The model can also be run in open-loop/ standalone conditions, which is necessary for initial assessments.

According to the condition, the force and acceleration vectors are measured or simulated numerically based on the derivatives of the position vector and the structural properties of the wind turbine model. The forces are measured by the sensor (loadcell) placed at the top of the tower. This loadcell measures the forces in 6DOF and provides the forces as a vector. The coordinate system of the loadcell however is not the same as the one used for the modelling, so the direction of the vector needs to be corrected. The gravitational are measured in the opposite directions

A MEMS triaxial accelerometer measures the acceleration and provides the acceleration in the translational directions (surge, sway and heave). The measured acceleration is used in the block for correcting the measured forces to derive the external aerodynamic force. Since the acceleration values in the rotational dimensions are not available, the calculated position vector from the previous time step is used to derive the acceleration. Only the rotational components of this acceleration are used in the force correction module. However, its influence on the results is not too significant since the torque on the system caused by aerodynamic forces on the rotor has a higher magnitude.

The external forces considered in the model are from the measured aerodynamic forces and numerically simulated hydrodynamic forces. The hydrodynamic forces simulated are divided into diffraction forces and radiation forces. The diffraction forces are modelled based on the wave input decided by the user, while the radiation forces are calculated based on the velocity of the floater. The blocks for the respective calculation are run with the help of MATLAB scripts that model the physics behind these forces. The aerodynamic force correction module on the other hand corrects the measured forces and outputs the external aerodynamic force applied on the system.

Finally, the 6DOF dynamics block solves the dynamics of the FOWT system based on Equation 4.1. The properties of the reference FOWT system are used inside this block to model the necessary mass, stiffness and damping terms. The external forces determined from the other blocks are used as input to this module. The structural dynamics, mooring line dynamics, hydrostatic and gravitational loads are all included within this block. It is also designed to have the option to isolate degrees of freedom to

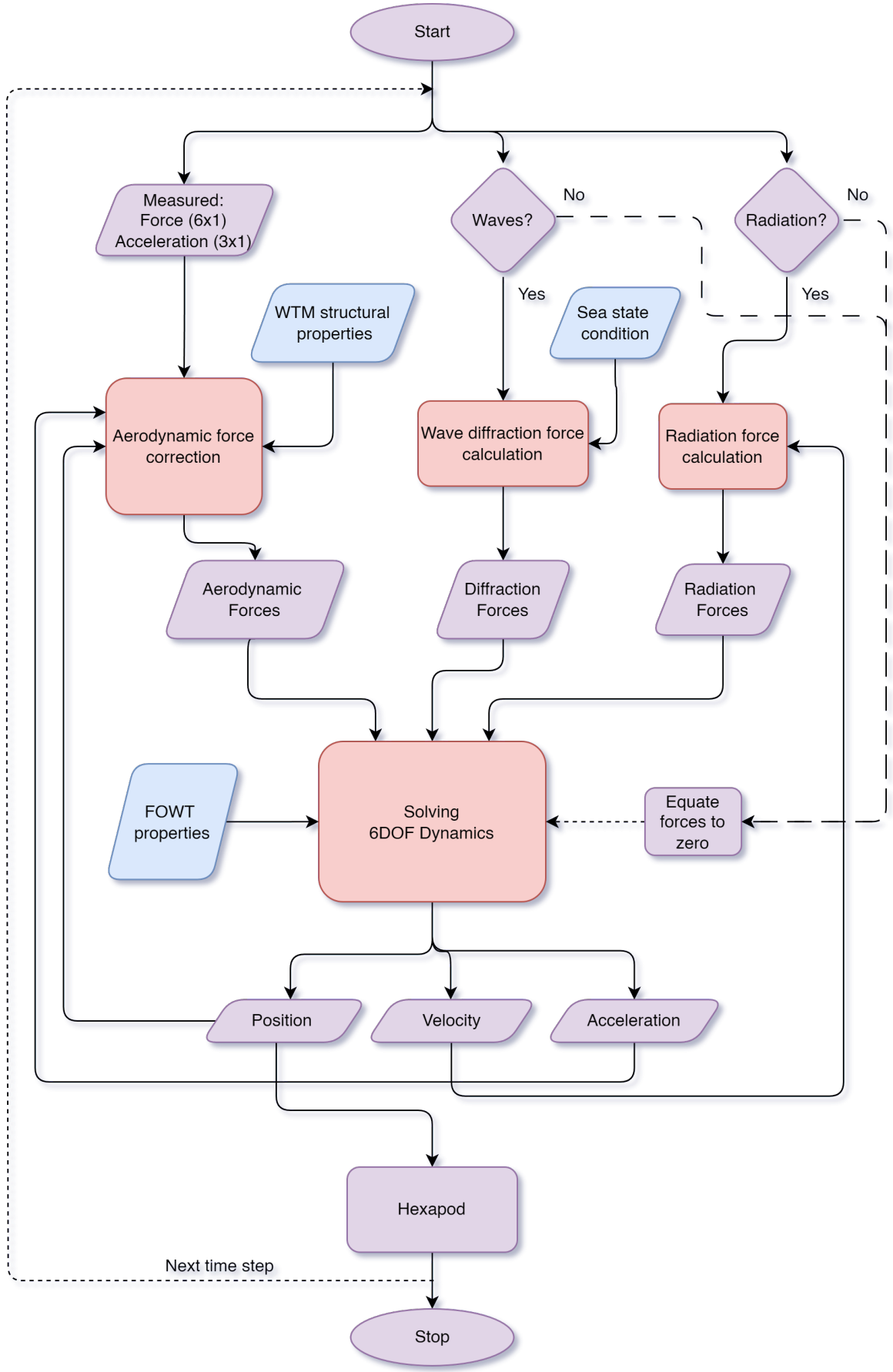

Figure 4.2: Simplified flowchart of the HIL simulink model in the closed loop condition. The blocks in blue are user-defined inputs and the blocks in red are the major calculations required.

understand specific dynamics better. Additional stiffness and damping terms can also be added to this to tune the numerical model for better accuracy.

4.3. Hydrodynamic Loads

The external hydrodynamic loads are modelled using the potential flow theory for fluid dynamics, where the motion of the fluid is described using scalar potentials. Under this theory, the fluid is assumed to be inviscid and irrotational. This means the viscosity of the fluid is assumed to be zero. The forces considered in this theory are diffraction forces, radiation forces, incident wave forces and hydrostatic forces. More details about the theory behind this method can be read in subsection 2.3.3. For this model, the hydrodynamic loads considered are only diffraction and radiation loads. This is also the methodology followed by the potential flow solver WAMIT. The outputs from WAMIT are used for modelling the hydrodynamics in this model.

$$F_{hydro} = F_{rad} + F_{diff} \tag{4.4}$$

WAMIT (Wave Analysis MIT)

WAMIT is a potential flow solver which uses the panel method in the frequency domain. It solves hydrodynamic forces by calculating velocity potentials and hydrostatic pressure on submerged structures. It divides the structure into geometric panels and solves the problem inside each panel. WAMIT also separates the problem into those dependent on the incident wave amplitude and those not. These are broadly described as diffraction forces and radiation forces respectively. They are solved simultaneously to obtain the coefficients necessary for modelling the hydrodynamic effects. This included terms such as added mass, excitation forces, damping coefficients and RAOs. These solutions are made in the frequency domain with the geometry of the floating structure as the main input. Only first-order linear effects can be solved in the frequency domain, hence WAMIT uses a separate module to model the second-order diffraction forces.

The developed HIL model is currently modelled to reproduce the linear hydrodynamics and second-order effects have not been included. WAMIT outputs for both the Triple Spar floater and the VolturnUS floater are utilized in the model. The coefficients for the radiation, diffraction and added mass are obtained from WAMIT output files. These files are non-dimensional, hence steps are taken to convert the coefficients into dimensional terms when necessary. The outputs ".hst",".1" and ".3" are used to model the radiation, diffraction, hydrostatic stiffness and the added mass. These are also the files used by HydroDyn within OpenFAST to model the first-order hydrodynamics. A basic description for the outputs from WAMIT are given below,

- "**.hst**" : This file provides the coefficients that account for hydrostatic restoring effects due to buoyant forces. The gravitational restoring is not included in this file and is modelled separately. The file contains a 6x6 matrix with non-dimensional values of hydrostatic stiffness.
- "**.1**" : This file contains the added mass matrix at 0 time period and infinite time period, which corresponds to infinite frequency and zero frequency added mass matrices respectively. The file also contains damping coefficients as 6x6 matrices, which are provided for a range of frequencies starting from 0 rad/s to 5 rad/s with an increment of 0.05 rad/s. These damping coefficients are used to find the radiation forces.
- "**.3**" : This file contains the first-order wave excitation loads or diffraction forces. This involves 3 forces and 3 moments for a full range of frequencies and wave headings (-180°to 180°). The forces and moments are non-dimensional values and are represented as magnitude and phase as well as real and imaginary. The real and imaginary representation is used for modelling in this project.

The values from the WAMIT outputs cannot be directly used to model the radiation and diffraction loads, even after dimensionalizing them. Radiation loads are dependent on the motion of the floater, while the coefficients provided are dependent on the frequency and wave direction. A similar case applies to the diffraction loads, which depend on the sea state condition. More details on how these forces are modelled are provided in the subsequent sections.

4.3.1. Radiation Loads

Radiation in the context of floating structures occurs due to the motion of the structure in water, this motion could be a response to environmental stimuli. The motion of the structure generates disturbances in the water that form waves, called radiated waves. Generating these waves results in a reactive force on the structure applied by the water, which is commonly called the radiation force. Since the radiation forces are reactive, they have a negative magnitude that helps dampen the motion of the structure under different environmental conditions. Hence, they are expressed using damping coefficients in many numerical models.

Another component involved with radiation forces is the added mass. When the structure accelerates in water, some of the water is also moved along with it. This created an added mass effect on the structure. This creates an inertial force that opposes the floater's motion. Since these forces are also dependent on the motion of the floater, they are also part of the radiation forces. However, instead of velocity, the forces due to added mass are dependent on the acceleration of the floater. The radiation forces can be described generally with Equation 4.5, where R is the radiation damping, and A is the added mass.

$$F_{rad} = -R \cdot \dot{x} - A \cdot \ddot{x} \tag{4.5}$$

The results from WAMIT give us the damping coefficients depending on frequency. To model the dynamics due to the radiation damping, the coefficients need to be utilized in the time domain. Using the state-space representation is a common approach for modelling the dynamics of radiation in the time domain. A state space representation can describe the system's state at any time. Another method of solving is using convolution integrals with Impulse Response Functions ($K(t)$), but they are difficult to solve in numerical simulations, so state space approximations are commonly made.

Fitting techniques are used to convert from the frequency domain to the time domain. Frequency Domain Identification (FDI) is the method used for fitting the state space matrices in this project. It is a methodology developed by NREL and its details are reported in [88]. This methodology uses the added mass and the damping coefficients from WAMIT to find the retardation function $K(\omega)$ according to Equation 4.6. Where $B(\omega)$ is the damping matrix, $A(\omega)$ is the added mass matrix and A_{inf} is the infinite frequency added mass matrix.

$$K(\omega) = B(\omega) + j\omega[A(\omega) - A_{inf}] \tag{4.6}$$

With an equation that provides the response to a frequency, the linear state space system can be identified with the FDI method. The outputs are then the A, B and C matrices. These matrices can be used to find the radiation forces dependent on the velocity of the floater as given in Equation 4.8, where $z(t)$ is the state vector and $\dot{x}$ is the velocity of the floating platform.

$$\dot{z}(t) = A \cdot z(t) + B \cdot \dot{x} \tag{4.7}$$

$$F_{rad}(t) = C \cdot z(t) \tag{4.8}$$

Different fitting techniques exist for modelling the state space matrices from coefficients from WAMIT. OpenFAST uses the same methodology as mentioned above, but also has the option to use other state space fitting methodologies. Another option that the numerical code has is using the convolution integral directly, but better results are obtained when using the state space fitting methodology.

A MATLAB script with the above-mentioned methodology is used for the state space fitting. The script is used to generate the state space matrices for the full-scale FOWT as well as the model scale FOWT. The matrices for the model scale will be used for the real-time HIL testing. The full-scale matrices are used for comparative analyses. Since two FOWTs are being used then a total of 4 sets of state space matrices are generated. The number of states identified for the VolturnUS floater and the TripleSpar floater was 62 and 38 states respectively. The full-scale and model-scale matrices have the same number of states since there is only a difference in the scaling factors.

4.3.2. Diffraction Loads

The diffraction loads in floating structures occur due to the surrounding waves interacting with the structure. The incoming waves are often disturbed due to floating structures causing a scatting of the waves. This effect causes the incoming wave to change direction and wave characteristics. The incoming waves are partly reflected and diffracted. This leads to two sources of loading in diffraction, first from the interaction from the incident wave and second from the reactive forces due to the scattering of the wave. Ultimately, diffraction forces are dependent on the characteristics of the incoming wave.

The incident wave forces are also called the Froude Krylov forces and are dependent on the pressure variations caused on the wetted surface of the floater due to the incoming waves. These forces are also the biggest source of non-linearity among hydrodynamic loads. WAMIT solves for diffraction forces in the first order and the second order. However, in this project only a simple linear model is built, hence the second-order effects are neglected. WAMIT obtains the force coefficients for diffraction using potential flow theory with BEM. Both the incident wave forces and the forces due to scattering are determined and given as non-dimensional force coefficients as a function of wave heading and wave period.

To use these forces in the time domain, the wave characteristics at each time step are needed. In the final HIL model, the wave forces are precalculated and saved as a time history. This time history of wave forces is loaded by the Simulink model. A MATLAB script developed in-house is used to numerically generate the waves for the specified sea state characteristics and simulation time. The data from this numerically generated wave is later used to identify the diffraction forces at each time step, this is saved as a time history file to be used in the Simulink model. Multiple wave cases are run for both floaters with varying simulation times.

The Joint North Sea Wave Project (JONSWAP) spectrum is used to simulate the irregular waves given the wave height, wave period, gamma and wave direction, as well as simulation settings such as wave duration and time step. OpenFAST has options to simulate irregular waves using the JONSWAP/Pierson-Moskowitz spectrum, a white noise spectrum or a user-defined spectrum. The JONSWAP spectrum is chosen for this project since it is a widely used model for representing the energy distribution of ocean waves over different frequencies in a given sea state. It was developed from data collected during the JONSWAP experiment.

The wave spectrum can be generated with the significant wave height (H_s), peak spectral period (T_p) and gamma factor which corresponds to the peakiness of the spectrum. Information on the H_s and T_p is provided in the definitions for the floaters [41][37]. The gamma factor would be 1 for a fully developed sea, which corresponds with the Pierson-Moskowitz spectrum. A default value for moderately developed sea is 3.3 and this value is used in this model. The force coefficients are also obtained from the WAMIT .3 output file. A script is run to obtain the WAMIT data, generate the wave using the input wave characteristics and determine the time history of the wave forces for the specific wave.

4.4. Mooring Line Model

Both the selected floating platforms are semi-submersible platforms with catenary mooring lines. The mooring line modelling approach chosen for this project is a quasi-static model. As mentioned in subsection 2.3.4 a quasi-static approach assumes the mooring line as a static spring-mass system. Viscous and drag effects on the mooring lines are neglected in this model, thus an equilibrium position is always assumed on the mooring lines. The loads from the mooring system are preliminarily dependent on the specifications of the mooring lines and the offset of the floater from the neutral position. This can be better visualized with the help of the Figure 4.3 below.

For the TripleSpar floater, a linearized mooring stiffness matrix was provided in the definition of the floater [82]. Two 6x6 matrices with stiffness coefficients were provided, one for the neutral position with 0 offset, and another for the rated condition position with maximum thrust and an estimated offset distance of 19.57 m. The mooring line stiffness matrix for the neutral position is used in the Simulink HIL model since only the below-rated operating region is tested experimentally. The stiffness term is used to model the loading due to mooring lines as can be seen in Equation 4.9. The FAST model for the DTU10MW wind turbine with TripleSpar floater is also set up with a quasi-static mooring line model with the same matrix for better comparability. The module in FAST that models the linear mooring

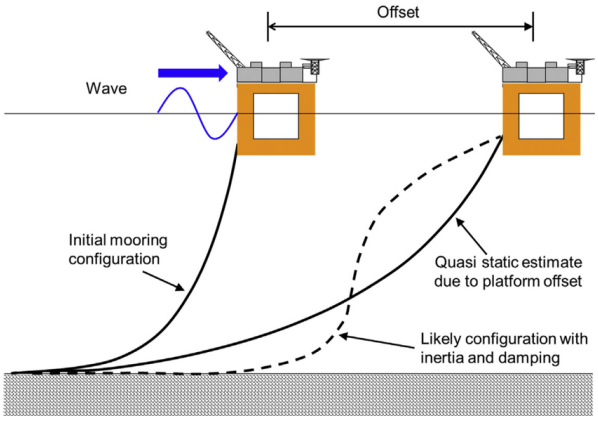

Figure 4.3: Quasi-static mooring line model approximation compared with a dynamic model [89]

line model is called the Mooring Analysis Program (MAP). It has been upgraded to MAP++ in recent versions of FAST and OpenFAST.

$$F_{moor} = K_{moor} \cdot x \tag{4.9}$$

The quasi-static approach for modelling the mooring lines is also taken for the VolturnUS floater for easy adaptability. However, the definition of the floater did not contain data for a linear mooring line model, only the specifications of the mooring line system that could be used with the dynamic model MoorDyn in OpenFAST. So the linearized mooring line matrix is derived for the VolturnUS floater. For this, the input file (.fst) for the OpenFAST model is used. The input file contains information about the water depth and density. The '.fst' file also leads to the MAP input file which entails information on the mooring system such as the weight and diameter of the lines, the number of nodes along the lines considered and their specifications. A Python module for MAP called 'pyMAP' developed by the NREL WISDEM team is used to determine the stiffness matrix [90].

The derived mooring stiffness matrix (K_{moor}) is added to the other stiffness terms that are part of the equation of motion. More details about the other stiffness terms will be discussed in the next section. The final mooring line stiffness matrices are added to Appendix A.

4.5. Stiffness and Damping

4.5.1. Hydrostatic and Gravitational Stiffness

The stiffness terms considered in the system are threefold, the mooring line stiffness discussed previously and then the hydrostatic (K_{hst}) and gravitational (K_{grav}) stiffness. This can be seen from Equation 4.10. The hydrostatic and gravitational effects provide restoring effects on the system and are modelled as stiffness terms in the equation of motion. This methodology is similar to that followed in OpenFAST. The hydrostatic and gravitational effects are modelled separately since dynamics of mass and inertia are accounted for by ElastoDyn, to avoid double counting, it is not considered in HydroDyn.

The WAMIT output '.hst' contains the coefficients for hydrostatic stiffness, also referred to as the hydrostatic restoring matrix. The coefficients from this file are non-dimensionalized, they can be used as the stiffness after re-dimensionalizing them. The '.hst' file only contains the restoring effects from buoyancy, not from the system's mass or the mooring lines. The restoring forces due to mass are added separately as gravitational stiffness.

$$K = K_{moor} + K_{hst} + K_{grav} + K_{tuning} \tag{4.10}$$

The hydrostatic forces in WAMIT are calculated using surface integrals over the mean wetted body area. The centre of buoyancy is considered at the still water level and the vertical centre of buoyancy is considered as 0, this is done to avoid including the gravitational restoring effects. The coefficients

calculated are non-dimensionalized as follows according to WAMIT [91].

$$\bar{C}(3,4) = C(3,4)/\rho g L^3$$
$$\bar{C}(3,5) = C(3,5)/\rho g L^3$$
$$\bar{C}(4,4) = C(4,4)/\rho g L^4$$
$$\bar{C}(4,5) = C(4,5)/\rho g L^4$$
$$\bar{C}(4,6) = C(4,6)/\rho g L^4$$
$$\bar{C}(5,5) = C(5,5)/\rho g L^4$$
$$\bar{C}(5,6) = C(5,6)/\rho g L^4$$

where C is the hydrostatic restoring coefficient, $\bar{C}$ is the non-dimensional coefficient, ρ is the water density, g is gravity and L is the length scale, defined by the variable ULEN in the WAMIT input files. The value of L for both the considered floaters is 1.

Restoring gravitational effects occur when the body undergoes pitching or rolling motion, causing the center of gravity to shift relative to the center of buoyancy and creating a restoring moment. The gravitational stiffness is determined by the product of the total weight of the FOWT system and the distance of the centre of mass above the SWL. This stiffness matrix is only non-zero in the pitch and roll degrees of motion, meaning the gravitational restoring force depends on the extent of pitch and roll displacement.

4.5.2. Viscous Damping

Viscous effects in FOWT systems are crucial for predicting the hydrodynamic response and damping characteristics of the structure. These effects, primarily due to viscous drag, oppose the structure's motion and dissipate energy. In the equation of motion for FOWTs, viscous effects are represented as a 6x6 damping matrix (R), accounting for resistance forces and moments in all six degrees of freedom (surge, sway, heave, roll, pitch, and yaw). Each matrix element corresponds to a specific damping coefficient, including the coupling between degrees of freedom.

The damping matrix is often provided in the definition of the floater. Quadratic damping matrices (R_2) are also commonly included to enable more realistic system behaviour. Both the linear and quadratic damping coefficients are determined using CFD tools or solving Morison's equation. For the TripleSpar floater a linear and diagonal viscous damping matrix is provided in the definition, this is obtained by solving the viscous term in Morison's equation using the approximation, $C_D = 0.61$ [82]. For the VolturnUS floater, the viscous damping matrix is solved with a CFD simulation using the OpenFOAM platform. The damping coefficients are quadratic for the VolturnUS floater.

4.6. Overall Dynamics

The overall dynamics ties all the above-mentioned forces together and solves the equation of motion Equation 4.1. The mass matrix is an important component of the dynamics and is represented as a diagonal 6×6 matrix. The rigid body assumption is taken for the whole wind turbine model, including the rotor and the tower. They have also been designed to be extra stiff, which is not realistic but it makes the HIL modelling less complex. So the modes of the tower and the blades are not taken into account.

The diagonal components correspond to the total mass of the system in the translational degrees of freedom and the inertia in the rotational degrees of freedom. The mass and inertia values in each degree of freedom are often provided in the definition of the floater. The total mass includes the mass of the nacelle, the rotor, the tower and the floating platform. The same value is used for the surge, sway and heave degrees of freedom. The pitch and roll inertia are identical due to symmetry and the yaw inertia is unique.

Another crucial part that hasn't been discussed yet is the aerodynamics. The measured forces are a vital part of the experiment. Since the testing is meant to be done in a wind tunnel, the aerodynamic forces are calculated from the force measurements. The force measurements also include the inertial

and gravitational effects of the wind turbine model's rotor nacelle assembly. A lengthy methodology is involved with the measurement and correction of the forces since only aerodynamic forces are needed in the end. This correction methodology be discussed in detail in the subsequent sections.

4.7. Necessity for Force Correction

There are two reasons why the correction methodology is necessary. First, the scaling methodology chosen for the HIL testing uses arbitrary scaling factors for the length and velocity scales. Thus the Froude similarity law is not followed. Following the Froude similarity law means the Froude number before and after scaling is identical, in addition to this acceleration is the same for both the full scale and the model scale and only the velocity and length terms are scaled. This includes gravity.

However with the scaling methodology followed, there is a scaling factor for gravitational acceleration that is not 1 (gravitational mismatch), and $g_M \neq g_F$. To be more specific, for the DTU10MW model with the TripleSpar floater, with $\lambda_l = 1 : 148$ and $\lambda_v = 1 : 3$ the gravitational acceleration would be $161.32 m/s^2$ for the wind turbine model in place of $9.8 m/s^2$. Similarly, for the VolturnUS the gravitational acceleration would be $312.35 m/s^2$. Due to this, the inertial and gravitational forces would be much higher even if the RNA was perfectly scaled for mass and inertia.

In addition to this, the mass of the Rotor Nacelle Assembly (RNA) in the model scale is much higher when scaled up compared to the mass of the nacelle in the full scale. The mass of the nacelle is 1.61kg approximately, if this is scaled according to the chosen scaling factors the value would be 3.9×10^6 kg and 9.5×10^6 for the DTU10MW and the IEA15MW respectively. While the actual RNA masses are around 6.7×10^5 and 1×10^6 respectively. So the masses in the scaled model are 8 to 12 times higher than they are meant to be. However, it is not possible to design an RNA with masses that are 8 to 12 times lower.

All these factors make the correction methodology necessary for obtaining the aerodynamic forces and moments. So the final aerodynamic thrust would be the measured forces minus the correction factor, this is represented in the Equation 4.11 below. The correction term represents the inertial and gravitational loads in the system. These are measured by the load cell since it is placed beneath the RNA but is not part of the force applied due to wind. The mass and inertia of the RNA are included in the numerical model, so measuring them again would also result in double-counting errors.

$$F_{aero} = F_{measured} - F_{corr} \tag{4.11}$$

Another crucial factor for implementing the force correction methodology is the transformation of the forces from the rotating frame to the fixed frame. This is done with the help of transformation matrices discussed in the section below.

4.8. Transformation Matrices

Transformation matrices are used to transfer from one reference frame to the other. This is necessary because the equations of motion for the system are solved in the fixed frame, while the acceleration and force measurements are taken by sensors attached to the wind turbine, which are in the rotating frame. The transformation matrices are first determined for converting from the rotating frame to the fixed frame. This is done for each angle of rotation. Figure 4.4 illustrates how the rotational transformation matrices are formed. The dotted lines represent the axes aligned with the turbine (rotating frame), while the solid lines represent the fixed frame. It is important to note that the pitch angle is considered negative. The right-hand rule is followed for the directional conventions.

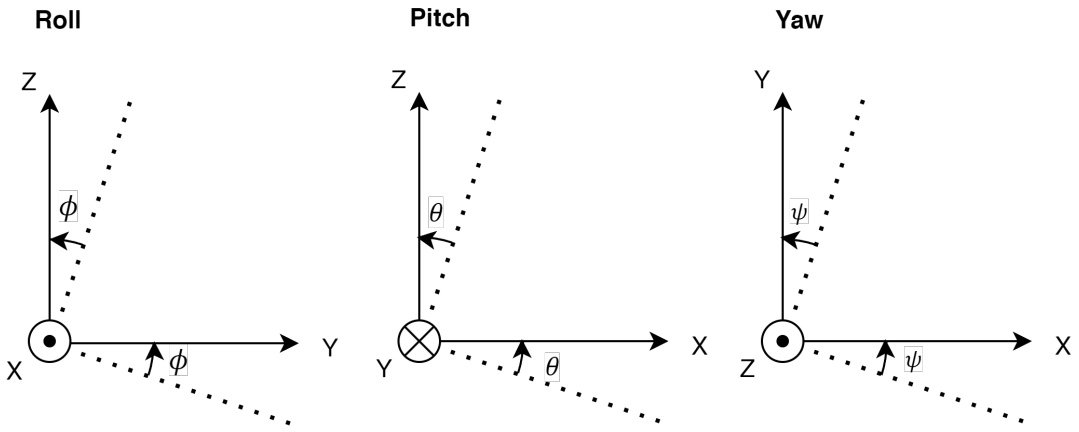

Figure 4.4: Representation of the frame transformation from rotating to fixed frame

The rotation matrices are,

Yaw Rotation:

$$R_z(\psi) = \begin{bmatrix} \cos(\psi) & -\sin(\psi) & 0 \\ 3\sin(\psi) & \cos(\psi) & 0 \\ 0 & 0 & 1 \end{bmatrix}$$

Pitch Rotation:

$$R_y(\theta) = \begin{bmatrix} \cos(\theta) & 0 & \sin(\theta) \\ 0 & 1 & 0 \\ -\sin(\theta) & 0 & \cos(\theta) \end{bmatrix}$$

Roll Rotation:

$$R_x(\phi) = \begin{bmatrix} 1 & 0 & 0 \\ 0 & \cos(\phi) & -\sin(\phi) \\ 0 & \sin(\phi) & \cos(\phi) \end{bmatrix}$$

The order of rotations, or the Euler sequence, plays a crucial role in the transformation matrix, as different sequences can yield different results. For a 6DOF system, the transformation matrices are multiplied threefold, so the rotation order must be set correctly to avoid amplifying errors. The generally accepted order of rotation is the Yaw-Pitch-Roll transformation [92][93]. When applying this transformation, the matrices are multiplied in the Roll-Pitch-Yaw order. The final rotation matrix is,

$$R = R_z(\psi)R_y(\theta)R_x(\phi) \tag{4.12}$$

This order of rotation is used to transform from the rotating reference frame to a fixed reference frame. The inverse of the transformation is used to convert from a rotating frame to a fixed frame. The inverse can be easily used by just transposing the final rotational matrix. This can also be achieved by transposing the individual rotational matrices and reversing the order of rotation, i.e. Roll-Pitch-Yaw. The forces are experienced in the rotating frame, but the final equation of motion in all the models is solved in the fixed frame. Hence transformations are necessary for modelling the external forces. The equation of motion is also solved in the MSL which would be the tower base in this project. Hence, a transformation of the forces to the tower base is also necessary.

4.9. Measured Force and Acceleration Estimation

To correct the inertial and gravitational forces, the first step is to understand the forces and accelerations that the sensors would be measuring. The force sensor (loadcell) is placed on top of the tower and under the nacelle, whereas the accelerometer is placed on top of the nacelle. This can be better visualized with Figure 4.5 The centre of gravity of the rotor nacelle assembly is considered as the yellow y-axis from the Figure 4.5 and on the axis of the tower. The distance between the centre of gravity of the RNA and the loadcell of the wind turbine model is $z_{lc} = 0.035m$. The distance between the accelerometer and the loadcell is considered as $z = 0.05m$.

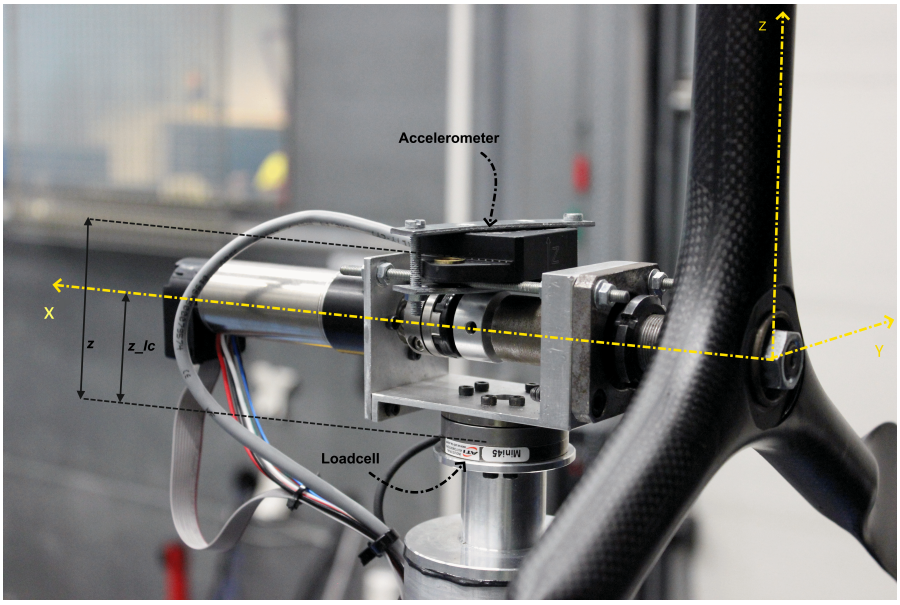

Figure 4.5: Image of the rotor nacelle assembly on the wind turbine model. The coordinate axes, the positions of the accelerometer and the loadcell are also mentioned.

The estimated forces in the load cell are from several sources.

- Aerodynamic forces from the wind acting on the rotor
- Gravitational forces from the weight of the rotor nacelle assembly
- Inertial forces due to acceleration in the surge, sway and heave directions.
- Forces due to the tangential and centripetal acceleration caused by the rotational acceleration of the WTM (roll, pitch or yaw acceleration).
- Torque caused by the acceleration of the WTM in the rotating degrees of freedom.
- Torque due to the tangential acceleration caused by the inertia of the RNA.

The aerodynamic forces and torques are the outputs required from the force correction methodology. To achieve this, all other forces estimated from the system's feedback need to be removed from the force measurements.

Fortunately, with the help of an accelerometer that is at a position close enough to the load cell, the acceleration effects can be approximately equal. Only the mass factor needs to be multiplied with acceleration readings. However, since only a triaxial accelerometer is equipped, rotational accelerations are not measured directly hence correcting torque values is difficult and requires extra steps. So first the theoretical estimation of the measured acceleration, forces and torques is done. The force effects mentioned above are written down in equation format below. The acceleration measurement is in the opposite direction of measured the forces because the measured forces are inertial and are opposite to the direction of acceleration. Gravitational force is measured downwards, but the MEMS accelerometer measures gravity upwards.

$$a_{meas} = R^{-1} \cdot \left(\underbrace{-1 \begin{bmatrix} 0 \\ 0 \\ -g \end{bmatrix}}_{a_{grav}} + \underbrace{\begin{bmatrix} \ddot{X} \\ \ddot{Y} \\ \ddot{Z} \end{bmatrix}}_{a_{trans}} + \underbrace{\left(\begin{bmatrix} \ddot{\phi} \\ \ddot{\theta} \\ \ddot{\psi} \end{bmatrix} \times \left(R \begin{bmatrix} 0 \\ 0 \\ h \end{bmatrix} \right) \right)}_{a_{tangential}} + \underbrace{\left(\begin{bmatrix} \dot{\phi} \\ \dot{\theta} \\ \dot{\psi} \end{bmatrix} \times \left(\begin{bmatrix} \dot{\phi} \\ \dot{\theta} \\ \dot{\psi} \end{bmatrix} \times \left(R \overbrace{\begin{bmatrix} 0 \\ 0 \\ h \end{bmatrix}}^{pos_{tt}} \right) \right) \right)}_{a_{centripetal}} \right) \tag{4.13}$$

The theoretical equation for measuring acceleration is provided in Equation 4.13. The acceleration equations are set up in the fixed frame and then finally transformed to the rotating frame, since the measured values will be from the rotating frame. It starts with the gravitational acceleration which is taken in the positive z direction since the accelerometer measures the gravity in the opposite direction. Then the translational acceleration (a_{trans}) of the WTM model is considered. This term can be estimated by double derivation of the position vector from either the previous time step or from the actual position data measured by the hexapod.

The last two terms of the equation are the two components of the translational acceleration of an object in rotational motion. These two accelerations are commonly referred to as centripetal and tangential acceleration. The tangential acceleration at each moment is in the direction of rotation and perpendicular to the centre of rotation. The common expression for calculating the tangential acceleration is $a_T = \alpha \times R$, where α is rotational acceleration in rad/s^2 and R is the radius of the circle of motion, in this case, it would be the height of the object of interest from the centre of rotation, which is the distance between the base of the tower and the accelerometer, this distance is approximately the height of the tower (h) which is 0.81m.

For simulating the rotational acceleration the position vector is double derivated. Since the position vector is in the fixed frame, so is the derived position vector. So the position of the tower top with respect to the tower base also needs to be determined in the fixed frame for calculating the accelerations. Thus the height of the tower is not directly used as the radius term and a rotational transformation is done to obtain the radius vector in the fixed frame.

The centripetal acceleration is less crucial than the tangential acceleration in this particular set-up because the acceleration is aligned to the axis of the tower and is in the negative z direction. This acceleration is also measured by the loadcell as a centrifugal force, hence it is easily corrected. This term is generally found with the expression $a_c = \omega^2 R$, where R is the radius as explained previously and ω is the rotational velocity in rad/s.

Finally, with all the acceleration terms determined in the fixed frame, they need to be transformed to the rotating frame. This is necessary since the accelerometer is moving along with the WTM and thus operates in the body-fixed frame. The body-fixed frame is the same as the rotating frame by the terminology followed in this report. For this the inverse of the rotational matrix determined in Equation 4.12 is used. The inverse is multiplied in scalar with the solved acceleration vector. This will result in the theoretical estimation of the accelerations measured.

The accelerations measured by the MEMS accelerometer are all in the direction they are physically in, with the exception of the gravitational forces, which are inverted in direction. This is in contrast to the loadcell which measures all the forces in the opposite direction to acceleration since they are inertial.

Theoretical force measurements in the translation direction would be the measured acceleration times the mass of the RNA, with an addition of the aerodynamic forces acting on the rotor. The effect of wind on the tower is not considered since the loadcell is measured on top of the tower, thus aerodynamic thrust on the rotor is the main component of aerodynamic forces that are measured. Wind on the rotor also causes torques that act on top of the tower and are measured by the loadcell. The rotation of the rotor also results in force fluctuations in the force measured but these fluctuations are periodic

depending on the rotational speed and have a mean value of zero hence they are ignored in the force correction methodology.

The theoretical forces in the translational directions can be determined using the same methodology to estimate the measured acceleration. Thus the measured forces estimation can be expressed as Equation 4.14. The final aerodynamic force vector is set in the fixed frame therefore it is added inside the parenthesis for rotational transformation from the fixed to the rotating frame. It can also be understood from the expression that measured forces can be easily corrected using the measured acceleration since the inertial and gravitational effects measured by the accelerometer and the loadcell are identical.

$$F_{meas} = \underbrace{\begin{bmatrix} F_{ax} \\ F_{ay} \\ F_{az} \end{bmatrix}}_{F_{aero}} + R^{-1} \left(+ \underbrace{\begin{bmatrix} 0 \\ 0 \\ -Mg \end{bmatrix}}_{F_{grav}} - \underbrace{\begin{bmatrix} M\ddot{X} \\ M\ddot{Y} \\ M\ddot{Z} \end{bmatrix}}_{F_{trans}} \underbrace{- M \left(\begin{bmatrix} \ddot{\phi} \\ \ddot{\theta} \\ \ddot{\psi} \end{bmatrix} \times \left(R \begin{bmatrix} 0 \\ 0 \\ h \end{bmatrix} \right) \right)}_{F_{tangential}} \underbrace{- M \left(\begin{bmatrix} \dot{\phi} \\ \dot{\theta} \\ \dot{\psi} \end{bmatrix} \times \left(\begin{bmatrix} \dot{\phi} \\ \dot{\theta} \\ \dot{\psi} \end{bmatrix} \times \left(R \overbrace{\begin{bmatrix} 0 \\ 0 \\ h \end{bmatrix}}^{pos_{tt}} \right) \right) \right)}_{F_{centripetal}} \right) \tag{4.14}$$

The correction of the measured torques and moments is more difficult since the accelerometer does not measure the rotational accelerations, hence the torque estimation depends on the translational acceleration measured and the double-derived position vector. A theoretical expression for the measured torques is provided below in Equation 4.15. It starts with the torque caused by inertia due to rotational acceleration followed by the torque on the tower top caused by the weight of the RNA. The general expression for calculating the torque in $T = F \times d$ where d is the length of the arm. In this case, the length of the arm is the z_{lc} value (0.035m) that can be visualized in Figure 4.5. Finally, the aerodynamic torques are added.

$$T_{meas} = -R^{-1} \underbrace{\begin{bmatrix} J_x\ddot{\phi} \\ J_y\ddot{\theta} \\ J_z\ddot{\psi} \end{bmatrix}}_{T_{inertia}} + \underbrace{\begin{bmatrix} -Ma_{meas}(y) \times z_{lc} \\ -Ma_{meas}(x) \times z_{lc} \\ 0 \end{bmatrix}}_{T_{mass}} + \underbrace{\begin{bmatrix} T_{ax} \\ T_{ay} \\ T_{az} \end{bmatrix}}_{T_{aero}} \tag{4.15}$$

4.10. Determining Aerodynamic Forces

Having the expressions for the estimation of the measured forces makes it easier to understand how the forces and the torques need to be corrected in order to obtain the aerodynamic forces. The expression for obtaining the aerodynamic forces is stated in Equation 4.11 and it is a simple subtraction of the correction term from the measured forces. The same expression also applies to the torques. Hence, the correction terms F_{corr} and T_{corr} need to be determined. This can be determined by simply substituting the measured estimation of forces (Equation 4.14 and Equation 4.15) into equation Equation 4.11. Torque are also similarly corrected ($T_{aero} = T_{meas} - T_{corr}$). This results in the following expressions for the correction,

$$F_{corr} = -M \cdot a_{meas} \tag{4.16}$$

$$T_{corr} = -R^{-1} \begin{bmatrix} J_x\ddot{\phi} \\ J_y\ddot{\theta} \\ J_z\ddot{\psi} \end{bmatrix} - \begin{bmatrix} Ma_{meas}(y) \times z_{lc} \\ Ma_{meas}(x) \times z_{lc} \\ 0 \end{bmatrix} \tag{4.17}$$

At each time step in the model, the acceleration and position are measured and the force measured is corrected according to the expressions above. Correcting the translational forces only required the acceleration measurement and the mass of the RNA which is predefined within the model. For correcting the torques the length of the arm, moment of inertia values and the rotational acceleration values are also necessary. However, the values for the moment of inertia of the RNA are not known and the values for rotational acceleration can also only be obtained by double deriving the position vector which causes a time delay. This issue is resolved by iterative testing with the HIL setup and finding suitable values.

This methodology for correction was tested with dummy values of aerodynamic thrust initially in MATLAB and the results were satisfactory. In the next stage, this is tested with the physical HIL setup without the use of the wind tunnel or the rotor. The hexapod is used along with the sensors and the numerical model with force correction. Physical forces were applied in all degrees of freedom and the response of the system was recorded for analysis of the correction methodology. Various moment of inertia values for the RNA were tested and the best results were observed by assuming the value as zero.

This is mainly due to the lag in obtaining the angular acceleration. There was a phase difference between the position and the acceleration calculated, the difference was approximately around 0.7 seconds. This phase difference is too high to be able to correct the torque due to rotational inertia. In addition to this, the torque caused by the mass of the RNA being at a distance from the load cell is of a higher magnitude. Hence, ignoring the torque due to the moment of inertia is the best choice. For a better correction method, a sensor to measure the acceleration in rotational degrees of freedom is necessary. For the scope of this project which is to test the HIL capability, this correction methodology is sufficient.

Another important step in force correction is the rotation and transportation of the forces. Since the required force is the aerodynamic force in the fixed domain. In the above equations, the aerodynamic force vector is in the rotating frame as it is part of the measured forces. Hence the final aerodynamic forces after correction need to be transformed from the rotating frame to the fixed frame. This can be done using the determined rotational matrix. The torques need to be transported to the base of the tower which is also the origin of the coordinate system. This is a crucial step since the aerodynamic torques acting on the system are required and the torque acting on the loadcell is not an accurate representation.

$$F_{aero,f} = R \cdot F_{aero} \tag{4.18}$$

$$T_{aero,f} = \begin{bmatrix} F_{aero,f}(x) \\ -F_{aero,f}(y) \\ F_{aero,f}(z) \end{bmatrix} \times \begin{bmatrix} pos_{tt}(x) \\ -pos_{tt}(y) \\ pos_{tt}(z) \end{bmatrix} + T_{aero} \tag{4.19}$$

The $F_{aero,f}$ and $T_{aero,f}$ terms are the final outputs of the force correction module. They indicate the final aerodynamic forces and torques that are acting on the system in the fixed reference frame. The negative sign for the torque due to the aerodynamic forces in the sway direction is necessary due to the chosen coordinate system. For example, positive sway results in a negative torque in the roll direction. These force terms are used in the dynamics module, where the equation of motion for the FOWT is solved and the position vector for the next time step is calculated. The MATLAB script used within the Simulink model for the force correction is provided in Appendix B

5

Tuning, Validation and Testing

In this chapter preliminary tests are conducted for both the FOWT model for tuning and verification. First in section 5.1, the open-loop tests are done where the results from the Simulink model are compared with the results from FAST/OpenFAST. This comparison also allowed for tuning the Simulink model with additional damping and stiffness terms. With the final tuned Simulink model, the floating dynamic performance was verified. Following this in section 5.2 closed-loop testing was conducted to verify the HIL setup. These tests are essential to ensure the correctness of the wind tunnel experiments. The validation and the feasibility of both models are commented on. Finally section 5.4 describes the experimental testing in wind tunnels and the preparation for it.

5.1. Initial Testing in Open Loop

A Simulink model was made for the HIL simulation according to the methodology detailed in the previous chapter. To recap, the HIL model included all the modules for force calculation, correction and solving the system's dynamics. The Simulink model was run with the help of a MATLAB script that initialized the FOWT properties, the wind turbine model properties, the sea state conditions and the scaling factors. The properties were also initially scaled within the script before running the simulation. Initial runs were made to check the outputs from every module. This was done for both the model-scale and full-scale setting and with both the FOWT designs. In these runs, the functioning of the force calculation modules (diffraction and radiation forces) and the aerodynamic force correction module were checked for reasonable output values in all degrees of freedom.

This preliminary testing in Simulink is also referred to as testing in Open-Loop since the hardware-in-loop is not used in these tests, they are done numerically without the hexapod. The open-loop testing is necessary to verify the floater dynamics of the model. This testing verifies the rigid body structural dynamics, the hydrodynamic forces simulation, mooring line dynamics, and the numerical wave generation for both FOWT models. The Open-Loop results are compared with FAST/OpenFAST for verification. Once the dynamics are verified for both the models in Open-Loop, the HIL is tested and verified by comparing it with results from Open-Loop.

Later a feature was built into the Simulink model which allows the selection of one or more degrees of freedom to simulate. This makes it possible to simulate all the degrees of freedom one by one and study the responses without interference. It also helps to understand the coupling between the different degrees of freedom and how they affect each other. It was found that the surge and pitch degrees of freedom are strongly coupled. Due to symmetry, the sway and roll responses are also coupled. With this feature, the decay responses simulated by the model can also be tested and compared with the same from FAST/OpenFAST. In addition to the decays, wave cases without wind were also compared between the Simulink model and FAST/OpenFAST.

5.1.1. Free Decay Tests

Free decay tests are often done on floating structures to test the added mass, stiffness and damping characteristics of the structure. These tests are done for each degree of freedom one by one. An initial displacement is made on the system and the response of the system to reach the equilibrium positions is recorded and studied. The oscillating motion of the floating platform provides information on the natural frequency and the damping ratio of the system for that particular DOF. The natural frequency of the system is a function of the stiffness, damping and added mass as can be seen from the expression below,

$$f_i = \frac{1}{2\pi}\sqrt{\frac{k_i}{m_i}} \tag{5.1}$$

where f is the natural frequency in Hz, k is the stiffness in N/m and m is the mass, i denotes the degrees of freedom.

Initial decay tests resulted in similar values for the natural frequency for both the DTU10MW+TripleSpar and the IEA15MW+VolturnUS model since the mass stiffness and damping matrices from the definition were used. However, the damping ratio did not match as accurately and the natural frequency values could also have a better match. Hence tuning was done to match the decay response using additional stiffness and damping values. These values were determined empirically by trial and error.

For calculating the natural frequency and the damping ratio from the time history of the position output from the model the 'findpeaks' function in MATLAB is used. It provides the values of local maxima in the time history along with its position in time. With this information, the damped frequency can be found as follows,

$$f_{damped} = \frac{1}{\text{time difference between peaks}} \tag{5.2}$$

To find the undamped natural frequency the damping ratio is required. The damping ratio can be calculated using the formula below,

$$\text{Damping ratio}(\zeta) = \frac{\frac{\delta}{2\pi}}{\sqrt{1+(\frac{\delta}{2\pi})^2}} \tag{5.3}$$

where δ is the logarithmic decrement which is depicted as,

$$\delta = log(\frac{Peak(1)}{Peak(2)}) \tag{5.4}$$

Finally, the undamped natural frequency can be found as a function of the damped frequency and the damping ratio as follows,

$$f_n = \frac{f_{damped}}{\sqrt{1-\zeta^2}} \tag{5.5}$$

With this method, the natural frequency and the damping ratio are determined for all the degrees of freedom for both the Simulink model outputs and from FAST/OpenFAST. Decay tests for both models are done full scale for easy comparison since the values from the FAST/OpenFAST model are not scaled. Small displacement values are taken since the equilibrium position is reached sooner. This is an advantage since the file sizes are small which makes it more computationally efficient. Small displacements also allow for better matching with the Simulink model since other structural effects do not interfere with the decay.

DTU 10MW + TripleSpar

The FAST model of the DTU10MW with the TripleSpar floater is used to run decay simulations with a similar setup to the Simulink model. The decays are run with all degrees of freedom turned off

except for the platform motions. The simulations are run in an environment with no wind or waves. There is also no control since the turbine is not operating. The mooring line model is turned on for the setup. On the other hand, the Simulink model is run in a standalone mode where there are no external forces measured. The force correction module and the radiation forces module are turned on while the diffraction forces are off.

The simulation time was set at 3600 seconds for all the simulations in both FAST and Simulink. The motion history outputs from FAST did not settle at the zero position for the surge and pitch decays since this is the direction of the incoming wind and an offset is considered within the FAST model. This offset is not incorporated in the developed Simulink model, hence for better comparison the output from FAST for these DOFs is offset to settle with zero as its equilibrium position. The initial displacement values and the offsets for each degree of freedom are provided in the Table 5.1.

DOFs	**Surge**	**Sway**	**Heave**	**Roll**	**Pitch**	**Yaw**
Initial Displacement	2m	2m	2m	2°	2°	2°
FAST Offset	-0.05m	-	-	-	+0.09°	-

Table 5.1: Initial conditions for free decay tests for the DTU10MW with TripleSpar model. The offset is added to the final motion history before comparison.

With the above-mentioned setup and initial conditions, the simulations were run for all the degrees of freedom. The decay results from FAST was used as the standard for tuning the Simulink model. If the natural frequency from the Simulink model was lower than from FAST, an additional stiffness term was added for that degree of freedom. If the natural frequency was lower, a negative additional stiffness value was added. Similarly damping ratio values were also adjusted by incorporating additional damping terms to match the results from FAST. The objective of the tuning process was to obtain identical free decay behaviour in both models. The tuning was done starting from surge and ending with yaw.

The final tuning resulted in additional stiffness and damping matrices, they are added in the appendix Equation A.5. The comparison between the decays for each DOF after tuning can be seen from Figure 5.1. The decays from the tuned Simulink HIL model closely resemble the decay response from the FAST model. The final values of the natural frequency and damping ratios are recorded in Table 5.2. As can be seen, the natural frequencies match perfectly between both models, with the exception of roll and yaw. The damping ratios in the translational directions seem to be slightly higher and the damping ratios in the rotational directions seem to be slightly lower. However, these discrepancies are small and the decay responses match well.

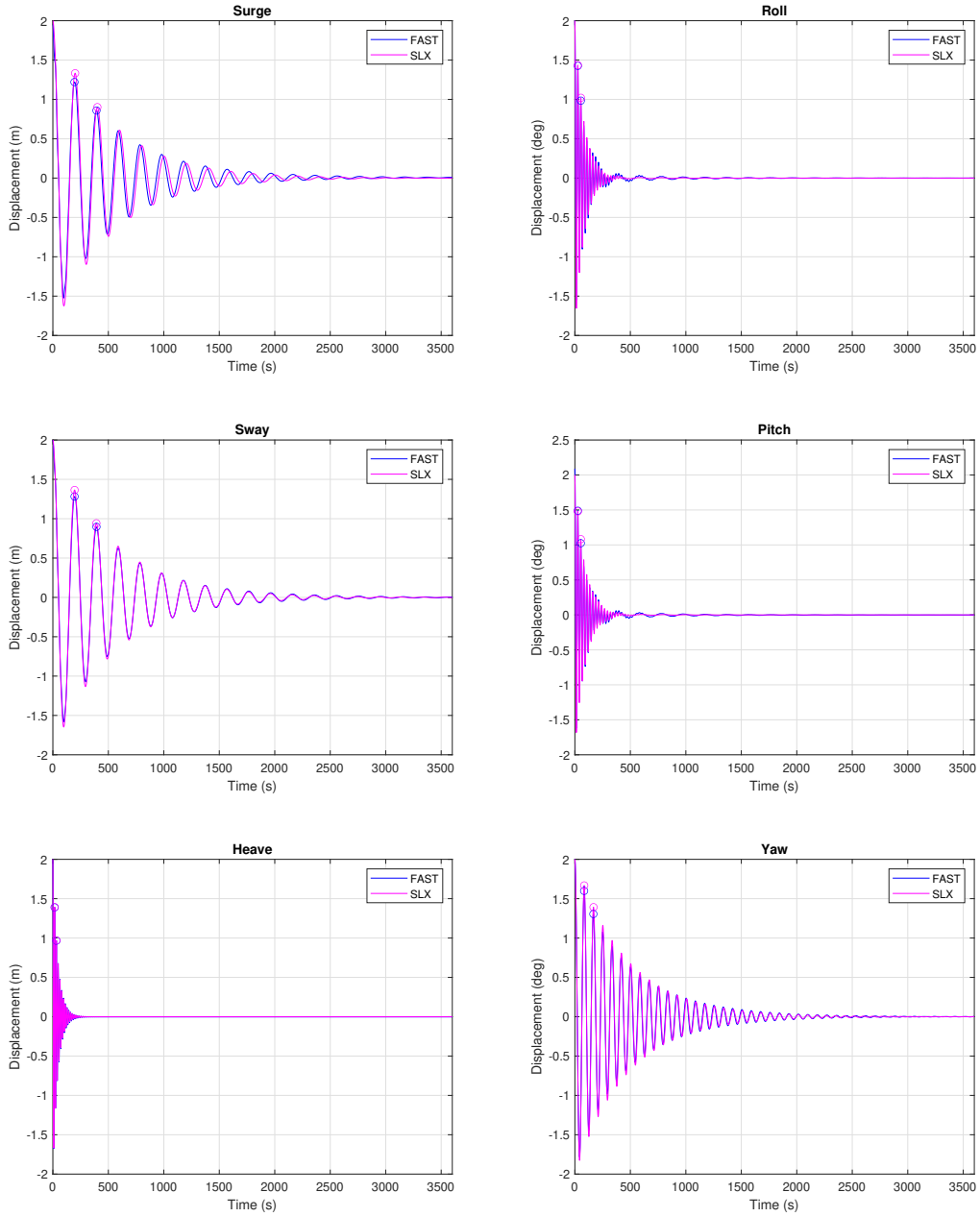

Figure 5.1: Free decay plot comparison between outputs from the HIL Simulink model and FAST tool for the DTU10MW wind turbine with TripleSpar floater. The decays from all six degrees of freedom are compared.

IEA15MW + VolturnUS

A similar tuning methodology was also implemented for the IEA15MW wind turbine model with the VolturnUS floater. In this case, the OpenFAST model for the FOWT model was used. The OpenFAST decay tests were set up identically to the one used for the DTU10MW with TripleSpar. The Simulink model was also similarly set up with the new FOWT model. Similar initial conditions were also used for the decays. One-hour-long decays were done with small displacement amplitudes. However, the offsets for the IEA15MW + VolturnUS model were found to be higher. These are recorded in Table 5.3 along with the initial displacement for each degree of freedom.

The offsets were added to the motion history from OpenFAST before comparing them with the results from the Simulink model. The motion history for surge decay from OpenFAST was noisy when it pre-

DOFs	FAST		Simulink HIL Model	
	Nat Freq. (Hz)	Damping Ratio (-)	Nat Freq. (Hz)	Damping Ratio (-)
Surge	0.005	0.0558	0.005	0.062
Sway	0.0051	0.0568	0.0051	0.0589
Heave	0.0628	0.0577	0.0628	0.0576
Roll	0.0375	0.059	0.0371	0.0541
Pitch	0.0376	0.0594	0.0375	0.0496
Yaw	0.012	0.0323	0.0119	0.0288

Table 5.2: Comparison of natural frequencies and damping ratios between FAST and Simulink numerical model for the DTU10MW+TripleSpar model

DOFs	Surge	Sway	Heave	Roll	Pitch	Yaw
Initial Displacement	2m	2m	2m	2°	2°	2°
FAST Offset	-0.3947m	-	+0.3548	-	+1.4021°	-

Table 5.3: Initial conditions for free decay tests for the IEA15MW with VolturnUS model

vented the natural frequency and damping ratios from being determined accurately. Hence a lowpass filter was added to this signal with a cut-off frequency of 0.03Hz to remove the disturbances in the motion history.

Another significant detail to notice was that the decays for the IEA15MW+VolturnUS FOWT never reached the equilibrium position, even with small amplitude displacements and an hour of simulation. The definition of the VoltunUS floater also does not specify any linear damping and only includes a quadratic damping matrix. Without a linear damping matrix reaching a stationary equilibrium position would be highly difficult.

Having continuous oscillations is less than ideal for HIL testing as well as in real-world conditions. Hence the quadratic damping matrix is replaced with a linear damping matrix with empirical values. With the linear damping matrix, the decays reach an equilibrium position. In addition to this, tuning of the stiffness and damping is done. Similar to what was carried out with the DTU10MW + TripleSpar model. The additional stiffness and damping terms are added in Equation A.11.

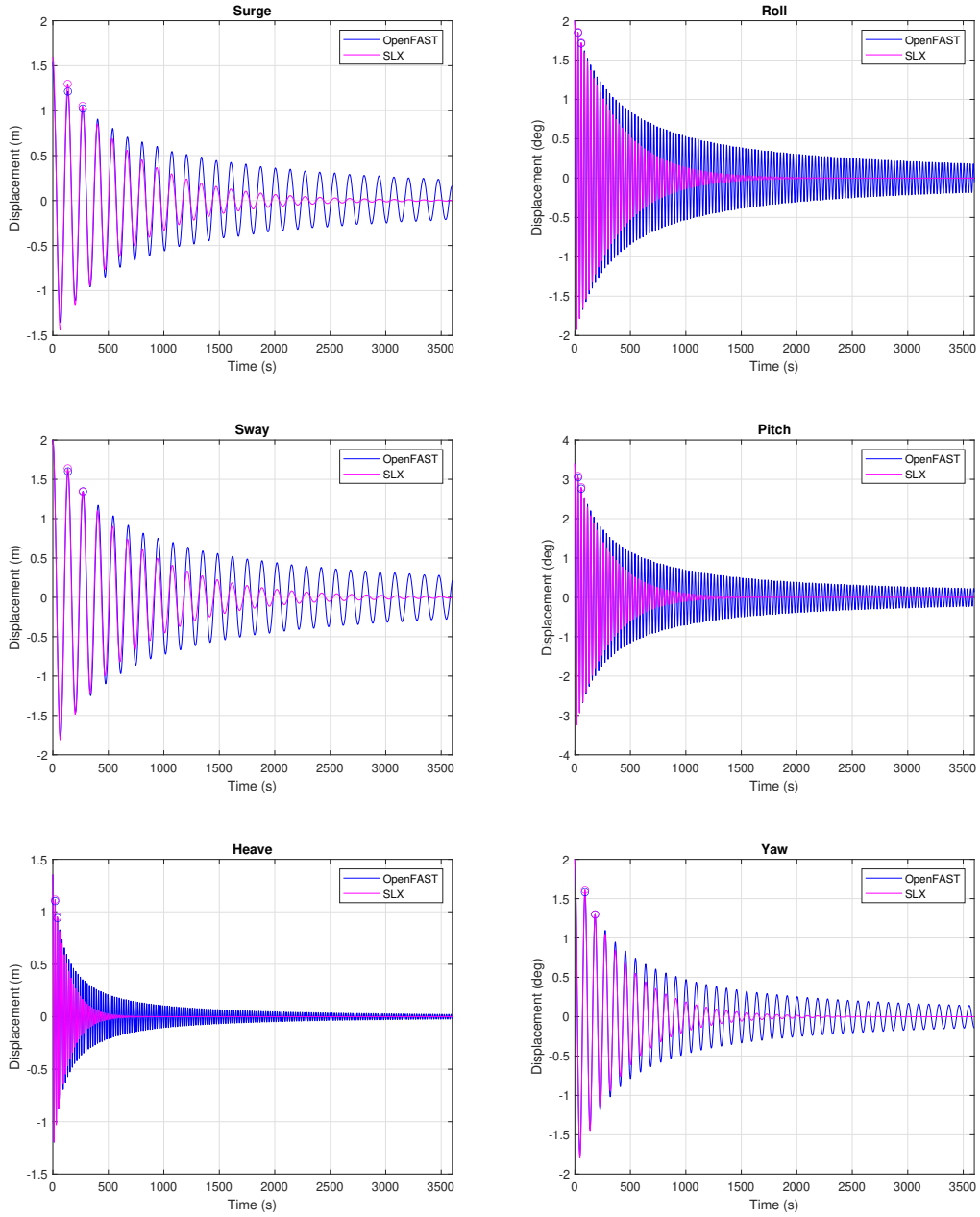

Figure 5.2: Free decay plot comparison between HIL Simulink model and OpenFAST for the IEA15MW wind turbine with VolturnUS floater.

The final natural frequencies and damping ratios for all the DOFs from OpenFAST and the Simulink HIL model are tabulated below in Table 5.4. The natural frequencies are matched accurately whereas the damping ratios for the Simulink model are slightly higher in some DOFs. The decay plots are compared in Figure 5.2. The decay for all the DOFs matches well in the initial seconds, later the decay from OpenFAST keeps oscillating whereas the decay from the Simulink model reaches equilibrium.

Although major modifications were made to the damping matrix from the original design, and the response from the Simulink HIL model for this FOWT design might not match the actual design response, the modifications to the damping were accepted and further testing was done to check the model's feasibility. This is because, despite the change in the damping matrix the natural frequencies and the damping ratios are the same and the motion response is also matched well in the initial stages.

DOFs	OpenFAST		Simulink HIL Model	
	Nat Freq. (Hz)	Damping Ratio (-)	Nat Freq. (Hz)	Damping Ratio (-)
Surge	0.0075	0.027	0.0075	0.0334
Sway	0.0074	0.0276	0.0074	0.0316
Heave	0.0484	0.0251	0.0485	0.0252
Roll	0.035	0.0123	0.035	0.012
Pitch	0.0351	0.0157	0.0351	0.0156
Yaw	0.011	0.0313	0.011	0.0342

Table 5.4: Comparison of natural frequencies and damping ratios between OpenFAST and the Simulink HIL model for the IEA15MW with VolturnUS FOWT design.

5.1.2. Testing Irregular Waves

Following the free decay tests, additional tests with simulated wave conditions were run to ensure that the dynamic response of the numerical model aligns with that of the response from FAST/OpenFAST. Initially, wave cases were simulated on FAST/OpenFAST, where the set-up included only the platform motions, hydrodynamics and mooring line dynamics. The wind inflow and the aerodynamics are neglected, this is done to mimic the HIL open-loop model setup. The HIL Simulink Model for this test includes diffraction forces as well as radiation forces. The simulations are set for one hour with identical sea state conditions but without the presence of wind.

The following results are compared once the simulation results are obtained from both the OpenFAST/-FAST tool and the HIL Simulink model.

- The motion history of the platform in 6DOF
- The spectra of the platform motion
- The spectra of the diffraction forces acting on the floater due to waves
- The spectra of the wave elevation
- Response Amplitude Operators

A FFT (Fast Fourier Transform) function was used to find the spectrum for the results mentioned in the above list. The spectrum of platform motion gives insight into the prominent motion frequencies and periods. The platform motion should be closely related to the diffraction forces and the incoming wave's elevation. Since the diffraction forces are a function of wave elevation and the platform motions are a function of the diffraction forces. This behaviour can be visualized by comparing the spectrum.

The spectrum represents the magnitude of the complex results derived after the FFT. The spectrum provides information about the excitement frequencies and the natural frequencies of the system. The broadness of the peaks provides information on the damping, broader peaks have more damping. The height of the peak relates to how quickly the system reaches equilibrium (rate of decay), smaller peaks have a faster rate of decay.

The results from the HIL simulink model and FAST/OpenFAST are compared first for the DTU10MW with the TripleSpar model and then the IEA15MW with the VolturnUS model. This was done using a MATLAB script. The plots for the wave cases analysis are compared in the subsequent sections.

DTU10MW + TripleSpar

The most important wave to consider while testing the dynamics is the wave at rated condition since it has the largest loading on the system during operating conditions. The sea state conditions at rated wind speed (11.4 m/s) have a significant wave height (H_s) of 3.04m and a peak time period (T_p) of 9.50s. The wave is generated numerically for a duration of one hour, based on the JONSWAP spectrum. The resulting wave elevation spectrum is provided in Figure 5.3.

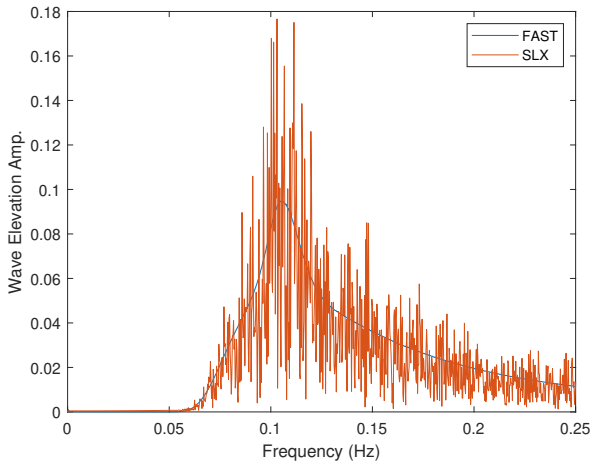

Figure 5.3: Wave elevation spectrum for an irregular wave at rated wind speed for the DTU10MW wind turbine with H_s of 3.04m and T_p of 9.50s. The spectrum of the wave generated in FAST is compared with that generated by the HIL Simulink Model (SLX).

With the generated irregular wave, the diffraction forces acting on the platform are simulated. The wave heading is considered to be 0°, hence diffraction forces only act on the surge, heave and pitch DOFs. The resulting spectrum of the wave diffraction forces can be visualized in Figure 5.4.

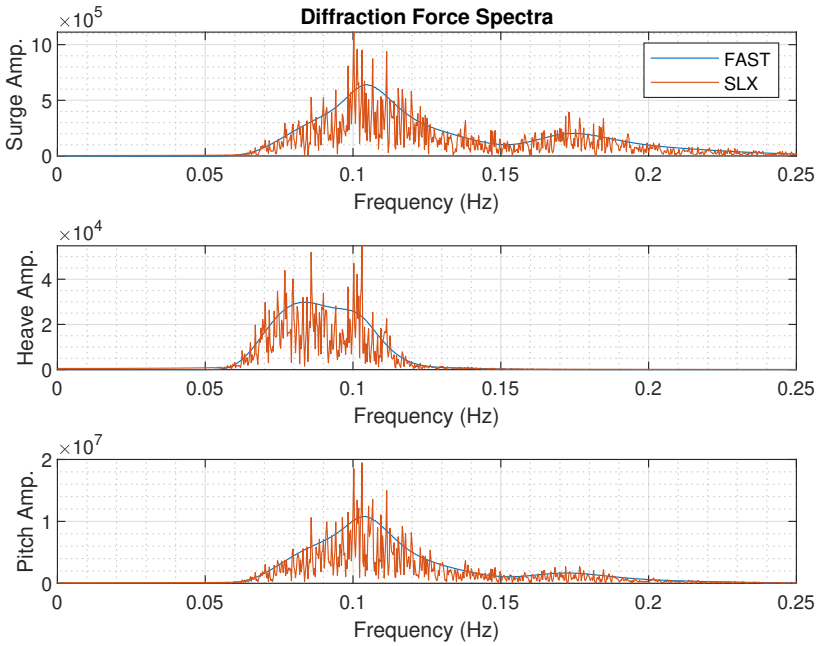

Figure 5.4: Diffraction force spectra for an incoming irregular wave with H_s of 3.04m and T_p of 9.50s. The spectra are compared between the output from FAST and the HIL Simulink model for the DTU10MW wind turbine with TripleSpar floater.

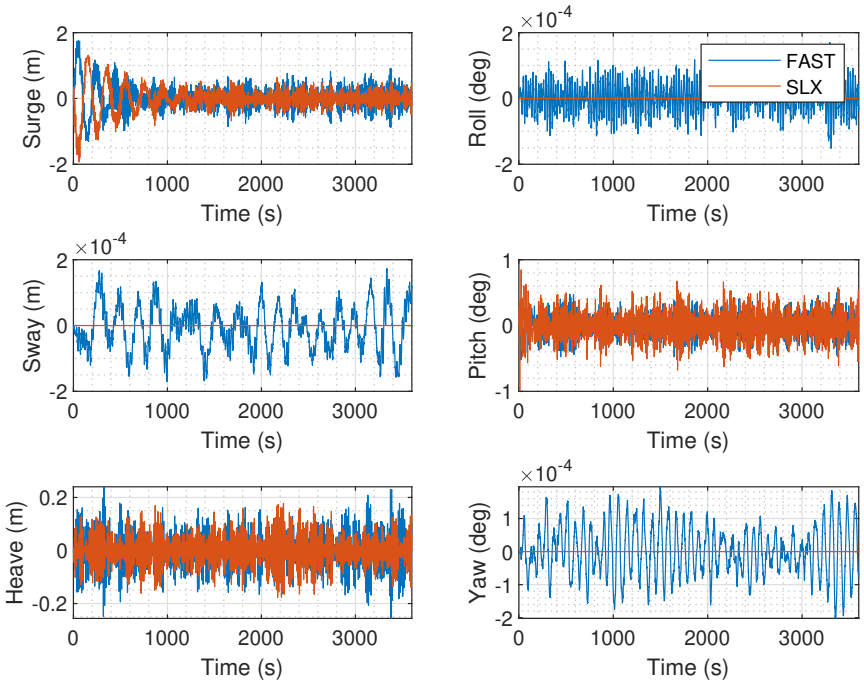

Figure 5.5: Motion time history of DTU10MW FOWT model with TripleSpar floater for the wave case at rated wind condition compared between HIL simulink model and FAST. The cases are compared assuming no wind.

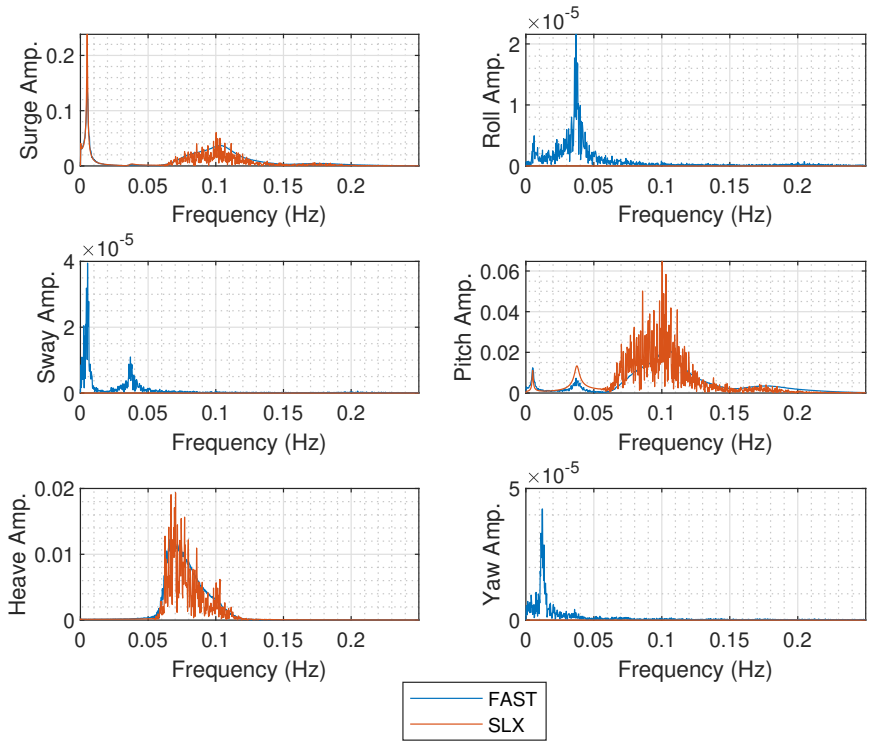

Figure 5.6: Motion spectra of DTU10MW FOWT model with TripleSpar floater for the wave case at rated wind condition compared between HIL simulink model and FAST. The cases are compared in all DOFs assuming no wind.

From Figure 5.5, it can be understood that the platform response for both models is comparable. The response in surge, pitch and heave degrees of motion are similar in amplitude. The difference is that the Simulink model assumes the motion to be insignificant for the other degrees of motion whereas the FAST model is accurate in identifying the smaller displacements. This approximation is accepted since the motion response in FAST is of a much smaller magnitude compared to the other DOFs.

Comparing the motion spectrum in Figure 5.6 the motion response frequency in the surge, pitch and heave DOFs are comparable. The peaks in the graphs of these DOFs match with the frequency of the wave elevation and wave diffraction forces. The initial peak in the surge and pitch DOFs correspond with the natural frequencies of the TripleSpar floater, the pitch DOF has two initial peaks since surge motion is coupled with pitching. Due to the diffraction force approximation, the response in the other DOFs is close to zero.

From Figure 5.7 the response amplitude operators (RAOs) can be compared between the FAST model and the Simulink model. The RAO is similar to a frequency response function of the platform motion depending on the wave amplitude. The RAOs depict the displacements in the different DOFs when facing waves with a particular amplitude. The methodology for calculating this is provided in Appendix C. As can be seen from the graph, the RAOs match well between the two models.

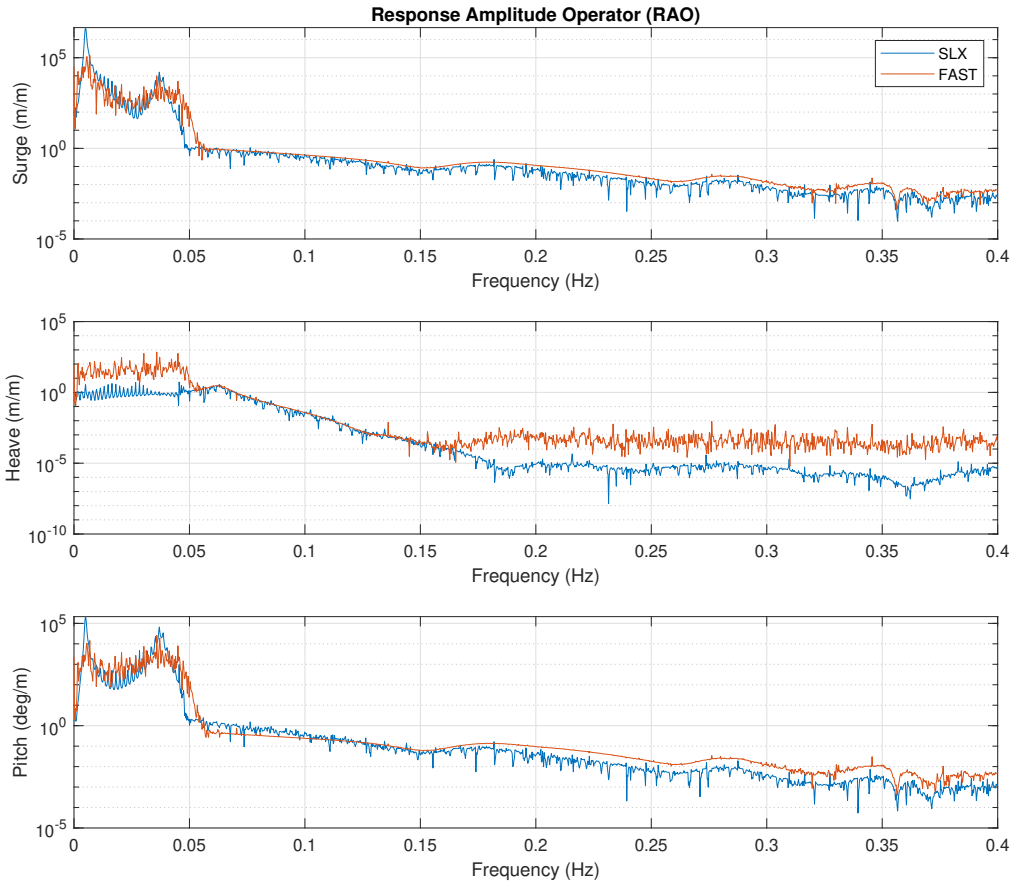

Figure 5.7: Comparision of RAO between the Simulink model and FAST for the simulated rated wave condition without wind.

IEA15MW+VolturnUS

A similar test and comparison is also done with the IEA15MW wind turbine with the VolturnUS Simulink model and the OpenFAST model of the same. In this case the rated condition wind speed is 10.59m/s, the data for the sea state conditions however are only available for the wind speed of 10m/s. Assuming

that the sea state conditions do not differ significantly between the actual rated condition and at 10m/s, the H_s and T_p values for the wave are considered as 1.54 m and 7.65 s. The irregular wave is generated and the diffraction forces are computed.

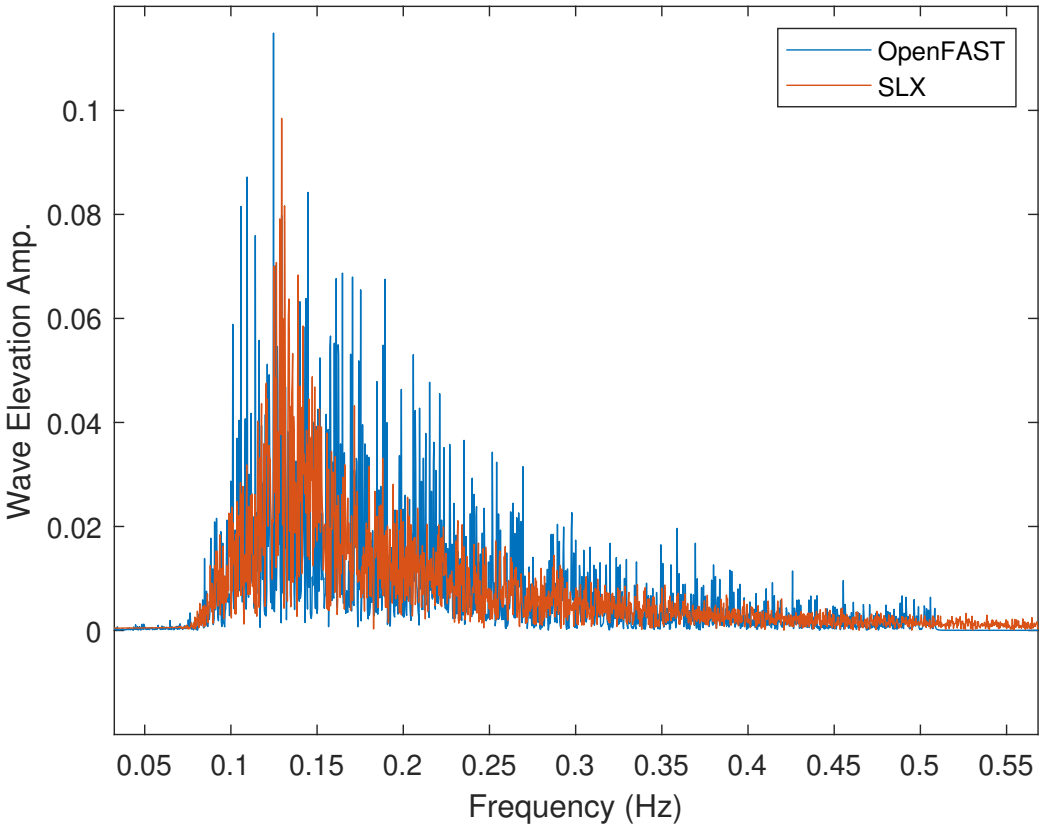

Figure 5.8: Wave elevation spectrum for an irregular wave at rated wind speed for the IEA15MW wind turbine with H_s of 1.53m and T_p of 7.65s. The spectrum of the wave generated in OpenFAST is compared with that generated by the HIL Simulink Model (SLX).

The wave elevation spectrum compares well between OpenFAST and the HIL Simulink Model. From Figure 5.8 the wave frequency can be identified, which is around 0.13 Hz. With the generated wave the diffraction forces are calculated assuming 0°wave heading. Then the floating dynamics of the system is solved to obtain the platform motion response which is depicted in Figure 5.9 The results from the OpenFAST model and the HIL Simulink model are compared. It can be seen that surge, pitch and heave DOFs have displacements, whereas the sway, roll and yaw DOFs have minor displacements.

It can also be noticed that the IEA15MW model takes longer to reach an equilibrium position compared to the DTU10MW. The motion response from the OpenFAST model resembles the response from the HIL Simulink Model, however the magnitude of displacements differs slightly. Since the Simulink model has linear damping and the OpenFAST model is designed with quadratic damping, there is some discrepancy in the initial displacements, however the responses match well towards the end. This discrepancy is accepted since the initial response is mainly due to the sudden application of wave forces from a neutral state, this transition period is cut off during the final HIL tests in the wind tunnel.

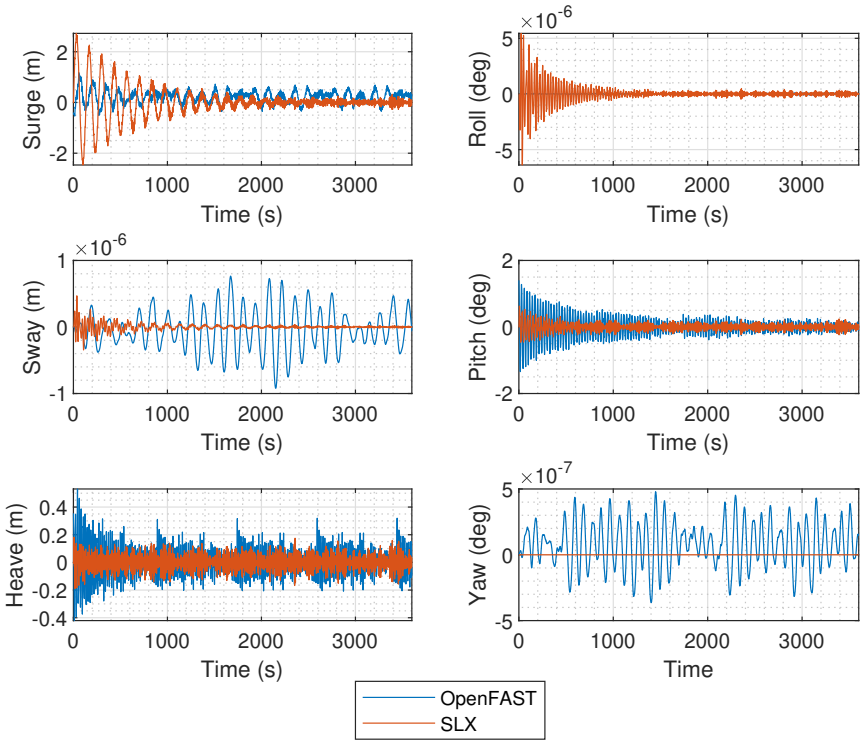

Figure 5.9: Motion time history of IEA15MW FOWT model with VolturnUS floater for the wave case at rated wind condition compared between HIL Simulink model and OpenFAST. The cases are compared assuming no wind.

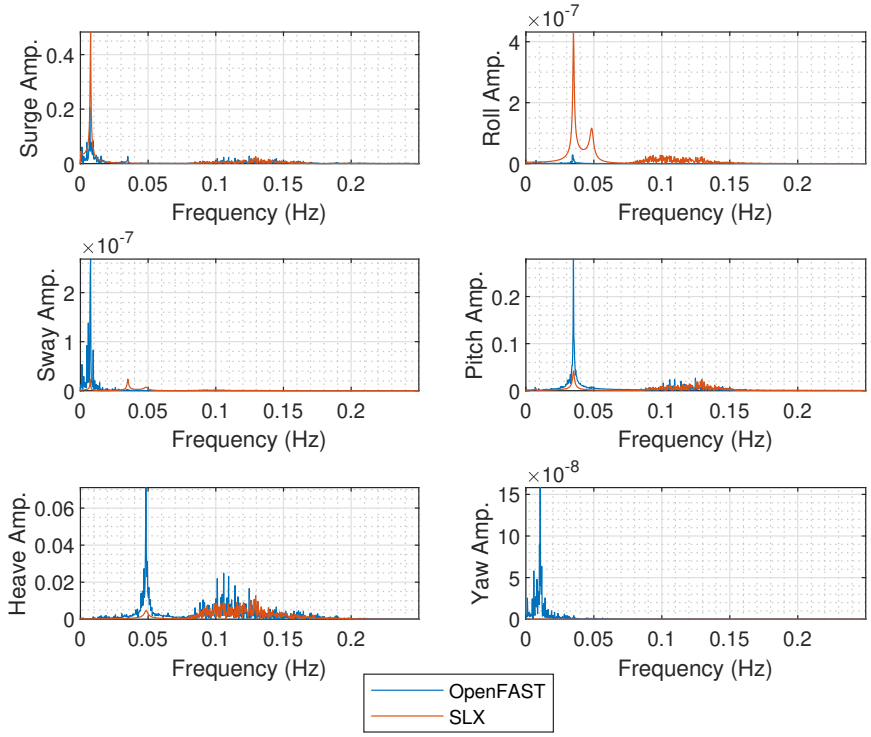

Figure 5.10: Motion spectra of IEA15MW FOWT model with VolturnUS floater for the wave case at rated wind condition compared between HIL simulink model and OpenFAST. The cases are compared in all DOFs assuming no wind.

The motion spectra of the VolturnUS floater under the influence of an irregular wave can be visualized in Figure 5.10. From the plots, it can be noticed that there is activity in the wave frequency range and in the natural frequency range. The spectra match well around the wave frequency but the peak amplitudes at the natural frequency range differ. This effect could also be attributed to the effects of the initial oscillations being different due to the different viscous damping mechanisms followed.

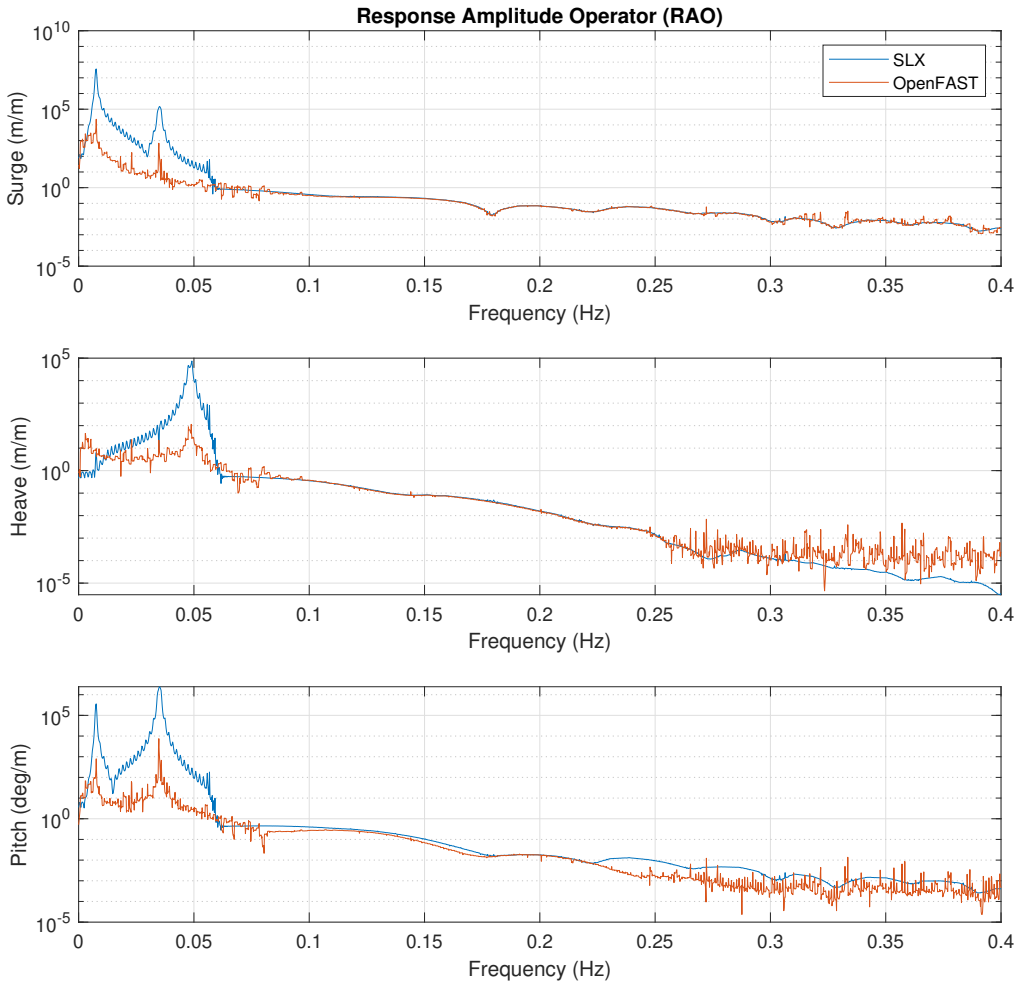

Figure 5.11: Comparision of the platform displacement RAO obtained for the Simulink and the OpenFAST model for the IEA15MW wind turbine with VolturnUS using the wave case at rated conditions assuming no wind.

From the RAO plots in Figure 5.11 it can be seen that the RAOs in the mid and higher frequency range (after 0.1 Hz) have good matching. The RAO peaks in the low-frequency range are consistently higher for the Simulink model compared to OpenFAST. This is due to the discrepancies in the damping mechanism. The Simulink model has a stronger response to the wave in lower frequencies, this is due to the linear damping modification. The matching in the higher-frequency range is much more significant for design and testing hence these results are considered acceptable.

5.2. Preliminary Closed Loop HIL Testing

After tuning and verifying the numerical floating dynamic performance of the FOWT by comparing the free decays of the Simulink HIL model with FAST/OpenFAST tool, the next stage of testing is done which is the closed loop HIL test. This test uses the HIL setup with the wind turbine, the hexapod, and the instrumentation system. The preliminary tests are done outside the wind tunnel in a laboratory and

with the rotor turned off.

The developed Simulink HIL model is integrated into the overall Simulink program, which interfaces with both the dSPACE system and the Hexapod. All force and acceleration sensors are set up to provide feedback to the HIL model. Consequently, a responsive dynamic FOWT model is established. With the established model, it is possible to provide external forces by manually applying them or controlling the WTM's motion with the Simulink program's help.

The testing with this setup is referred to as closed-loop testing since the HIL setup is utilized. However this is different from the final experiment since it is not done in a wind tunnel, hence only preliminary tests are done with this setup for verification. This test is essential for verifying the force feedback mechanisms, the force correction and also the system's motion actuation. This test also helps make sure the latency of the HIL setup is not too high.

First, the HIL Simulink model of the DTU10MW wind turbine with the TripleSpar floater is tested. Manual force is applied to the model for every DOF. The response to the manual force was found to be appropriate and the system reached an equilibrium position in due time. Forces in multiple DOFs were also applied simultaneously to the system and this also had a satisfactory result. So the force feedback and the actuation were verified and the latency of the system was also acceptable.

The force correction methodology was also verified with the help of these tests. Analysing the data recorded during the tests, the signals for the corrected aerodynamic forces swiftly settled at zero after the applied external force was removed. This was checked in all the degrees of freedom. Due to the methodology chosen for correction, the yaw DOF does not have any correction implemented. This makes sense logically since the inertial and gravitational effects in this DOF are small.

The same kind of preliminary tests were also done for the IEA15MW + VolturnUS model. The HIL system was set up with the new FOWT properties and scaling factors. Unfortunately, upon the application of physical force, the system did not approach equilibrium. The oscillations grew and the system quickly became unstable. Decays with the HIL setup were also simulated, but the decay motions diverged instead of damping. The reasons for this instability are explored in the next section.

5.3. Feasibility of IEA15MW + VolturnUS model

From the open-loop testing, the IEA15MW with VolturnUS FOWT model produced satisfactory results when compared with the OpenFAST model. However, in a closed-loop setup, the results did not match. The system grew unstable in closed-loop with the oscillations rapidly growing. To troubleshoot the problem a step-by-step approach was taken to check the numerical model for errors in the structural, hydrodynamics and mooring line properties of the FOWT model. The consistency of scaling factors used was also verified throughout the model. Slightly higher velocity factors around 1:2.7 were also tested with no success. The instability of the model is likely due to a combination of the following factors:

1. Modifications to viscous damping:

   The official UMain's VoltunUS model was designed without any linear viscous damping terms. The provided viscous damping matrix was quadratic which made reaching an equilibrium position impossible for the floater. A continuous oscillating response is difficult to model in a HIL system and it is also not realistic to have a floater with continuous oscillation. Hence, the linear viscous damping terms were empirically chosen based on the decay response.

   Having a linear damping matrix is easier to model however they do not capture the system's nonlinearities. Since the damping terms were identified empirically, they could introduce errors in the system. This could be a cause of the instability since it does not reflect the actual design as per the documentation.

2. Overambitious scaling factors:

   The scaling factors chosen for the wind turbine model are more stringent than the DTU10MW with the TripleSpar model. The scaling factors for the mass and force are very small ($\lambda_{mass} = 1/7,900,827.58$ and $\lambda_{force} = 1/247,929.62$), mass scaling factor is around 2.5 times smaller for

the IEA15MW model compared to the DTU10MW. Similarly, the force is 25% smaller. This means that the forces and inertia measured are much smaller than in real-life conditions. Minute errors in the forces measured or the mass and inertia identified can result in numerical instability.

Another issue is the large scaling factors for frequency ($\lambda_{freq} = 1/0.013$), this is 62% larger than the frequency scaling factor for the DTU10MW model. This means that the dynamics that are simulated happen at much shorter durations. Accurately simulating the dynamics over this small period is difficult in a responsive system. Having a noisy input or having a time step that is too big makes this problem more significant and could lead to an unstable system.

3. System identification errors:

   The system identification for the wind turbine model was done analytically by observing the force and acceleration measurements in imposed motions. Knowing the acceleration and the force, the mass of the RNA could be derived easily. The inertia of the RNA was approximated to 0 after testing the force correction module.

   The accuracy of the mass and inertia values is not that good since either an empirical or analytical approach is taken for its determination. This accuracy is more important for the IEA15MW model due to the drastic scaling for mass. Errors in the system identification thus also result in numerical instability.

4. Lack of signal filter:

   The system's response to the measured forces is more sensitive for the IEA15MW model due to the small force scaling factor. Since no signal filtering is implemented in the HIL system, the signal noise from the sensors could be interpreted as external forces acting on the system potentially leading to instability. An implementation of a lowpass filter was tested but it failed to comply with the real-time conditions and, hence was discarded.

5. Latency the HIL system:

   Latency is often defined as the delay between the input signal and response in a system. A high latency can cause a phase difference in the loop and potentially cause oscillations and instability. The HIL model is a dynamic system that is dependent on feedback and on time. With a feedback delay, the system could become inaccurate and unstable. The time scaling factor for the IEA15MW model is 38% smaller which means the latency has a higher chance of causing issues for this model.

After a thorough analysis, the reasons for instability were determined. However, the solutions to these problems are not easily achieved. Identifying a new viscous damping matrix can be done with the help of Morison's equation or with CFD, however, the data on the geometry of the floater is not available so this could not be done. The scaling factors also cannot be modified much since the length scale is fixed by the size of the wind turbine model and changing the velocity scale by 0.2 points resulted in the same instability.

The system identification could be improved to have more accuracy if the 3D model of the wind turbine model is available with material properties. Or with the help of a 6DOF accelerometer. More time could be invested to also develop a lowpass filter for the signals resulting in a lower delay. More analysis of the latency could be done to identify the biggest cause and make the system more efficient and accurate.

These solutions could be carried out in future research. However, they were too time-intensive for the scope of this project, thus with the current setup the IEA15MW model with the VoltunUS floater was deemed unfeasible for HIL testing in wind tunnels. The DTU10MW model with the TripleSpar floater on the other hand was successfully validated with FAST and can be further tested in the wind tunnels.

5.4. Final HIL test in the Wind Tunnel

The validated DTU10MW with the TripleSpar model was finally tested in the wind tunnel at the OJF in TU Delft. A series of experiments were conducted whose main objective was to assess the capability of the

HIL model to reproduce real-world conditions. The full dynamic capability of the model was also aimed to be tested and validated. The response of the model to various environmental conditions was also tested. All the input signals, measurements and responses were recorded for further analysis.

The tests in the wind tunnel were carried out in three parts. The first part involved static cases where only the aerodynamic forces acting on the rotor at different operating conditions (wind speeds and rotor speeds) were recorded. The operating conditions were determined using the full scaling operating parameters. The wind speed and rotor speed from the full-scale FOWT model were scaled down, and the relevant points below and at rated conditions were tested. Additional operating points with a fixed tip speed ratio were also included in the experiment.

The second part involves decay tests. These tests were done in a closed-loop setting inside the wind tunnel. The HIL model was controlled with an interface developed in-house for previous experiments. A user-defined external force was applied to the model at each degree of freedom. Once the model reached an equilibrium position with the applied force, the force was removed and the response was recorded for decay tests. Each degree of freedom was tested with three different force magnitudes, with and without the presence of wind in a closed loop. This results in a total of 36 test cases. The maximum force magnitude for each test was also initially tested in open-loop, i.e. with HIL disabled to make sure the initial displacement was within the workspace of the hexapod.

The third and final part involves testing with irregular waves based on the JONSWAP spectrum. Different sea state conditions are simulated with the help of the HIL Simulink model, starting from calm seas to rougher seas. The wind speed in the tunnel and the rotor speeds are also changed to match the sea state condition. The response of the HIL model for the different wave cases is recorded and analysed. The waves were generated using the MATLAB script mentioned in subsection 4.3.2.

5.4.1. Preparation for the Test Campaign

To prepare for the testing the wind turbine model was assembled in the low-speed wind tunnel in the OJF. The test area was cleared and the best location for the HIL setup was determined based on knowledge of the wind quality. The HIL setup was placed at the closest location to the nozzle of the wind tunnel and at a height where the wind turbine is facing the nozzle parallelly and is approximately in the middle of the wind tunnel's nozzle height. The height of the set-up is fixed with the help of a table with adjustable height. The hub height was finally measured to be 2355mm from the floor. The rotor hub's distance from the nozzle was approximately 100mm.

The hexapod, the wind turbine model and whole instrumentation is assembled at the location and the orientation is verified with the help of a laser level. Before the testing, checks were done to assess the loadcell and accelerometer measurements in all DOFs. The rotor of the wind turbine model is also checked along with the breaking resistor. Next the hexapod and the user interface to control the whole system is also checked. The user interface is setup in the control room adjacent to the wind tunnel so the tests could be conducted remotely.

Later, the HIL Simulink model was loaded with the interface and the model's response was checked in open-loop and close-loop briefly, similar to what was done during the preliminary tests. Finally, the wind speeds within the wind tunnel were checked with an fan anemometer. After all the checks the setup was ready for the official testing. The data from each test was recorded and analysed. The main results from the data analysis are discussed in the next chapter.

6

Results and Discussion

In this chapter the results from the experimental testing done in the wind tunnel are documented. The chapter is mainly divided into three sections based on the type of test conducted. The first section discusses static cases that are important in understanding the performance of the wind turbine model under different uniform wind speed conditions. The second section discusses the decay tests which are crucial for analysing the floating dynamic performance of the HIL model, the effects of wind on these tests are also explored. The last section discusses the wave conditions with both wind and wave loading on the system, the capability of the HIL model to handle the loading is tested and its accuracy is verified. The contents of this chapter mostly deal with the wind turbine model and the HIL system in the wind tunnel, hence most of the values presented are in the model scale.

6.1. Static Case

In the static cases the wind turbine is in a fixed position with the rotor operational. The performance of the wind turbine model is analysed in these tests. The signals from the motor and from the loadcell are used to determine the aerodynamic thrust, rotor torque and power. Uniform wind from the wind tunnel is used to test various operating points. The rotor speed is fixed manually according to the wind speed.

Two sets of operating points are tested in the static case. The first set was formed assuming a constant TSR to derive the rotor speed according to the wind speed. The design tip speed ratio for the DTU10MW wind turbine is used which is 7.5. For example, for a wind speed of 9 m/s at full scale the rotor speed was 7.23 rpm according to the TSR formula. The wind speed and the rotor speed are scaled down to the model scale using the defined scaling factors, resulting in a wind speed of 3 m/s and a rotor speed of 357 rpm. For the second set of operating parameters the wind speed and rotor speed values from the DTU10MW definition [81] are directly scaled.

For evaluating the performance of the wind turbine model, the thrust, torque and power values are needed. The aerodynamic thrust and the rotor torque are measured by the load cell placed on top of the tower. Aerodynamic thrust is taken as the x component of the force measured. The torque is taken as the ϕ (roll) component of the force measured. The power is calculated using the relation $P = T_x \times \omega$ where T_x is torque in x axis and ω is the rotational speed in rad/s.

Another approach to finding the power and torque is using the signals from the motor encoder. The torque is directly obtained from the encoder signal, to obtain the rotor torque this value needs to be multiplied by the transmission ratio, in addition to this, the units of the torque from the encoder are N.mm so a factor of 10^-3 is multiplied to the values. The power can be found from the torque using the same relation as before. The transmission ratio according to the specifications of the motor is 5.8.

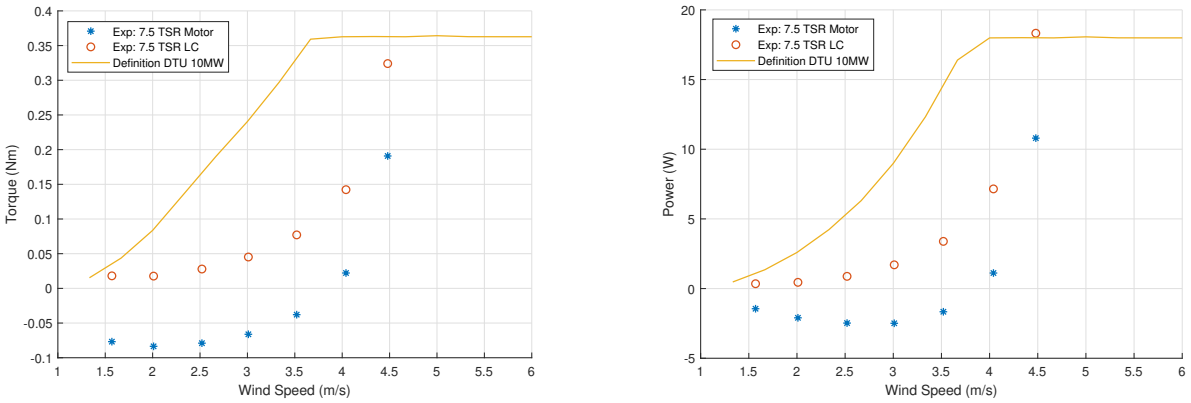

Figure 6.1: Comparison of torque and power (left and right resp.) values from the motor and the loadcell with the values from the DTU10MW definition.

From Figure 6.1, the torque and power results can be compared with the values from the definition. The values are all scaled down to the model scale. The values from the load cell for both the torque and power are closer to the values in the definition. This is because the current in the motor varies a lot depending on the input voltage and the temperature. Thus, in the rest of the report, the thrust, torque and power values are derived from the loadcell measurements.

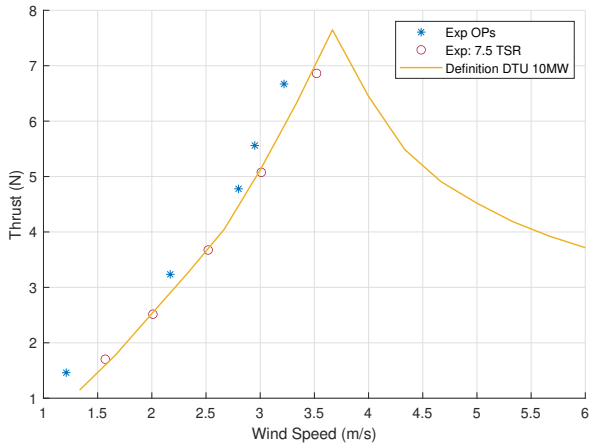

Figure 6.2: Thrust curve

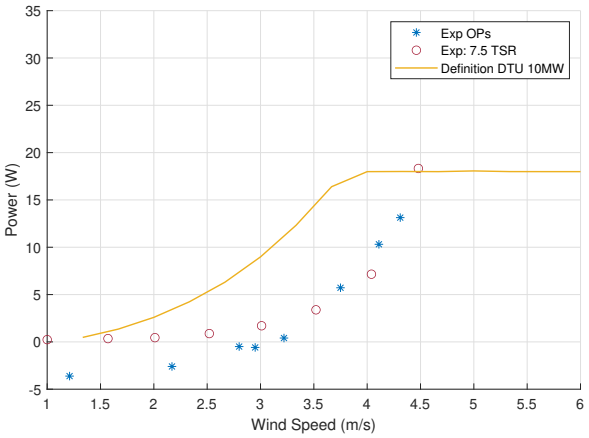

Figure 6.3: Power curve

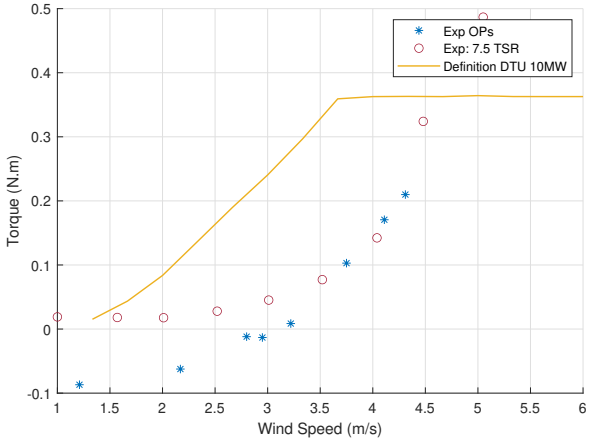

Figure 6.4: Torque curve

The aerodynamic performance of the wind turbine model is verified by comparing the thrust, power and torque curves obtained from the definition and the experiments conducted. Both sets of operating parameters are plotted in the graphs for comparison. As seen from Figure 6.2, in the below-rated region, the results from the constant TSR operating points provide a better match with the values from the definition. The power and torque comparison can be visualized with Figure 6.3 and Figure 6.4. The results from the experiments do not match perfectly with the curves from the definition however they are in the range. This result is as expected since the wind turbine model was designed to reproduce aerodynamic thrust and not power or torque. With this, the aerodynamic performance is verified successfully.

6.2. Decay Test Cases

Decay tests are an efficient way of testing the dynamics of floating structures. These tests were conducted for all six degrees of freedom with varying initial displacements. Initially, tests were done in open-loop (purely numerical), followed by closed-loop with system feedback, and finally in closed-loop with wind at rated condition i.e. wind at 4 m/s with the rotor operating at 480 rpm. The applied wind offset the hexapod from zero position, this was corrected to keep decay motions within the workspace. Motion time history results were adjusted later during data analysis to approximate equilibrium at zero position. In this test the performance of the simulated floater was assessed. The effects of wind and different initial displacements on the decays are also examined.

The process of comparison of results follows the schematic provided in Figure 6.5. It starts with the comparison between FAST/OpenFAST with the Simulink model to validate the numerical model. This is the first step and is discussed in the previous chapter. With the validated Simulink model the next step is to validate the HIL system. Following these validation steps the main experiment is conducted with the presence of wind. The third and final step compares the results without and without wind to understand its influence. In this section steps 2 and 3 are discussed which involve three data sets, i.e. Open-Loop (OL), Closed-Loop (CL) and Closed-Loop with Wind (CL+W). The results from the Simulink model discussed in the previous chapter are the same as the results from the Open-Loop setting, there is only a difference in the scaling factors. Steps 2 and 3 are conducted on model-scale while step 1 is done on full-scale.

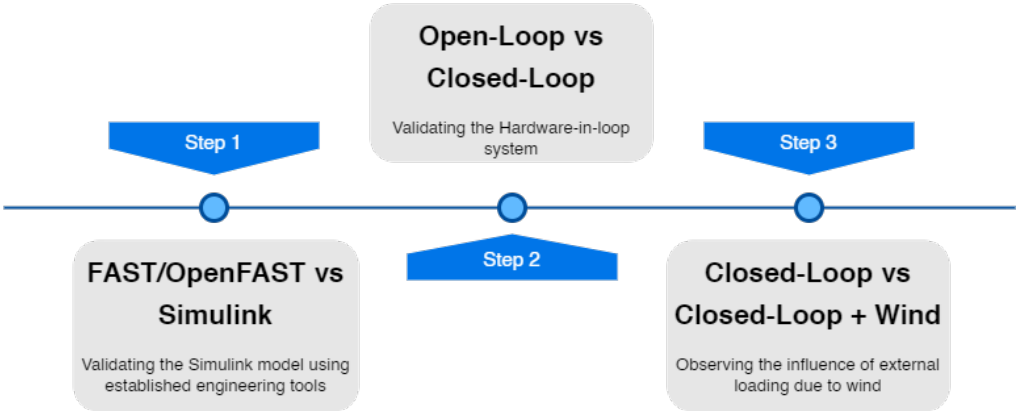

Figure 6.5: Schema of the step-by-step process taken for HIL testing in wind tunnels

6.2.1. Open-loop vs Closed-loop

Comparison between open-loop and closed-loop is necessary before proceeding with the real experimental tests with wind. The results from the open-loop and closed-loop should match sufficiently to be able to proceed. This ensures that the HIL system is working correctly. The HIL system referred to here involves specifically the feedback mechanisms, the force correction, the motion actuation, and the latency. A comparable result means the above-mentioned systems are working correctly and this will ensure that the results from the tests with wind are accurate. The comparison between open-loop and closed-loop is only done for the highest displacement for all the DOFs. The highest displacement tests the limits of the setup, hence if the results for this match then the lower displacements would also

match. The decay motion comparison is depicted in Figure 6.6.

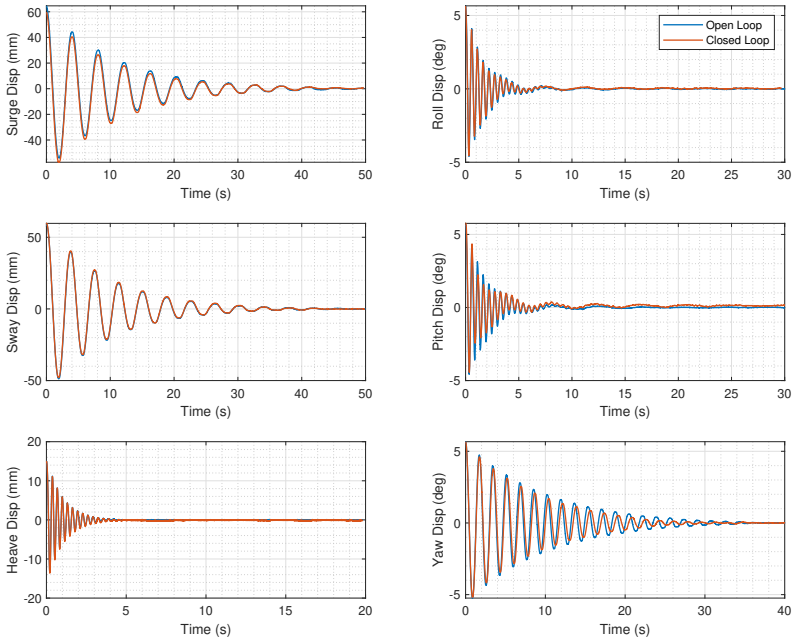

Figure 6.6: Decay motion history comparison between open-loop and closed-loop setting in 6DOF with maximum initial displacement. The DTU10MW model with the TripleSpar floater is used for the simulation.

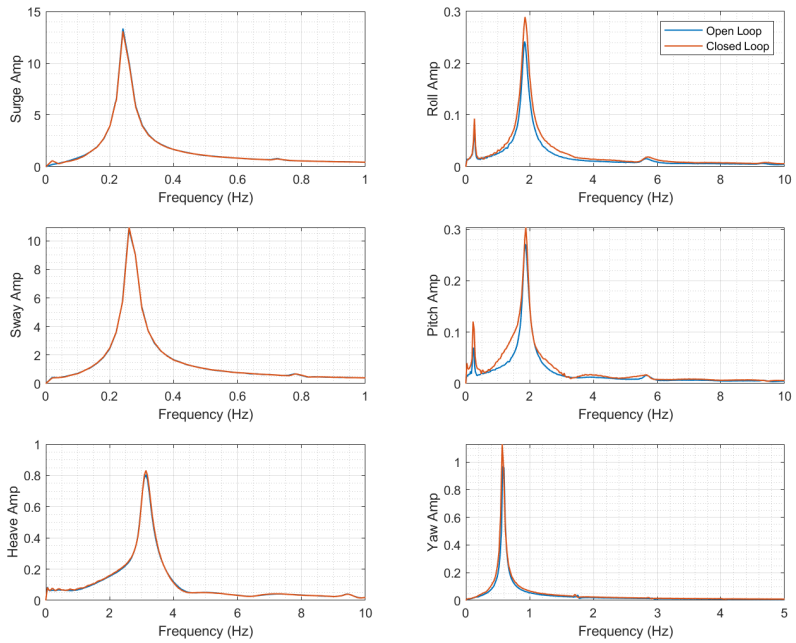

Figure 6.7: Decay motion spectra comparison between open-loop and closed-loop setting in 6DOF with maximum initial displacement. The DTU10MW model with the TripleSpar floater is used for the simulation.

The OL motion history depicted above is the numerical results for the initial displacement solved by the HIL Simulink program. The closed-loop results are with the HIL system, and it depicts the actual position measured by the hexapod. From the comparison, it can be seen that the responses from open-loop and closed-loop are virtually identical. To further study the response, an FFT was performed on the motion history to obtain the motion spectra, which are provided in Figure 6.7. The spectra in the translational motion match perfectly whereas the discrepancies are noticed slightly in the rotational motion. This is more pronounced due to the smaller displacements in these DOFs making it more difficult for the HIL system to achieve perfect actuation. Nevertheless, the shapes of the peaks and the positions match perfectly, thus validating the HIL. Following this, the HIL experimental testing with wind was done.

6.2.2. Large Displacement

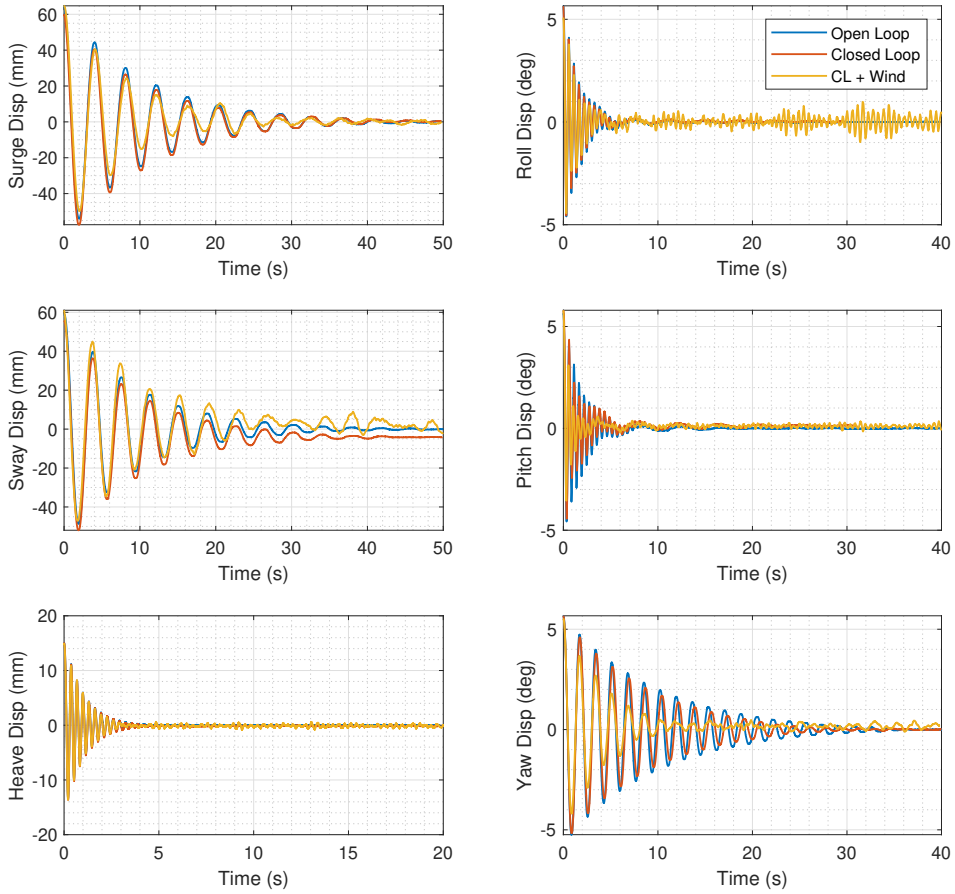

Figure 6.8: Decay motion history in 6DOF with maximum initial displacement. The decay tests were held with the HIL setup in the windtunnel with the DTU10MW with TripleSpar numerical model. The motion history from open-loop, closed-loop and closed-loop with wind are compared.

The decay motions in Figure 6.8 correspond to the actual position, measured by the hexapod and saved as a time history. The motion time history shows that closed loop and open loop responses follow the same path in all degrees of freedom. The closed-loop with wind case however is more erratic. It has a noisy response in the roll DOF, however, this could be explained due to the rotor's rotation in this DOF. Since roll and sway are coupled the sway response is also disturbed. The presence of wind can be noticed clearly in the surge, pitch and yaw decays. The wind causes disturbance to the oscillating motion, however unlike with the effect of the rotor, the disturbance due to wind causes a dampening

effect of the decay in these particular DOFs allowing it to reach an equilibrium position faster. The damping effects can be better visualized with the help of a spectrum for the decay motion of each DOF, this is provided in Figure 6.9.

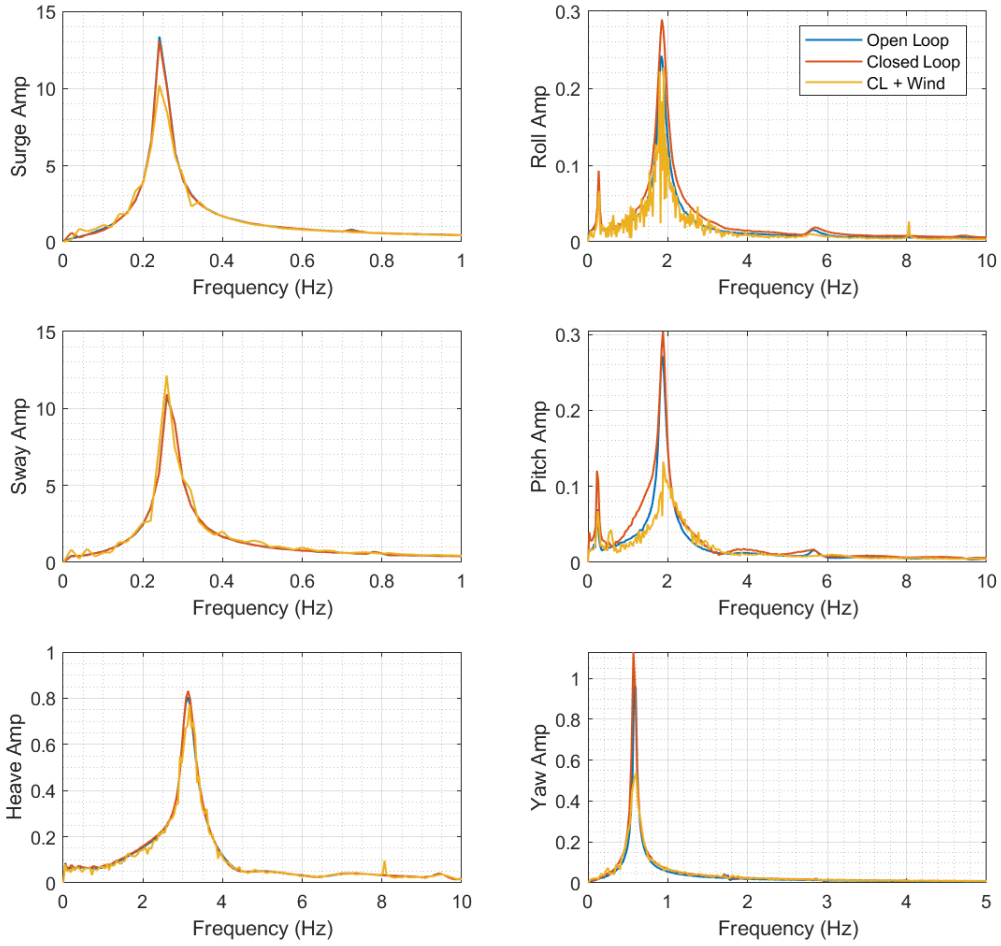

Figure 6.9: Spectrum of decay motion done with HIL testing in 6DOF with maximum initial displacement. The sprectrum from decays in open-loop, closed-loop and closed-loop with wind are compared.

The Figure 6.9 provides the natural frequency of the DOFs, this is the biggest peak visible in the plots. The frequencies are in the model scale, when they are scaled to the full scale, the values match with the results from FAST. There is another peak visible in the roll and pitch DOFs before the peak of the natural frequency, this is the natural frequency of sway and surge respectively. This peak is visible since roll and pitch are coupled to sway and surge. Another tiny peak is visible around 8Hz in the heave and roll DOF, this is the 1P frequency of the rotor. Only the roll and heave DOFs have a peak for the 1P frequency since there are directions in which the rotational acceleration of the rotor is aligned.

The spectrum with the wind has peaks are that lower in height and broader in the surge, pitch and yaw degrees of freedom, this means that the wind provides damping. The thrust force from the wind acting on the rotor has a damping effect on the motion in these DOFs since these motions are against the direction of wind flow (x-direction). The aim of this test is to analyse the natural frequency and the damping, thus a quantitative analysis is also done and the results are tabulated in Table 6.1.

DOFs	Open-loop		Closed-loop		Closed-loop + Wind	
	Nat Freq. (Hz)	Damping (-)	Nat Freq. (Hz)	Damping (-)	Nat Freq.(Hz)	Damping (-)
Surge	0.005	0.0614	0.005	0.675	0.005	0.0743
Sway	0.0054	0.0628	0.0054	0.0678	0.0056	0.0459
Heave	0.0666	0.0523	0.0665	0.0509	0.0665	0.0461
Roll	0.038	0.0581	0.0377	0.062	0.0378	0.0797
Pitch	0.0384	0.0498	0.0384	0.0452	0.0401	0.169
Yaw	0.012	0.0277	0.0116	0.0309	0.0118	0.0493

Table 6.1: Natural frequencies and damping ratios obtained from decay tests done using the HIL setup with large initial displacements, for different DOFs under different test settings. The values have been scaled from model-scale to full-scale.

6.2.3. Medium displacement

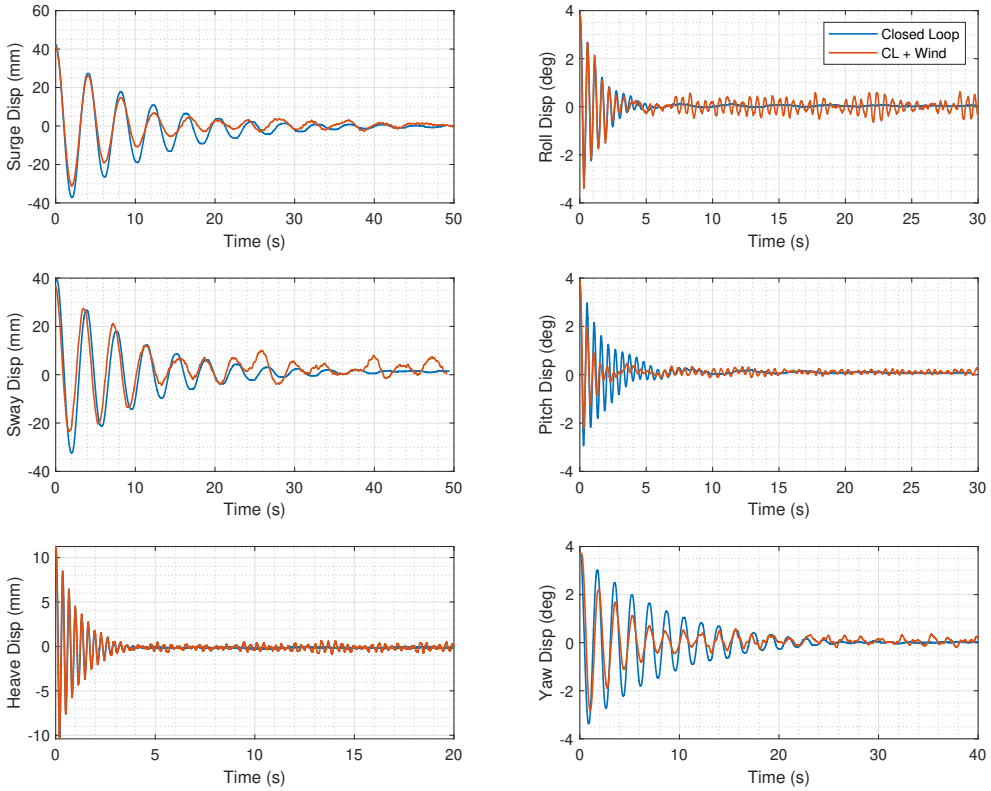

Figure 6.10: Decay motion history with medium displacement from HIL testing with and without wind in a closed-loop setting. The decays are done in model scale for all the 6DOFs with the DTU10MW numerical model.

The decay tests were done again with a lower initial displacement compared to before. Since the results from open-loop and closed-loop settings were roughly the same in the previous tests, only the closed-loop with and without wind settings were chosen to test this case.

From Figure 6.10, similar decay behaviour can be observed compared to the previous test case. As seen before, the roll and sway DOFs have disturbances due to the rotor operating. Surge, pitch and yaw DOFs reach equilibrium faster due to disturbances caused by the wind. The effect of wind on the decay motion is more pronounced with a smaller initial displacement.

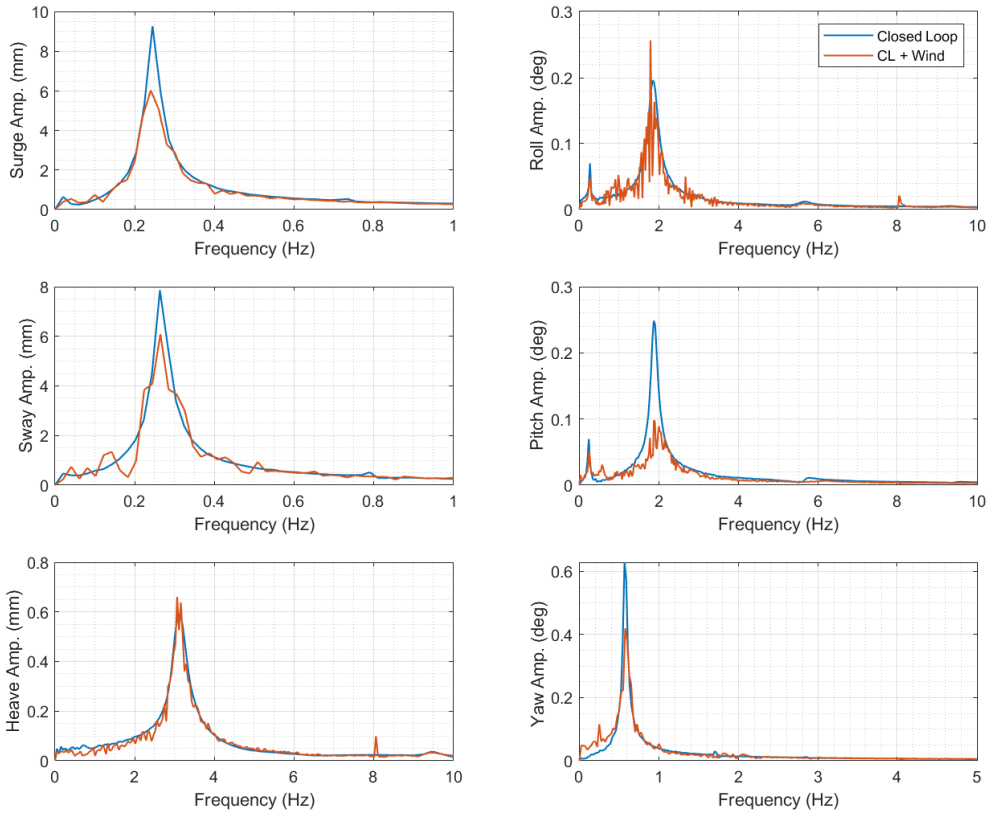

Figure 6.11: Spectrum of decay motion with medium initial displacement. The decay motion tests were conducted in a HIL setup with and without the presence of wind.

The spectrum of the decay motion with medium displacement is shown in Figure 6.11. The peaks still have approximately the same shape as in the previous test case. The smaller peaks are also visible, these are due to the rotor and coupling effect in roll and pitch as previously discussed. However, the amplitude of the spectrum is much lower, since the displacements are smaller. The effect of wind on the spectrum is more visible due to this since the magnitude of wind speed has not been changed. The damping effect can be clearly seen in the surge and pitch DOFs and also in yaw. Although, the damping in yaw is not as pronounced. This is also reflected in the quantitative analysis tabulated in Table 6.2

	Closed-Loop		**Closed-loop + Wind**	
DOFs	**Nat Freq. (Hz)**	**Damping Ratio (-)**	**Nat Freq. (Hz)**	**Damping Ratio (-)**
Surge	0.0051	0.0668	0.0051	0.0748
Sway	0.0054	0.0669	0.0054	0.0428
Heave	0.0646	0.0523	0.0642	0.0453
Roll	0.0354	0.0556	0.038	0.035
Pitch	0.0379	0.0518	0.0401	0.1318
Yaw	0.0117	0.0364	0.012	0.0404

Table 6.2: Natural frequencies and damping ratios obtained from decay tests done using the HIL setup with medium initial displacements, for different DOFs under different test settings. The values have been scaled from model-scale to full-scale.

6.2.4. Small Displacement

The decay tests are conducted again with a smaller displacement. The decay motion history and the spectrum obtained after FFT are provided in Figure 6.12 and Figure 6.13 respectively.

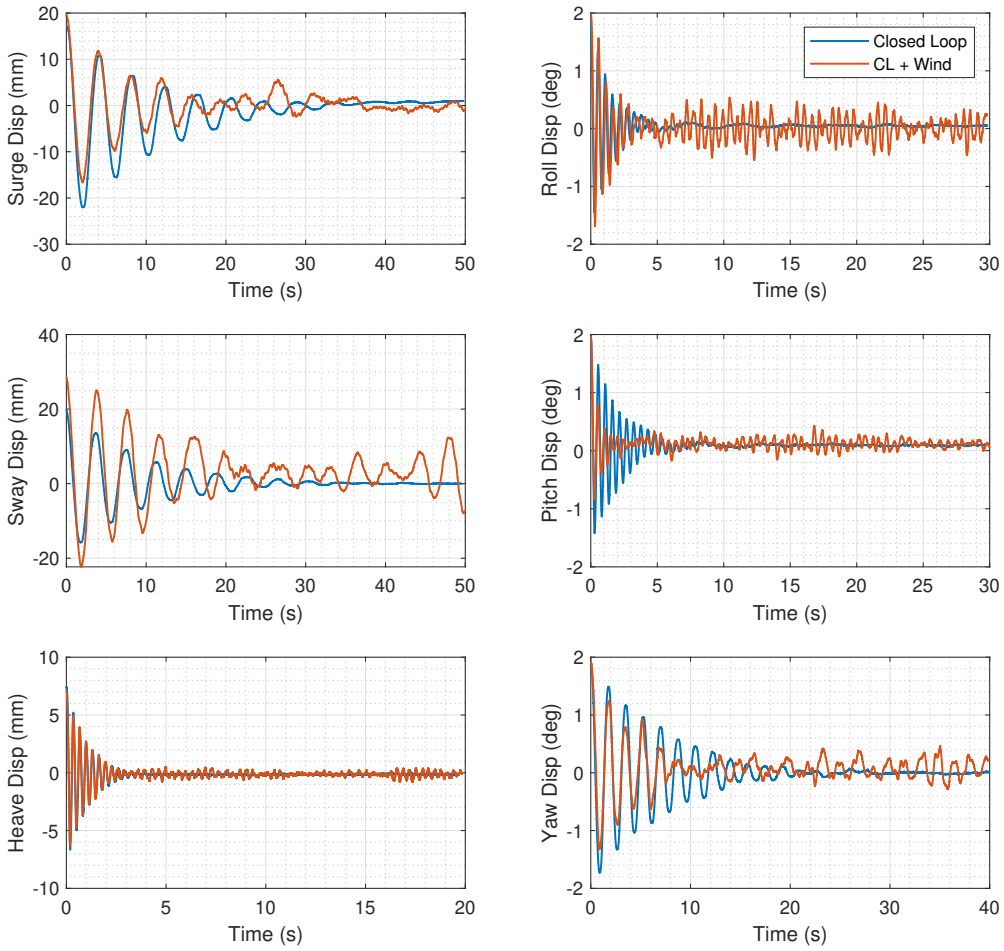

Figure 6.12: Decay motion history with small initial displacement from HIL testing with and without wind in a closed-loop setting. The decays are done in model scale for all the 6DOFs with the DTU10MW numerical model.

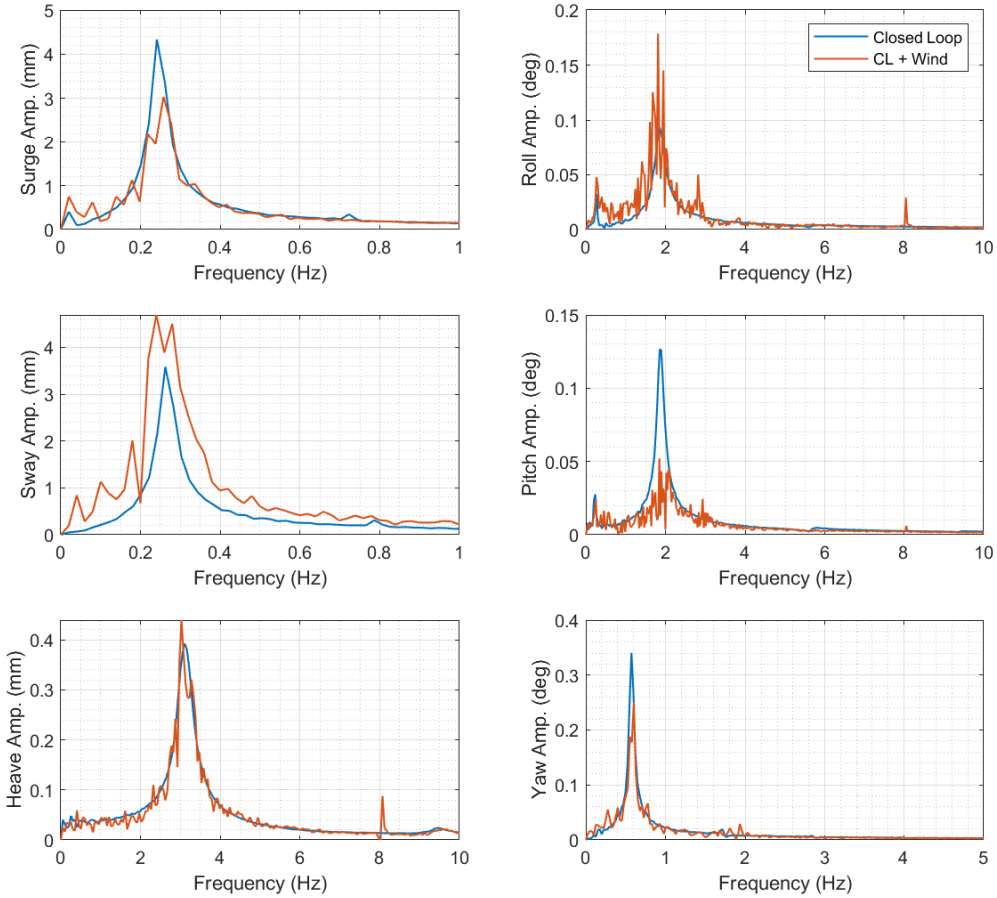

Figure 6.13: Spectrum of decay motion with small initial displacement. The decay motion tests were conducted in a HIL setup with and without the presence of wind.

From Figure 6.12 and Figure 6.13, it is visible that the disturbances in the motion is more drastic with the presence of wind in closed-loop setting. This is especially evident in the sway motion history which turns slightly unstable. The magnitude of displacement towards the end of the decay in the surge for the setting with wind is around 10mm. It is the also approximately the same magnitude in the tests done previously with different initial displacement.

However the spectrum matches poorly between the two different closed-loop settings. The setting with wind have bigger peaks that engulf the spectrum of the motion without wind. Despite this, the damping effect of the wind on the surge, pitch and slightly on the yaw DOF is still clearly visible. The peaks from the 1P rotor frequency and from the natural frequency of surge and sway on pitch and roll respectively is also visible. The motions in the presence of wind are more erratic, thus calculating a FFT for this signal proves more challenging with the small data sets, this results in a spectrum that is not as smooth as it is for closed-loop.

The natural frequencies and the damping ratios were calculated from the motion history in this test case with small displacement, they are documented in Table 6.3. The natural frequency values are highly accurate with only a maximum of 5% difference observed among the different decay test cases conducted. The damping ratios are more erratic, however the damping effects of wind on the surge, pitch and yaw motions are undeniable.

DOFs	Closed-loop		Closed-loop + Wind	
	Nat Freq. (Hz)	Damping Ratio (-)	Nat Freq. (Hz)	Damping Ratio (-)
Surge	0.005	0.0729	0.0051	0.0977
Sway	0.0053	0.0643	0.0053	0.0406
Heave	0.0634	0.0494	0.063	0.0372
Roll	0.0376	0.0584	0.0359	0.1073
Pitch	0.0381	0.044	0.0396	0.1386
Yaw	0.0116	0.0388	0.0125	0.072

Table 6.3: Natural frequencies and damping ratios for different degrees of freedom (DOFs) under closed-loop and closed-loop with wind conditions.

6.3. Irregular Wave Cases

In this test case, the ability of the HIL model to respond to wind and wave loads accurately similar to the real-world situation is tested and analysed. Irregular waves within the operational range of the FOWT were tested. Five sea states are tested in total, starting from calm seas to rougher seas, the met-ocean conditions at the five different sea states are provided in the Table 6.4 in full scale. The waves are aligned with the direction of the wind, and wind-wave misalignment effects are not tested in this case.

The irregular waves were generated using the JONSWAP spectrum for a wave period of 18000s or 5 hrs. In the model scale, this results in a simulation duration of approximately 365s or 6 minutes. However, the initial few transition seconds are not recorded. The waves are generated numerically in the HIL Simulink model which also scales the waves to model scale. The wind and the rotor speed were scaled and set manually for each sea state.

Since the wind turbine model lacks pitch control, wind speeds and rotor speeds are capped at the rated condition. Therefore, cases with higher wind speeds are approximated by the rated wind speed. The model experiences the highest aerodynamic loading at the rated condition, making wave cases above the rated wind speed more challenging than they would be in reality. This results in the system potentially overperforming, which is acceptable for this experiment aimed at testing capability.

Case	Wind speed (m/s)	Rotor speed (rpm)	Wave H_s (m)	Wave T_p (s)
WC1	7	6	1.38	7
WC2	7.1	6.04	1.67	8
WC3	10.3	8.27	2.2	8
WC4	11.4	9.6	3.04	9.5
WC5	11.4	9.6	4.29	10

Table 6.4: Irregular wave test cases with corresponding wind speeds, rotor speeds, wave heights (H_s), and wave peak periods (T_p).

All of the test cases in Table 6.4 were carried out in the wind tunnel with the HIL model. All the motions were within the limits of the hexapod and the dynamics were solved and actuated successfully. The input and output signals from the experiment were stored. The time history of the actual position, measured by the hexapod is used to create the spectrum of motion for all wave cases in all DOFs using FFT. The RAO of the wave cases were also computed and are documented in Equation C.1 [94].

The spectrum of the wave cases from the FFT provides useful information about the behaviour of the floating dynamics and the effect of the rotor and wind. The motion history is seen as a noisy oscillation with varying magnitudes, this is filtered using a lowpass filter and detrended before performing the FFT analysis to obtain useful spectrum data. The wave elevation spectrum would be the same as previously tested during the preliminary open-loop tests, except in the model scale. Thus only the spectrum of the motion history is provided below.

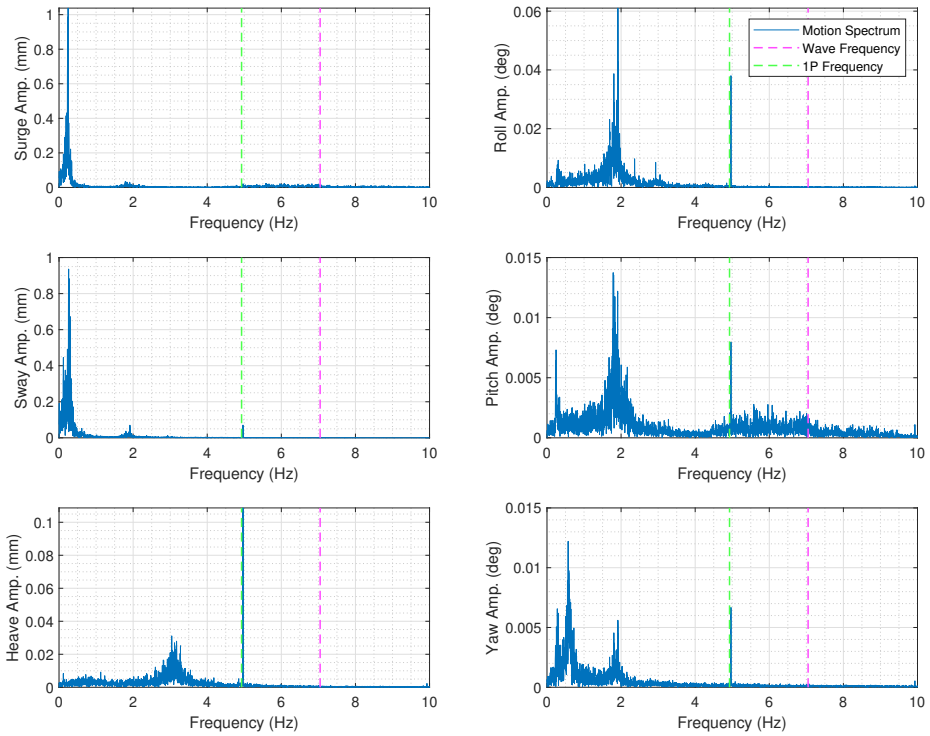

Figure 6.14: Sprectrum obtained after FFT of motion history for irregular wave case 1 tested in the wind tunnel.

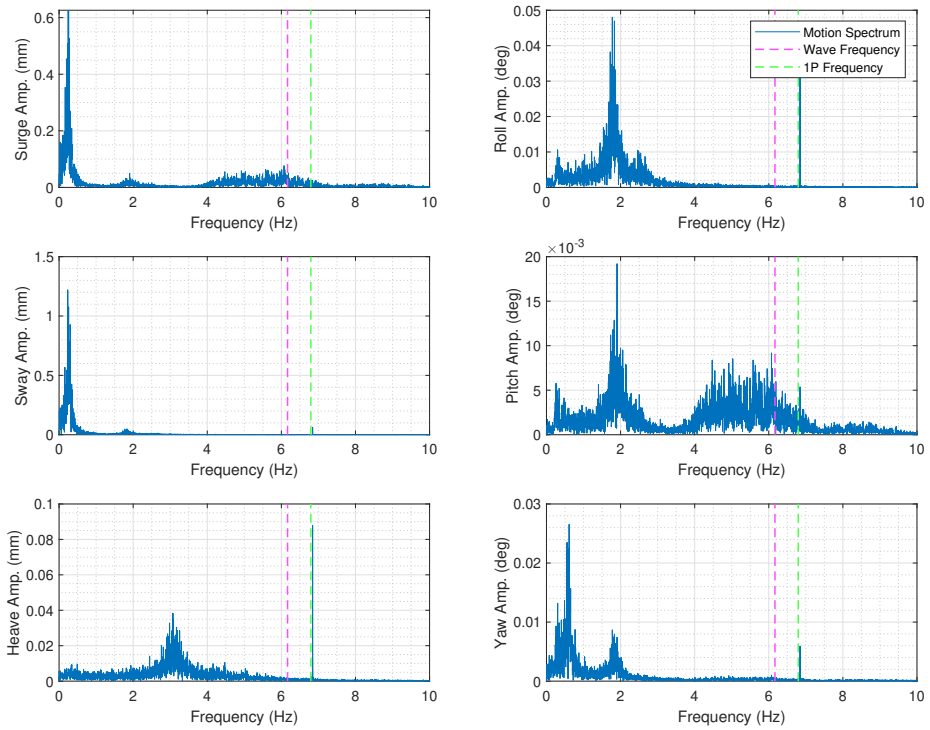

Figure 6.16: Sprectrum obtained after FFT of motion history for irregular wave case 3 tested in the wind tunnel.

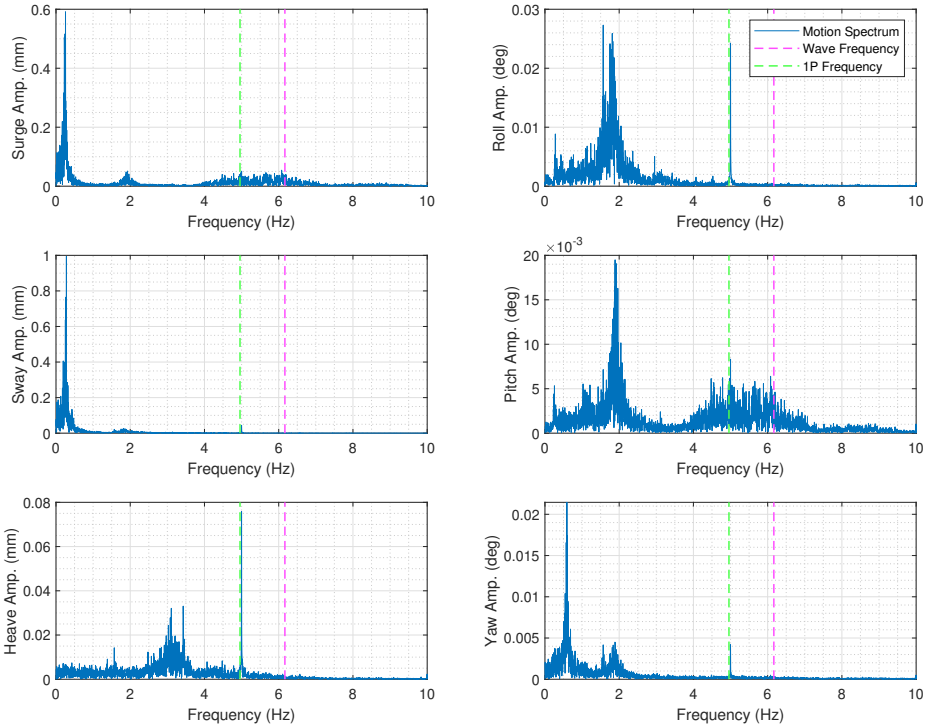

Figure 6.15: Sprectrum obtained after FFT of motion history for irregular wave case 2 tested in the wind tunnel.

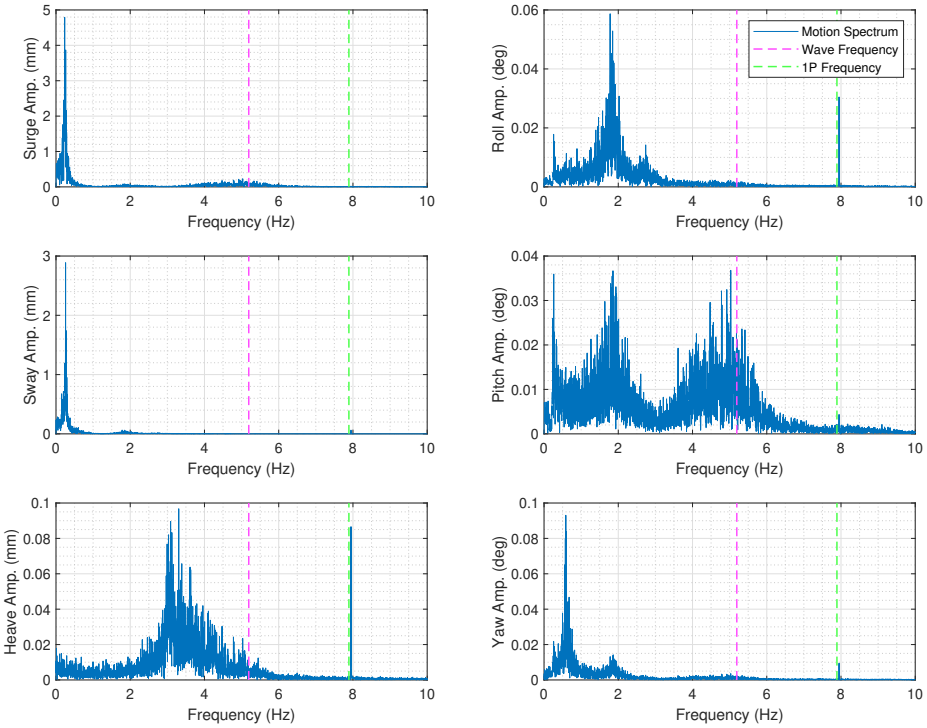

Figure 6.17: Sprectrum obtained after FFT of motion history for irregular wave case 4 tested in the wind tunnel.

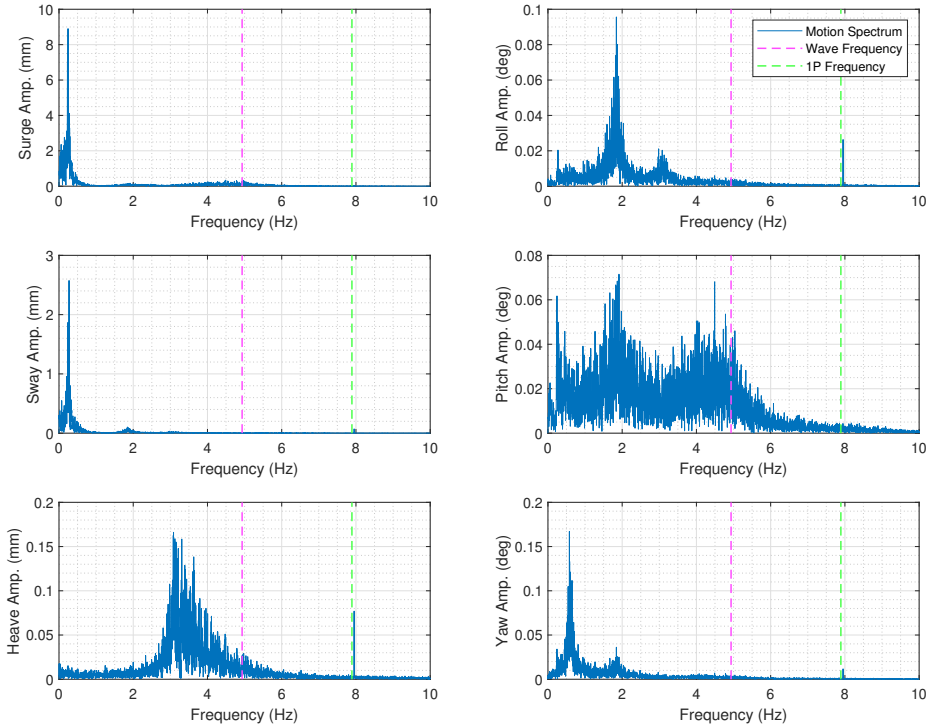

Figure 6.18: Sprectrum obtained after FFT of motion history for irregular wave case 5 tested in the wind tunnel.

From the motion history spectra above for the various wave cases, it is visible that there are two significant areas of activity. The first is near the natural frequency range of the floating platform, which is towards the lower frequency range this is also the region where the effects of wind are visible. The second area is around the wave frequency which is depicted with the purple dashed line, a broad region around this dashed line is affected by the waves. In the calmer waves, the peaks near the wave frequency are very small compared to the natural frequency peaks, this slowly shifts in the rougher seas where the peaks in the wave frequency range are as tall as the natural frequency peak. This is seen especially in the case of pitch in wave cases 4 and 5.

The magnitude of the spectrum also varies drastically between surge and sway and between roll and pitch. From this, it can be understood that the surge, pitch and heave DOFs have the most activity, especially in the wave frequency range. This is because the incoming wave forces only act in these DOFs since the waves and the wind are aligned at 0°, which is along the x-axis. The response in the roll DOF around the natural frequency range is also significant, the cause of this response is mainly due to the torque of the rotor.

The 1P frequency is the rotational speed of the rotor. This is closer towards the natural frequencies in the calmer sea states, it also had a relatively bigger amplitude and is visible in the roll, pitch, heave and yaw DOFs. In the rougher sea states it is mainly visible in roll and heave. The magnitude of the 1P frequency response is the highest in wave case 3 since the difference between the wave frequency and the 1P frequency is the least.

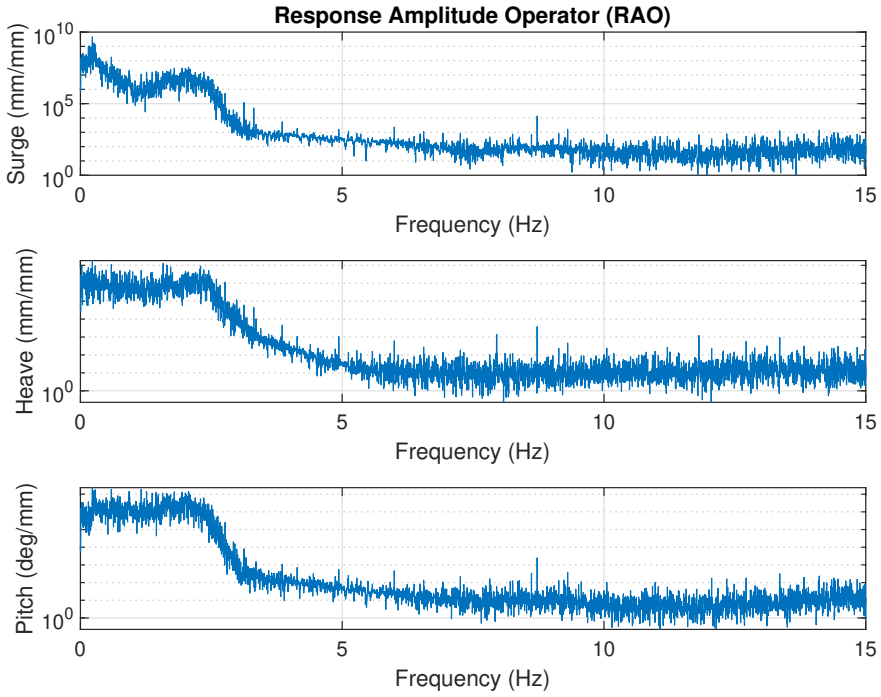

Figure 6.19: RAO obtained from the platform motion for wave case 4

The RAOs obtained for all the wave cases closely match as expected. The plots for the RAO obtained from the different wave cases are provided in Appendix C. From Figure 6.19 the RAO for the wave case 4 can be visualized. The shape of the curves closely resembles the plots in Figure 5.7. However, the results from the wind tunnel test are in the model scale, so the magnitudes cannot be directly compared. The RAO obtained from the experimental data is much noisier compared to the numerical data, the reasons for this can be due to the effects of scaling and the disturbances due to the wind and the rotor. Despite that, the peaks of the RAO are still clearly visible from which the dynamic responses of the FOWT model can be analysed.

7

Conclusion

This project aimed to develop a numerical model that can solve the dynamics of a scaled floating offshore wind turbine model in real-time with applied external aerodynamic loads and predefined met-ocean conditions. The work of this thesis is just one part of a bigger project that is to develop a functional hardware-in-loop setup in a wind tunnel that can simulate the dynamic behaviour of a floating offshore wind turbine. This setup is meant to be used for experimental testing to understand the special aerodynamic effects that occur in FOWTs.

The work of this project was divided into four sub-questions whose answers were necessary to achieve the main aim. The defined questions and the answers to each of them are concluded after a thorough research below,

1) How are the dynamics of a fully coupled FOWT system with given aerodynamic loads and met-ocean conditions modelled in real-time for use in Hardware-in-loop testing in a wind tunnel?

The short version of the answer for this would be that the dynamics of the FOWT in this project are solved with the Cummins equation. This equation is also commonly used in research and the industry for solving the dynamics of floating structures. However, each component of the equation also needs to be derived before it can be solved. The right side of the equation consists of external loading from the waves and the aerodynamic forces. On the other side the mass and inertia, hydrostatic stiffness, mooring-line stiffness, added mass, viscous damping, radiation damping, gravitational stiffness and additional stiffness and damping terms need to be obtained.

Most of the necessary terms are obtained either from the definition of the floater or using WAMIT outputs. WAMIT is a potential flow solver that provides hydrodynamic coefficients. The radiation, diffraction and mooring-line effects and calculated separately with the help of MATLAB scripts that were developed previously in-house or by other researchers. Modifications to these scripts were made to adjust to the FOWT of choice. All the terms were modelled as matrices. Once all the necessary terms were obtained, the dynamics in 6DOF were solved with the help of a Simulink MATLAB model. The scaling for all the matrices was done within the model before the dynamics were solved.

2) What is the methodology for correcting the aerodynamic force for a non-Froude scaled FOWT in HIL wind tunnel testing?

The scaling methodology used in this project does not follow Reynold's or Froude's similarity laws, instead, an arbitrary scaling factor is chosen that provides the best wind speeds and the least Reynold's mismatch according to this particular setup. Since the Froude similarity law is not followed, the accelerations need to be scaled. This means that the gravitational forces and inertial forces need to be scaled as well. Creating a scaled RNA for the wind turbine model is impractical, thus a correction methodology is necessary.

An important component of the external forces necessary for solving the dynamics is the aerodynamic

force. This force can be obtained using the forces measured by the load cell that is placed beneath the RNA. However, this also measures the inertial and gravitational forces of the RNA. Thus to obtain the aerodynamic forces, the components of inertia and gravitation need to be removed from the measured forces. This is done so with the help of an accelerometer that is placed on top of the nacelle.

The accelerometer present measures the triaxial acceleration, with the acceleration and the mass known the inertial forces can be corrected. The gravitational forces can also be corrected easily because the MEMS accelerometer measures gravitational acceleration in the opposite direction, making it easy to identify and correct. Correction of the torque measured is slightly more complicated since there is no accelerometer present on the model that can measure rotational acceleration. A theoretical estimation for the biggest components in the measured torque forces is made and these terms are subtracted to obtain aerodynamic torque.

3) How to make the numerical model adaptable with different floaters and wind turbines?

The numerical model that solves the dynamics of FOWT is built in Simulink. This is also the model that is responsible for the real-time simulation that is necessary for HIL testing. The Simulink model is in turn run with the help of MATLAB scripts that initialize and define values and manage settings. The properties of the chosen floater and the wind turbine model can thus be easily changed by having separate scripts for the different FOWT designs. However, the scaling methodology needs to be individually done for any selected FOWT for the wind turbine model. The obtained scaling factors can then be used with the Simulink model.

In this project, two FOWT designs were modelled and tested. The first was with the DTU10MW wind turbine and the TripleSpar floater, the second was the IEA15MW wind turbine with the VolturnUS floater. They are both open-source FOWT designs that have their aerodynamic, structural and hydrodynamic properties publicly available. The scaling for the DTU10MW was previously done and tested during previous experiments, the same methodology was implemented with the IEA15MW to obtain the scaling factors.

With the scaling factors, the properties of the floater were identified and modelled into matrices that can be used by the Simulink model. The information on the met-ocean conditions during the operation was also different for this floater so different waves were generated and sea-state conditions were set. After the modelling the Simulink model was used to run tests and the results were validated. However, the model failed in the closed-loop setting with the HIL feedback. The reasons for this were explored and the most plausible causes were listed.

4) How accurate is the HIL model at modelling dynamics of FOWT compared to established engineering models like OpenFAST?

To assess the accuracy of the developed Simulink model for the different FOWT designs, the dynamic response was compared between the outputs from Simulink and from the FAST/OpenFAST setup. A FAST setup was used to verify and validate the DTU10MW with the TripleSpar model while an OpenFAST setup was used for the IEA15MW with the VolturnUS model. Free decay tests were done to compare the motion response and also compare the natural frequency and damping ratio of the simulated floating dynamics. Wave cases were also simulated and the wave spectrum, diffraction force spectrum (incident wave force) and motion spectrum were compared between the Simulink model and FAST/OpenFAST.

Overall, there was a good match between the FAST model and the DTU10MW with the TripleSpar model. The natural frequencies matched perfectly with the lowest accuracy rate being around 99%. The damping ratio's accuracy was slightly lower at 92% average accuracy. For the IEA10MW model, the natural frequency has an average of 100% accuracy. There was some discrepancy in the damping ratio, this was due to a modification in the damping done on the model, linear damping values were assumed in the Simulink model whereas the OpenFAST model was equipped with quadratic damping. This resulted especially in the surge and sway DOFs being more damped than in OpenFAST. Despite this, the average accuracy of the damping ratios was 92%. The wave case spectrum was plotted and the peaks were visually matched. This concluded the validation of the Simulink model.

The validated Simulink model was then compared with the experimented HIL results from the wind tunnel. The Simulink model results are essentially the same as the HIL results in open-loop. The

open-loop results also closely matched the close-loop setting. This validated the HIL system. Later, the closed-loop result was compared to the closed-loop setting with wind and rotor operating. This comparison gave insight into the effect of wind and rotor loading on the HIL system.

Suggestions for future work

While working on this project each step was faced with new challenges, and often due to the limitation of time and resources the simplest solution was adopted. In future works, the following suggestions could be considered to develop a better model.

1. More time could be spent on each aspect of the model to increase the fidelity while also balancing it with computational efficiency. So the first recommendation would be to develop the model further to include more non-linear effects thus gradually increasing the fidelity of the numerical model.
2. In the force correction methodology the correction of measured torque was approximated since there was no sensor measuring rotational accelerations. Another sensor could be installed on the wind turbine model to allow this. That, in turn, will enable a force correction module that is more accurate and robust.
3. The signals in the HIL system were not filtered in real-time, having a lowpass filter for the input signals of the HIL model such as the measured force and acceleration will possibly improve the performance. It will remove or at the least reduce the instances where noise in the signals is considered an external force.
4. Finally during the test campaign in the wind tunnel, wind wave misalignment cases can also be tested. This case is not the highest loading experienced by the FOWT system, however, it can help with analysing the dynamic responses better in the different degrees of freedom.

References

[1] *WMO confirms that 2023 smashes global temperature record*. Jan. 2024.

[2] *WEF The Global Risks Report 2024*. Tech. rep. 2024. URL: www.weforum.org.

[3] United Nations Secretary-General. *UN SG's Acceleration Agenda Ad_17JULd*. Tech. rep.

[4] International Energy Agency. *Net Zero by 2050 - A Roadmap for the Global Energy Sector*. Tech. rep. 2050. URL: www.iea.org/t&c/.

[5] International Energy Agency. *Renewables 2023 - Analysis and forecast to 2028*. Tech. rep. URL: www.iea.org.

[6] International Renewable Energy Agency. *Offshore wind energy: Patent insight report*. Tech. rep. 2023.

[7] Z. Janipour. *Floating Offshore Wind Energy: Reaching Beyond the Reachable by Fixed-Bottom Offshore Wind Energy*. Sept. 2023.

[8] WindEurope. *Floating Offshore Wind Vision Statement*. Tech. rep. 2017.

[9] M. Leimeister, A. Kolios, and M. Collu. "Critical review of floating support structures for offshore wind farm deployment". In: *Journal of Physics: Conference Series*. Vol. 1104. 1. Institute of Physics Publishing, Nov. 2018. DOI: 10.1088/1742-6596/1104/1/012007.

[10] S. Butterfield et al. *Engineering challenges for floating offshore wind turbines*. Tech. rep. National Renewable Energy Lab.(NREL), Golden, CO (United States), 2007.

[11] S. Whitfield. "Offshore Wind: The New Frontier in Powering Platforms?" In: *Journal of Petroleum technology* 72.01 (2020), pp. 38–40.

[12] URL: https://www.equinor.com/energy/hywind-tampen.

[13] C. Allen et al. *Definition of the UMaine VolturnUS-S Reference Platform Developed for the IEA Wind 15-Megawatt Offshore Reference Wind Turbine Technical Report*. Tech. rep. 2020. URL: www.nrel.gov/publications..

[14] J. M. Jonkman, M. L. Buhl, et al. *FAST user's guide*. Vol. 365. National Renewable Energy Laboratory Golden, CO, USA, 2005.

[15] A. Pegalajar-Jurado, M. Borg, and H. Bredmose. "An efficient frequency-domain model for quick load analysis of floating offshore wind turbines". In: *Wind Energy Science* 3.2 (2018), pp. 693–712. ISSN: 23667451. DOI: 10.5194/wes-3-693-2018.

[16] E. Faraggiana et al. *A review of numerical modelling and optimisation of the floating support structure for offshore wind turbines*. Aug. 2022. DOI: 10.1007/s40722-022-00241-2.

[17] F. Lemmer et al. "Multibody modeling for concept-level floating offshore wind turbine design". In: *Multibody System Dynamics* 49.2 (June 2020), pp. 203–236. ISSN: 1573272X. DOI: 10.1007/s11044-020-09729-x.

[18] S. Deng, Y. Liu, and D. Ning. "Fully coupled aero-hydrodynamic modelling of floating offshore wind turbines in nonlinear waves using a direct time-domain approach". In: *Renewable Energy* 216 (Nov. 2023), p. 119016. ISSN: 09601481. DOI: 10.1016/j.renene.2023.119016.

[19] J. M. Jonkman et al. "AeroDyn v15 user's guide and theory manual". In: *NREL Draft Report* 46 (2015).

[20] A. Beardsell et al. "Beyond OC5 - Further advances in floating wind turbine modelling using Bladed". In: *Journal of Physics: Conference Series*. Vol. 1102. 1. Institute of Physics Publishing, Oct. 2018. DOI: 10.1088/1742-6596/1102/1/012023.

[21] A. Otter et al. *A review of modelling techniques for floating offshore wind turbines*. May 2022. DOI: 10.1002/we.2701.

[22] C. Ferreira et al. "Dynamic inflow model for a floating horizontal axis wind turbine in surge motion". In: *Wind Energy Science* 7.2 (Mar. 2022), pp. 469–485. ISSN: 23667451. DOI: 10.5194/wes-7-469-2022.

[23] E. Branlard et al. "Dynamic inflow and unsteady aerodynamics models for modal and stability analyses in OpenFAST". In: *Journal of Physics: Conference Series*. Vol. 2265. 3. Institute of Physics, June 2022. DOI: 10.1088/1742-6596/2265/3/032044.

[24] K. Shaler et al. “Preliminary Introduction of a Free Vortex Wake Method into OpenFAST”. In: *Journal of Physics: Conference Series*. Vol. 1452. 1. Institute of Physics Publishing, Mar. 2020. DOI: 10.1088/1742-6596/1452/1/012064.

[25] A. Subbulakshmi et al. *Recent advances in experimental and numerical methods for dynamic analysis of floating offshore wind turbines — An integrated review*. Aug. 2022. DOI: 10.1016/j.rser.2022.112525.

[26] American Automatic Control Council. *Proceedings of the 2009 American Control Conference : Hyatt Regency St. Louis Riverfront, Saint Louis, Mo, USA, June 10-12, 2009*. IEEE, 2009. ISBN: 9781424445240.

[27] S. Salehyar, Y. Li, and Q. Zhu. “Fully-coupled time-domain simulations of the response of a floating wind turbine to non-periodic disturbances”. In: *Renewable Energy* 111 (2017), pp. 214–226. ISSN: 18790682. DOI: 10.1016/j.renene.2017.04.017.

[28] T. C. Chuang, W. H. Yang, and R. Y. Yang. “Experimental and numerical study of a barge-type FOWT platform under wind and wave load”. In: *Ocean Engineering* 230 (June 2021). ISSN: 00298018. DOI: 10.1016/j.oceaneng.2021.109015.

[29] J. B. Thomsen, A. Têtu, and H. Stiesdal. “A comparative investigation of prevalent hydrodynamic modelling approaches for floating offshore wind turbine foundations: A tetraspar case study”. In: *Journal of Marine Science and Engineering* 9.7 (July 2021). ISSN: 20771312. DOI: 10.3390/jmse9070683.

[30] A. M. Viselli, A. J. Goupee, and H. J. Dagher. “Model Test of a 1:8-Scale Floating Wind Turbine Offshore in the Gulf of Maine1”. In: *Journal of Offshore Mechanics and Arctic Engineering* 137.4 (Aug. 2015). ISSN: 0892-7219. DOI: 10.1115/1.4030381.

[31] F. Driscoll et al. “Validation of a FAST Model of the Statoil-hywind Demo Floating Wind Turbine”. In: *Energy Procedia* 94 (Sept. 2016), pp. 3–19. ISSN: 18766102. DOI: 10.1016/j.egypro.2016.09.181.

[32] R.-Y. Yang et al. “The 1:20 scaled hydraulic model test and field experiment of barge-type floating offshore wind turbine system”. In: *Ocean Engineering* 247 (Mar. 2022), p. 110486. ISSN: 00298018. DOI: 10.1016/j.oceaneng.2021.110486.

[33] W. Shi et al. *Real-time hybrid model tests of floating offshore wind turbines: Status, challenges, and future trends*. Dec. 2023. DOI: 10.1016/j.apor.2023.103796.

[34] C. Cermelli and A. Aubault. *OTC 20674 Qualification of a Semi-Submersible Floating Foundation for Multi-Megawatt Wind Turbines*. Tech. rep. 2010, pp. 3–6. URL: http://onepetro.org/OTCONF/proceedings-pdf/10OTC/All-10OTC/OTC-20674-MS/1719099/otc-20674-ms.pdf/1.

[35] S. Bahramiasl, M. Abbaspour, and M. Karimirad. “Experimental study on gyroscopic effect of rotating rotor and wind heading angle on floating wind turbine responses”. In: *International Journal of Environmental Science and Technology* 15.12 (Dec. 2018), pp. 2531–2544. ISSN: 17352630. DOI: 10.1007/s13762-017-1519-4.

[36] A. J. Goupee et al. “Experimental comparison of three floating wind turbine concepts”. In: *Journal of Offshore Mechanics and Arctic Engineering* 136.2 (Mar. 2014). ISSN: 1528896X. DOI: 10.1115/1.4025804.

[37] A. N. Robertson et al. *Summary of Conclusions and Recommendations Drawn from the DeepCWind Scaled Floating Offshore Wind System Test Campaign Preprint SUMMARY OF CONCLUSIONS AND RECOMMENDATIONS DRAWN FROM THE DEEPCWIND SCALED FLOATING OFFSHORE WIND SYSTEM TEST CAMPAIGN*. Tech. rep. 2013. URL: http://www.osti.gov/bridgeonlineordering:http://www.ntis.gov/help/ordermethods.aspx.

[38] A. J. Goupee et al. “Additional Wind/Wave Basin Testing of the DeepCwind Semi-Submersible With a Performance-Matched Wind Turbine”. In: *Volume 9B: Ocean Renewable Energy*. American Society of Mechanical Engineers, June 2014. ISBN: 978-0-7918-4554-7. DOI: 10.1115/OMAE2014-24172.

[39] A. N. Robertson et al. “OC5 Project Phase II: Validation of Global Loads of the DeepCwind Floating Semisubmersible Wind Turbine”. In: *Energy Procedia* 137 (Oct. 2017), pp. 38–57. ISSN: 18766102. DOI: 10.1016/j.egypro.2017.10.333.

[40] E.-J. de Ridder et al. “Development of a Scaled-Down Floating Wind Turbine for Offshore Basin Testing”. In: *Volume 9A: Ocean Renewable Energy*. American Society of Mechanical Engineers, June 2014. ISBN: 978-0-7918-4553-0. DOI: 10.1115/OMAE2014-23441.

[41] H. Bredmose et al. “The Triple Spar campaign: Model tests of a 10MW floating wind turbine with waves, wind and pitch control”. In: *Energy Procedia*. Vol. 137. Elsevier Ltd, 2017, pp. 58–76. DOI: 10.1016/j.egypro.2017.10.334.

[42] Y. s. Zhao et al. “Experimental Study on New Multi-Column Tension-Leg-Type Floating Wind Turbine”. In: *China Ocean Engineering* 32.2 (Apr. 2018), pp. 123–131. ISSN: 21918945. DOI: 10.1007/s13344-018-0014-0.

[43] G. Doisenbant et al. “Application to reduced scale model testing”. In: *Wind Engineering* 42.2 (2018), pp. 108–114. ISSN: 0309524X, 2048402X. URL: https://www.jstor.org/stable/90019972.

[44] A. Connolly et al. “Fully Coupled Aero-Hydro-Structural Simulation of New Floating Wind Turbine Concept”. In: *ASME 2018 1st International Offshore Wind Technical Conference*. American Society of Mechanical Engineers, Nov. 2018. ISBN: 978-0-7918-5197-5. DOI: 10.1115/IOWTC2018-1016.

[45] C. Chen, Y. Ma, and T. Fan. *Review of model experimental methods focusing on aerodynamic simulation of floating offshore wind turbines*. Apr. 2022. DOI: 10.1016/j.rser.2021.112036.

[46] J. E. Carrion and B. F. Spencer. *NSEL Report Series Model-based Strategies for Real-time Hybrid Testing*. Tech. rep. 2007. URL: http://www.terragalleria.com/.

[47] Y. Cao and G. Tahchiev. “A Study on an Active Hybrid Decomposed Mooring System for Model Testing in Ocean Basin for Offshore Platforms”. In: *Volume 1: Offshore Technology*. American Society of Mechanical Engineers, June 2013. ISBN: 978-0-7918-5531-7. DOI: 10.1115/OMAE2013-11471.

[48] J. Azcona et al. “Aerodynamic Thrust Modelling in Wave Tank Tests of Offshore Floating Wind Turbines Using a Ducted Fan”. In: *Journal of Physics: Conference Series* 524 (June 2014), p. 012089. ISSN: 1742-6596. DOI: 10.1088/1742-6596/524/1/012089.

[49] J. Azcona, F. Bouchotrouch, and F. Vittori. “Low□frequency dynamics of a floating wind turbine in wave tank–scaled experiments with SiL hybrid method”. In: *Wind Energy* 22.10 (Oct. 2019), pp. 1402–1413. ISSN: 1095-4244. DOI: 10.1002/we.2377.

[50] E. Oguz et al. “Experimental and numerical analysis of a TLP floating offshore wind turbine”. In: *Ocean Engineering* 147 (Jan. 2018), pp. 591–605. ISSN: 00298018. DOI: 10.1016/j.oceaneng.2017.10.052.

[51] C. Wright et al. “Experimental comparison of dynamic responses of a tension moored floating wind turbine platform with and without spring dampers”. In: *Journal of Physics: Conference Series*. Vol. 628. 1. Institute of Physics Publishing, July 2015. DOI: 10.1088/1742-6596/628/1/012056.

[52] C. Desmond, J.-C. Hinrichs, and J. Murphy. “Uncertainty in the Physical Testing of Floating Wind Energy Platforms’ Accuracy versus Precision”. In: *Energies* 12.3 (Jan. 2019), p. 435. ISSN: 1996-1073. DOI: 10.3390/en12030435.

[53] C. Matoug et al. “An hybrid approach for the comparison of VAWT and HAWT performances for floating offshore wind turbines”. In: *Journal of Physics: Conference Series* 1618.3 (Sept. 2020), p. 032026. ISSN: 1742-6588. DOI: 10.1088/1742-6596/1618/3/032026.

[54] M. Andersen. *Floating Foundations for Offshore Wind Turbines*. English. PhD supervisor: Professor Søren R.K. Nielsen, Aalborg University Assistant PhD supervisor: Associate Professor Peter B. Frigaard, Aalborg University. 2016. DOI: 10.5278/vbn.phd.engsci.00175.

[55] A. Otter, J. Murphy, and C. J. Desmond. “Emulating aerodynamic forces and moments for hybrid testing of floating wind turbine models”. In: *Journal of Physics: Conference Series* 1618.3 (Sept. 2020), p. 032022. ISSN: 1742-6588. DOI: 10.1088/1742-6596/1618/3/032022.

[56] J. A. Armesto et al. “TELWIND: Numerical Analysis of a Floating Wind Turbine Supported by a Two Bodies Platform”. In: *Volume 10: Ocean Renewable Energy*. American Society of Mechanical Engineers, June 2018. ISBN: 978-0-7918-5131-9. DOI: 10.1115/OMAE2018-77587.

[57] O. Pires et al. “Inclusion of rotor moments in scaled wave tank test of a floating wind turbine using SiL hybrid method”. In: *Journal of Physics: Conference Series*. Vol. 1618. 3. IOP Publishing Ltd, Sept. 2020. DOI: 10.1088/1742-6596/1618/3/032048.

[58] E. E. Bachynski, V. Chabaud, and T. Sauder. “Real-time Hybrid Model Testing of Floating Wind Turbines: Sensitivity to Limited Actuation”. In: *Energy Procedia* 80 (2015), pp. 2–12. ISSN: 18766102. DOI: 10.1016/j.egypro.2015.11.400.

[59] M. Thys et al. “Real-Time Hybrid Model Testing of a Semi-Submersible 10MW Floating Wind Turbine and Advances in the Test Method”. In: *ASME 2018 1st International Offshore Wind Technical Conference*. American Society of Mechanical Engineers, Nov. 2018. ISBN: 978-0-7918-5197-5. DOI: 10.1115/IOWTC2018-1081.

[60] E. E. Bachynski et al. “Real-Time Hybrid Model Testing of a Braceless Semi-Submersible Wind Turbine: Part II — Experimental Results”. In: *Volume 6: Ocean Space Utilization; Ocean Renewable Energy*. American Society of Mechanical Engineers, June 2016. ISBN: 978-0-7918-4997-2. DOI: 10.1115/OMAE2016-54437.

[61] M. Hall and A. J. Goupee. “Validation of a hybrid modeling approach to floating wind turbine basin testing”. In: *Wind Energy* 21.6 (June 2018), pp. 391–408. ISSN: 1095-4244. DOI: 10.1002/we.2168.

[62] A. Meseguer and R. Guanche. “Wind turbine aerodynamics scale-modeling for floating offshore wind platform testing”. In: *Journal of Wind Engineering and Industrial Aerodynamics* 186 (Mar. 2019), pp. 49–57. ISSN: 01676105. DOI: 10.1016/j.jweia.2018.12.021.

[63] I. Bayati et al. “Scale model technology for floating offshore wind turbines”. In: *IET Renewable Power Generation*. Vol. 11. 9. Institution of Engineering and Technology, July 2017, pp. 1120–1126. DOI: 10.1049/iet-rpg.2016.0956.

[64] I. Bayati et al. “Aerodynamic design methodology for wind tunnel tests of wind turbine rotors”. In: *Journal of Wind Engineering and Industrial Aerodynamics* 167 (Aug. 2017), pp. 217–227. ISSN: 01676105. DOI: 10.1016/j.jweia.2017.05.004.

[65] M. Thys. *D7.9 Guidance and Recommended Methods for Hybrid/HIL-based FOWT Experimental Testing; D7.9 Guidance and Recommended Methods for Hybrid/HIL-based FOWT Experimental Testing*. Tech. rep. 2019.

[66] I. Bayati et al. “Wind Tunnel Wake Measurements of Floating Offshore Wind Turbines”. In: *Energy Procedia* 137 (Oct. 2017), pp. 214–222. ISSN: 18766102. DOI: 10.1016/j.egypro.2017.10.375.

[67] I. Bayati et al. “Analysis of FOWT dynamics in 2-DOF hybrid HIL wind tunnel experiments”. In: *Ocean Engineering* 195 (Jan. 2020), p. 106717. ISSN: 00298018. DOI: 10.1016/j.oceaneng.2019.106717.

[68] I. Bayati et al. “Design of a 6-DoF Robotic Platform for Wind Tunnel Tests of Floating Wind Turbines”. In: *Energy Procedia* 53 (2014), pp. 313–323. ISSN: 18766102. DOI: 10.1016/j.egypro.2014.07.240.

[69] M. Belloli et al. “A hybrid methodology for wind tunnel testing of floating offshore wind turbines”. In: *Ocean Engineering* 210 (Aug. 2020). ISSN: 00298018. DOI: 10.1016/j.oceaneng.2020.107592.

[70] I. Bayati et al. *OMAE2018-77804 6-DOF HYDRODYNAMIC MODELLING FOR WIND TUNNEL HYBRID/HIL TESTS OF FOWT: THE REAL-TIME CHALLENGE*. Tech. rep. 2018.

[71] I. Bayati et al. “A wind tunnel/HIL setup for integrated tests of Floating Offshore Wind Turbines”. In: *Journal of Physics: Conference Series* 1037 (June 2018), p. 052025. ISSN: 1742-6588. DOI: 10.1088/1742-6596/1037/5/052025.

[72] M. Thys et al. *IOWTC2019-7575 HYBRID MODEL TESTS FOR FLOATING OFFSHORE WIND TURBINES*. Tech. rep. 2019. DOI: 10.1115/IOWTC2019-7575. URL: https://lifes50plus.eu/.

[73] A. Fontanella, A. Facchinetti, and M. Belloli. “Wind tunnel hardware-in-the-loop experiments about the global response of a 15 MW floating wind turbine”. In: *Journal of Physics: Conference Series*. Vol. 2626. 1. Institute of Physics, 2023. DOI: 10.1088/1742-6596/2626/1/012059.

[74] S. Rockel et al. “Experimental Study on Influence of Pitch Motion on the Wake of a Floating Wind Turbine Model”. In: *Energies* 7.4 (Mar. 2014), pp. 1954–1985. ISSN: 1996-1073. DOI: 10.3390/en7041954.

[75] B. Schliffke, S. Aubrun, and B. Conan. “Wind Tunnel Study of a “Floating” Wind Turbine’s Wake in an Atmospheric Boundary Layer with Imposed Characteristic Surge Motion”. In: *Journal of Physics: Conference Series* 1618.6 (Sept. 2020), p. 062015. ISSN: 1742-6588. DOI: 10.1088/1742-6596/1618/6/062015.

[76] F. Taruffi et al. “An experimental study on the aerodynamic loads of a floating offshore wind turbine under imposed motions”. In: (2023). DOI: 10.5194/wes-2023-86. URL: https://doi.org/10.5194/wes-2023-86.

[77] TU Delft - Aerospace Engineering. *The Open Jet Facility*. URL: https://www.tudelft.nl/lr/organisatie/afdelingen/flow-physics-and-technology/facilities/low-speed-wind-tunnels/open-jet-facility.
[78] L. Lignarolo et al. “Experimental analysis of the wake of a horizontal-axis wind-turbine model”. In: *Renewable Energy* 70 (Oct. 2014), pp. 31–46. ISSN: 09601481. DOI: 10.1016/j.renene.2014.01.020.
[79] Q. Inc. *Hexapod*. https://www.quanser.com/products/hexapod/. Accessed: 2024-06-17. 2024.
[80] Quanser Inc. *Quanser 6 DOF Hexapod - User Manual*. Tech. rep. 2016. URL: http://www.quanser.com.
[81] C. ; Bak et al. *General rights The DTU 10-MW Reference Wind Turbine). The DTU 10-MW Reference Wind Turbine. Sound/Visual production (digital)*. Tech. rep. 2013.
[82] F. Lemmer et al. *Definition of the SWE-TripleSpar Floating Platform for the DTU 10MW Reference Wind Turbine*. Tech. rep.
[83] A. Fontanella, G. Da Pra, and M. Belloli. “Integrated Design and Experimental Validation of a Fixed-Pitch Rotor for Wind Tunnel Testing”. In: *Energies* 16.5 (Mar. 2023). ISSN: 19961073. DOI: 10.3390/en16052205.
[84] E. Gaertner et al. *Definition of the IEA Wind 15-Megawatt Offshore Reference Wind Turbine Technical Report*. Tech. rep. 2020. URL: www.nrel.gov/publications..
[85] W. Cummins et al. “The impulse response function and ship motions”. In: (1962).
[86] Z. Zhao et al. “Dynamic analysis of a novel semi-submersible platform for a 10 MW wind turbine in intermediate water depth”. In: *Ocean Engineering* 237 (Oct. 2021). ISSN: 00298018. DOI: 10.1016/j.oceaneng.2021.109688.
[87] J. M. Jonkman. “Dynamics of offshore floating wind turbines-model development and verification”. In: *Wind Energy* 12.5 (2009), pp. 459–492. ISSN: 10991824. DOI: 10.1002/we.347.
[88] T. Duarte et al. *State-Space Realization of the Wave-Radiation Force within FAST: Preprint*. Tech. rep. 2013. URL: http://www.osti.gov/bridgeonlineordering:http://www.ntis.gov/help/ordermethods.aspx.
[89] G. do Amaral. “Analytical Assessment of the Mooring System Stiffness”. PhD thesis. Mar. 2020. DOI: 10.13140/RG.2.2.28848.38401.
[90] N. W. Team. *WISDEM/pyMAP*. 2020. URL: https://github.com/WISDEM/pyMAP/tree/master.
[91] WAMIT. *WAMIT USER MANUAL v7.2*. Tech. rep. URL: www.wamit.com.
[92] J. A. Mulder et al. *Flight Dynamics Lecture Notes*. Tech. rep. 2013.
[93] R. C. Hibbeler. *Engineering mechanics: dynamics*. Pearson Educación, 2004.
[94] G. K. V. Ramachandran et al. *Investigation of Response Amplitude Operators for Floating Offshore Wind Turbines: Preprint*. Tech. rep. 2013. URL: www.nrel.gov/publications..

A

Property Matrices

A.1. DTU10MW + TripleSpar

Hydrostatic Stiffness:

$$K_{hst} = \begin{bmatrix} 0 & 0 & 0 & 0 & 0 & 0 \\ 0 & 0 & 0 & 0 & 0 & 0 \\ 0 & 0 & 5.30 \times 10^{6} & 0 & -4.948 & 0 \\ 0 & 0 & 0 & -6.441 \times 10^{9} & 0 & -1.246 \times 10^{4} \\ 0 & 0 & -4.948 & 0 & -6.441 \times 10^{9} & 0 \\ 0 & 0 & 0 & 0 & 0 & 0 \end{bmatrix} \quad \text{(A.1)}$$

Added Mass:

$$M_{inf} = \begin{bmatrix} 2.78 \times 10^{7} & 0 & -0.2955 & 0 & -7.44 \times 10^{8} & 0 \\ 0 & 2.78 \times 10^{7} & 0 & 7.44 \times 10^{8} & 0 & 1.48 \times 10^{3} \\ -1.40 & 0 & 4.36 \times 10^{6} & 0 & 65.3 & 0 \\ 0 & 7.44 \times 10^{8} & 0 & 2.70 \times 10^{10} & 0 & 3.98 \times 10^{4} \\ -7.44 \times 10^{8} & 0 & 49.2 & 0 & 2.70 \times 10^{10} & 0 \\ 0 & 1.38 \times 10^{3} & 0 & 4.07 \times 10^{4} & 0 & 1.75 \times 10^{10} \end{bmatrix} \quad \text{(A.2)}$$

Linear Viscous Damping:

$$R_{visc} = \begin{bmatrix} 1.70 \times 10^{5} & 0 & 0 & 0 & 0 & 0 \\ 0 & 1.70 \times 10^{5} & 0 & 0 & 0 & 0 \\ 0 & 0 & 1.35 \times 10^{6} & 0 & 0 & 0 \\ 0 & 0 & 0 & 7.37 \times 10^{8} & 0 & 0 \\ 0 & 0 & 0 & 0 & 7.37 \times 10^{8} & 0 \\ 0 & 0 & 0 & 0 & 0 & 1.09 \times 10^{8} \end{bmatrix} \quad \text{(A.3)}$$

Mooring Line Stiffness Matrix:

$$K_{moor} = -\begin{bmatrix} -8.33 \times 10^{4} & 4.06 \times 10^{-5} & 5.82 \times 10^{-11} & 5.61 \times 10^{-3} & -2.85 \times 10^{6} & 6.30 \times 10^{-7} \\ -3.20 \times 10^{-5} & -8.33 \times 10^{4} & 1.16 \times 10^{-10} & 2.85 \times 10^{6} & 0 & 3.69 \times 10^{-7} \\ 3.51 & 3.76 \times 10^{-5} & -5.73 \times 10^{4} & 4.65 \times 10^{-3} & 9.37 \times 10^{2} & 0 \\ 1.24 \times 10^{-3} & 2.84 \times 10^{6} & 0 & -2.00 \times 10^{8} & 1.42 \times 10^{-7} & 3.28 \times 10^{-4} \\ -2.84 \times 10^{6} & 1.38 \times 10^{-3} & -3.73 \times 10^{-9} & 1.89 \times 10^{-1} & -2.00 \times 10^{8} & -5.67 \times 10^{-4} \\ -5.55 \times 10^{-7} & 7.65 \times 10^{1} & 0 & -1.57 \times 10^{5} & 0 & -2.69 \times 10^{8} \end{bmatrix} \quad \text{(A.4)}$$

Addition stiffness and damping, determined after tuning:

$$K_{add} = \begin{bmatrix} -24 & 0 & 0 & 0 & 0 & 0 \\ 0 & -16 & 0 & 0 & 0 & 0 \\ 0 & 0 & -1 & 0 & 0 & 0 \\ 0 & 0 & 0 & 65 & 0 & 0 \\ 0 & 0 & 0 & 0 & 65 & 0 \\ 0 & 0 & 0 & 0 & 0 & -18 \end{bmatrix} \quad \text{(A.5)}$$

$$R_{add} = \begin{bmatrix} 45 & 0 & 0 & 0 & 0 & 0 \\ 0 & 50 & 0 & 0 & 0 & 0 \\ 0 & 0 & 15 & 0 & 0 & 0 \\ 0 & 0 & 0 & 180 & 0 & 0 \\ 0 & 0 & 0 & 0 & 160 & 0 \\ 0 & 0 & 0 & 0 & 0 & 60 \end{bmatrix} \quad \text{(A.6)}$$

A.2. IEA15MW + VolturnUS

Hydrostatic Stiffness:

$$K_{hst} = \begin{bmatrix} 0 & 0 & 0 & 0 & 0 & 0 \\ 0 & 0 & 0 & 0 & 0 & 0 \\ 0 & 0 & 4.45 \times 10^{6} & 0 & -4.03 \times 10^{3} & 0 \\ 0 & 0 & 0 & 2.19 \times 10^{9} & 0 & -9.13 \times 10^{4} \\ 0 & 0 & -4.03 \times 10^{3} & 0 & 2.19 \times 10^{9} & 0 \\ 0 & 0 & 0 & 0 & 0 & 0 \end{bmatrix} \quad \text{(A.7)}$$

Added Mass:

$$\text{MMainf} = \begin{bmatrix} 9.64 \times 10^{6} & 0.00 & -2.18 \times 10^{1} & 0.00 & -1.01 \times 10^{8} & 0.00 \\ 0.00 & 9.64 \times 10^{6} & 0.00 & 1.01 \times 10^{8} & 0.00 & -1.89 \times 10^{3} \\ -3.61 \times 10^{1} & 0.00 & 2.48 \times 10^{7} & 0.00 & -1.83 \times 10^{4} & 0.00 \\ 0.00 & 1.01 \times 10^{8} & 0.00 & 1.16 \times 10^{10} & 0.00 & -5.26 \times 10^{4} \\ -1.01 \times 10^{8} & 0.00 & -1.85 \times 10^{4} & 0.00 & 1.16 \times 10^{10} & 0.00 \\ 0.00 & -1.59 \times 10^{3} & 0.00 & -4.61 \times 10^{4} & 0.00 & 2.01 \times 10^{10} \end{bmatrix} \quad \text{(A.8)}$$

Linear Viscous Damping (these values were determined arbitrarily):

$$K_{moor} = \begin{bmatrix} 10.00 \times 10^{4} & 0 & 0 & 0 & 0 & 0 \\ 0 & 10.00 \times 10^{4} & 0 & 0 & 0 & 0 \\ 0 & 0 & 7.60 \times 10^{5} & 0 & 0 & 0 \\ 0 & 0 & 0 & 2.80 \times 10^{8} & 0 & 0 \\ 0 & 0 & 0 & 0 & 2.80 \times 10^{8} & 0 \\ 0 & 0 & 0 & 0 & 0 & 2.30 \times 10^{8} \end{bmatrix} \quad \text{(A.9)}$$

Mooring Line Stiffness:

$$K_{moor} = \begin{bmatrix} 7.31 \times 10^{4} & -1.64 \times 10^{-1} & 2.82 \times 10^{-3} & 7.64 & -6.75 \times 10^{5} & 1.01 \\ 0 & 7.31 \times 10^{4} & -1.73 \times 10^{-1} & 6.75 \times 10^{5} & -1.01 & -1.10 \\ -3.21 \times 10^{-3} & -5.76 \times 10^{-3} & 6.11 \times 10^{4} & -1.62 \times 10^{-1} & 1.32 \times 10^{-1} & 6.05 \times 10^{-4} \\ 0 & 6.76 \times 10^{5} & 1.03 \times 10^{3} & 4.01 \times 10^{8} & 2.18 \times 10^{1} & -2.10 \times 10^{1} \\ -6.76 \times 10^{5} & -1.03 \times 10^{3} & -3.70 \times 10^{-2} & -2.61 \times 10^{4} & 4.01 \times 10^{8} & 2.18 \times 10^{1} \\ 0 & -1.10 & 0 & -2.36 \times 10^{1} & -1.21 \times 10^{-3} & 2.56 \times 10^{8} \end{bmatrix} \quad \text{(A.10)}$$

Additional stiffness and damping:

$$K_{add} = \begin{bmatrix} -1 & 0 & 0 & 0 & 0 & 0 \\ 0 & 7 & 0 & 0 & 0 & 0 \\ 0 & 0 & 4 & 0 & 0 & 0 \\ 0 & 0 & 0 & 26 & 0 & 0 \\ 0 & 0 & 0 & 0 & 26 & 0 \\ 0 & 0 & 0 & 0 & 0 & -7 \end{bmatrix} \quad \text{(A.11)}$$

$$R_{add} = \begin{bmatrix} 0 & 0 & 0 & 0 & 0 & 0 \\ 0 & 0 & 0 & 0 & 0 & 0 \\ 0 & 0 & 0 & 0 & 0 & 0 \\ 0 & 0 & 0 & 30 & 0 & 0 \\ 0 & 0 & 0 & 0 & 30 & 0 \\ 0 & 0 & 0 & 0 & 0 & 0 \end{bmatrix} \quad \text{(A.12)}$$

A.3. Structural Matrices

These are used for both the numerical model,

$$M = \begin{bmatrix} M_{tot} & 0 & 0 & 0 & 0 & 0 \\ 0 & M_{tot} & 0 & 0 & 0 & 0 \\ 0 & 0 & M_{tot} & 0 & 0 & 0 \\ 0 & 0 & 0 & J_{xx} & 0 & 0 \\ 0 & 0 & 0 & 0 & J_{yy} & 0 \\ 0 & 0 & 0 & 0 & 0 & J_{zz} \end{bmatrix} \quad \text{(A.13)}$$

Where,

$M_{tot} = M_{floater} + M_{windturbine}$

$J_{xx} = Jx_{floater} + Jx_{windturbine} + M_{floater} * H^2_{floater,COM}$

$J_{yy} = Jy_{floater} + Jy_{windturbine} + M_{floater} * H^2_{floater,COM}$

$J_{zz} = Jz_{floater} + Jz_{windturbine}$

$$K_{grav} = \begin{bmatrix} 0 & 0 & 0 & 0 & 0 & 0 \\ 0 & 0 & 0 & 0 & 0 & 0 \\ 0 & 0 & 0 & 0 & 0 & 0 \\ 0 & 0 & 0 & -M_{tot} * H_{com} * G & 0 & 0 \\ 0 & 0 & 0 & 0 & -M_{tot} * H_{com} * G & 0 \\ 0 & 0 & 0 & 0 & 0 & 0 \end{bmatrix} \quad \text{(A.14)}$$

where K_{grav} is the gravitational stiffness, H_{com} is the height of the centre of mass of the whole FOWT model from the mean sea level.

B

Force Correction MATLAB Script

Below is the script used inside the Simulink model for the correction of measured forces to obtain external aerodynamic force.

```
function [F_aero_est_out,T_aero_est_out]= forcecorr(pos,r_acc,Fmeas,
    i_trans, i_FgComp, acc_meas)

F_meas=Fmeas(1:3);
T_meas=Fmeas(4:6);

ar=r_acc(4);
ap=r_acc(5);
ay=r_acc(6);

r=pos(4);
p=pos(5);
y=pos(6);

Jr=0;
Jp=0;
Jy=0;

g=9.81;
M=1.7;
z=0.035;
h=0.81;

% tt position wrt tb in zero pos
pos_tt_tb_0=[0 0 h]';

%rotation roll+pitch+yaw
Rot_r=[1 0 0
       0 cos(r) -sin(r)
       0 sin(r) cos(r)];
Rot_p=[cos(p) 0 sin(p)
       0 1 0
       -sin(p) 0 cos(p)];
Rot_y=[cos(y) -sin(y) 0
       sin(y) cos(y) 0
       0 0 1];
```

```
36
37  Rot_rpy=Rot_y*Rot_p*Rot_r;
38
39  Fcorr=-M*acc_meas;
40
41  Fz_ofs_comp=-[0; 0; +M*g];
42  if i_FgComp==1
43      Faero_est=F_meas-Fcorr+Fz_ofs_comp;
44  else
45      Faero_est=F_meas-Fcorr;
46  end
47  T_in=[-Jr*ar;-Jp*ap;-Jy*ay];
48  T_in_r=Rot_rpy\T_in;
49
50  Tcorr=[+acc_meas(2)*M*z;-acc_meas(1)*M*z; -0]+T_in_r;
51
52
53  Taero_est=T_meas-Tcorr;
54
55
56  %% Force rotation and transport
57
58  % rotate F_aero_est form rotating to fixed
59
60  Faero_est_tt_r=Faero_est;                              %tower top rotating
61  F_aero_est_tt_nr=Rot_rpy*Faero_est_tt_r;               %tower top fixed
62  T_aero_est_tt=Taero_est;
63
64  F_aero_est_out=F_aero_est_tt_nr;
65
66
67  % transport F_aero_est from tt to tb
68  pos_tt_tb=Rot_rpy*pos_tt_tb_0;
69  if i_trans==1
70
71      T_aero_est_trans=[-F_aero_est_tt_nr(2)*pos_tt_tb(3)+F_aero_est_tt_nr
            (3)*pos_tt_tb(2)
72                        F_aero_est_tt_nr(1)*pos_tt_tb(3)-F_aero_est_tt_nr
                              (3)*pos_tt_tb(1)
73                        -F_aero_est_tt_nr(1)*pos_tt_tb(2)+F_aero_est_tt_nr
                              (2)*pos_tt_tb(1)];
74
75      T_aero_est_out=T_aero_est_tt+T_aero_est_trans;
76  else
77      T_aero_est_out=T_aero_est_tt;
78
79  end
```

C

Response Amplitude Operators

$$RAO = H(\omega) = \frac{S_{xy}(\omega)}{S_{xx}(\omega)} \tag{C.1}$$

Where x denotes wave amplitude and y denotes the motion of the platform.

Sample MATLAB code for plotting RAO: The below code was used with the FAST outputs. An additional lowpass filter was used for the data from the wind tunnel experiments.

```
% RAO analysis

window = hanning(length(time));
Fs=1/(time(2)-time(1));
wave_elev = detrend(wave_elev);
ptfm_surge = detrend(ptfm_surge);
ptfm_heave=detrend(ptfm_heave);
ptfm_pitch=detrend(ptfm_pitch);

[wave_psd, f] = pwelch(wave_elev, window, [], [], Fs);
[cross_psd_surge, ~] = cpsd(wave_elev,ptfm_surge, window, [], [], Fs);
[cross_psd_heave, ~] = cpsd(wave_elev,ptfm_heave, window, [], [], Fs);
[cross_psd_pitch, ~] = cpsd(wave_elev,ptfm_pitch, window, [], [], Fs);

% Compute RAO
rao_surge = cross_psd_surge ./ wave_psd;
rao_heave = cross_psd_heave ./ wave_psd;
rao_pitch = cross_psd_pitch ./ wave_psd;

% Plot RAO
figure()
subplot(3,1,1)
plot(f, abs(rao_surge));
set(gca, 'YScale', 'log')
xlabel('Frequency (Hz)');
ylabel('Surge RAO');
title('Response Amplitude Operator (RAO)');
xlim([0 0.4])
grid on

subplot(3,1,2)
plot(f, abs(rao_heave));
```

```
set(gca, 'YScale', 'log')
xlabel('Frequency (Hz)');
ylabel('Heave RAO');
xlim([0 0.4])
grid on;

subplot(3,1,3)
plot(f, abs(rao_pitch));
set(gca, 'YScale', 'log')
xlabel('Frequency (Hz)');
ylabel('Pitch RAO');
xlim([0 0.4])
grid on;
```

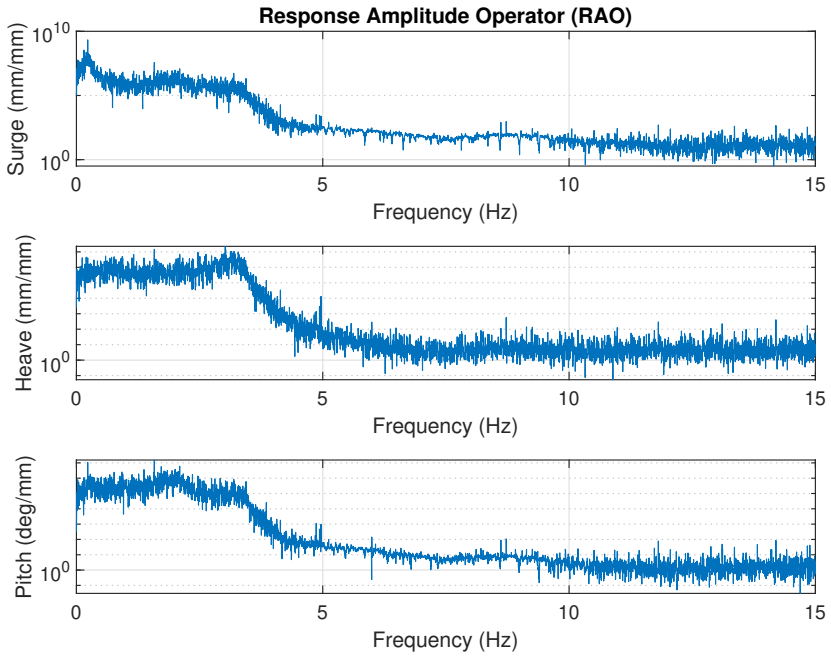

Figure C.1: RAO of Wave Case 1 tested in the wind tunnel.

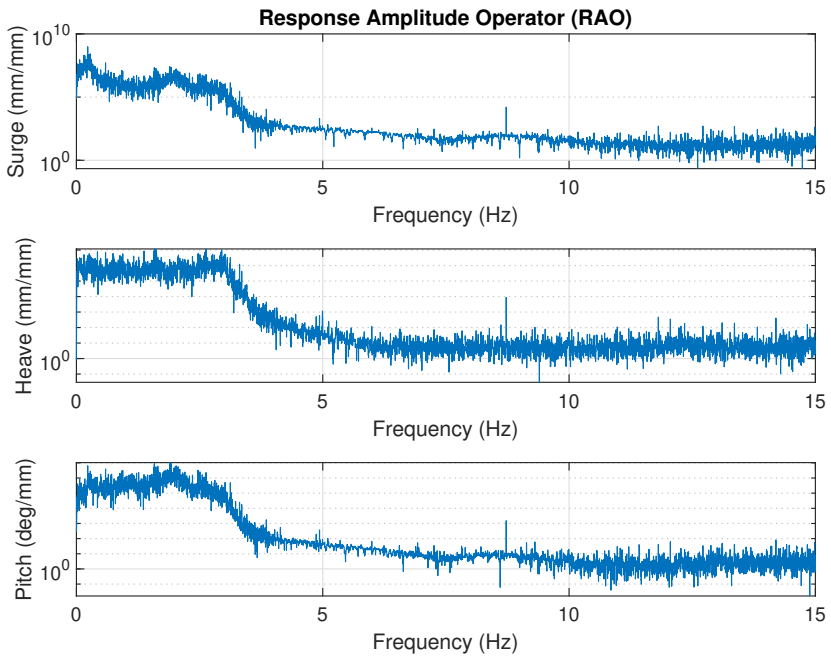

Figure C.2: RAO of Wave Case 2 tested in the wind tunnel.

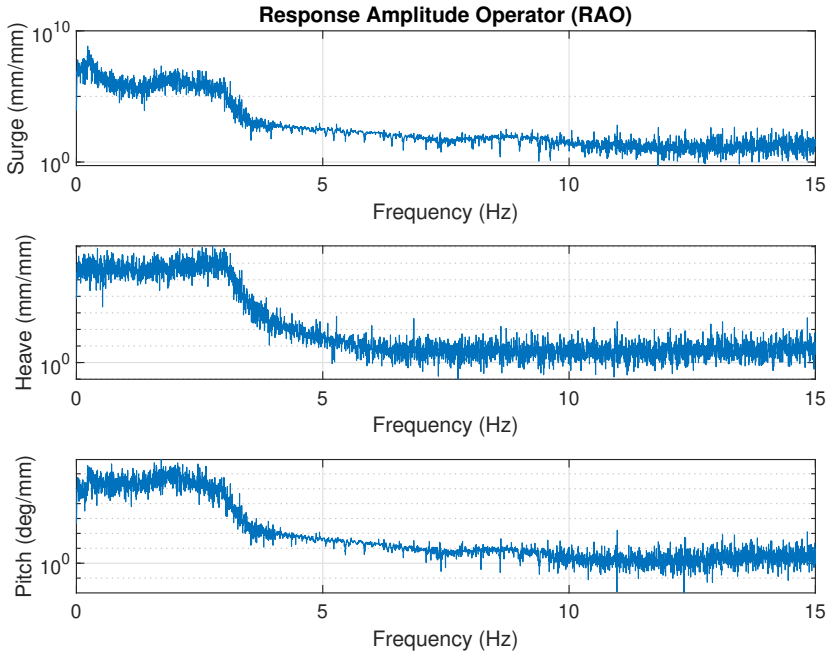

Figure C.3: RAO of Wave Case 3 tested in the wind tunnel.

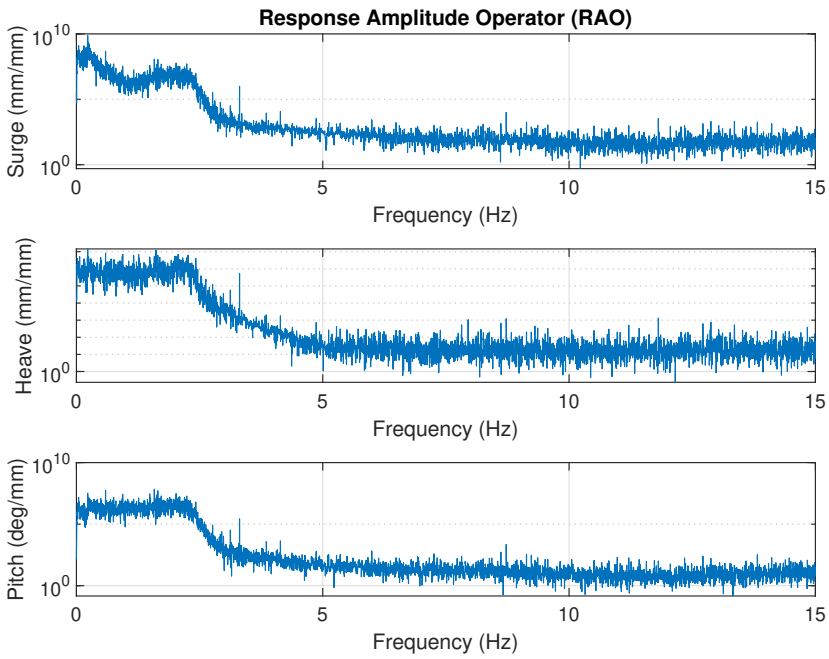

Figure C.4: RAO of Wave Case 4 tested in the wind tunnel.

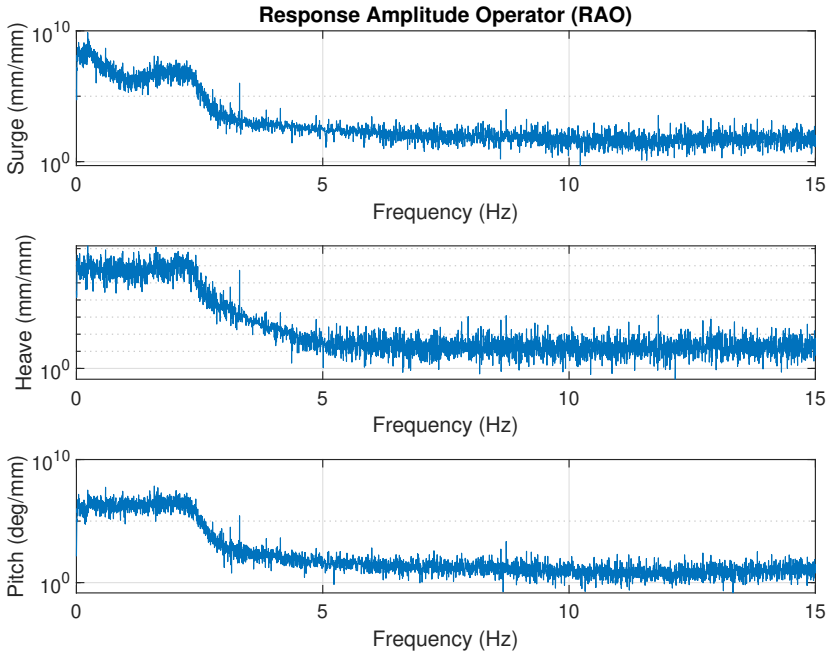

Figure C.5: RAO of Wave Case 5 tested in the wind tunnel.